S³ Advanced Optical Conceptual Design Report

S³: The Super Separator Spectrometer for LINAG Beams

Abstract:

S³ (Super Separator Spectrometer) is a device designed for experiments with the very high intensity stable beams of LINAG, the superconducting linear accelerator of GANIL, which will be built in the framework of SPIRAL2. These beams, which will provide in a first phase of SPIRAL2 ions with A/q = 3, can reach intensities exceeding 100 pμA for lighter ions—A < 40-50—depending on the final choice of the ECR (Electron Cyclotron Resonance) ion source. These unprecedented intensities open new opportunities in several physics domains, e.g. superheavy and very-heavy nuclei, spectroscopy at and beyond the proton dripline, isomers and ground state properties, multi-nucleon transfer and deep-inelastic reactions. An international collaboration has been formed for proposing physics experiments and developing technical solutions for this new instrument. The aim of this document is to present the status of the ion-optical design, magnet designs, safety studies and mechanical integration of the full S³ system in order to inform the decision on technologies to be used for the hardware components. This includes performance evaluations, construction and operating cost estimates and a project timeline. This document does not include discussion of sub-systems such as target systems, focal plane detection systems and the low energy branch except where necessary for clarification of interface issues and overall budget estimate.

Authors:

Matthew Amthor (GANIL)
Martial Authier (Irfu/SIS)
David Boutin (Irfu/SPhN)
Lise Bouvet (Irfu/SENAC)
Olivier Delferière (Irfu/SACM)
Antoine Drouart (Irfu/SPhN)
Maurice Duval (GANIL)
Shashikant Manikonda (ANL)
Jerry Nolen (ANL)
Jacques Payet (Irfu/SACM)
Hervé Savajols (GANIL)
Marc-Hervé Stodel (GANIL)
Aymeric Van Lauwe (Irfu/SENAC)

Contents

1 Introduction and project objectives

The Super Separator Spectrometer (S^3) is a device designed for experiments with the very high intensity stable beams of the superconducting linear accelerator of the SPIRAL2 facility. These heavy-ion beams (from carbon to uranium) will reach unprecedented currents, up to 1 mAe for light ions, with energies from 0.75 to 14.5 MeV/u. This will enable the production and study of radioactive nuclei with low production cross sections: superheavy elements (SHE) or neutron-deficient nuclei produced with fusion-evaporation reactions or neutron-rich nuclei produced by multi-nucleon transfers. Then delayed and prompt spectroscopy studies of secondary reactions and ground state properties can be performed to study these rare nuclei. These physics cases will be presented in the following section and more details can be found in the SPIRAL2 Letter of Intent [1].

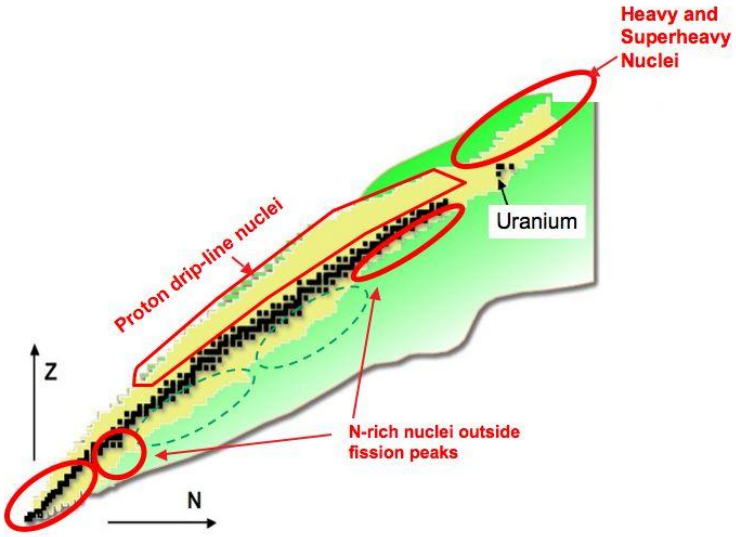

Figure 1: Main physics area covered by S^3

All of the experiments mentioned have the common feature of requiring the separation of very rare events from intense backgrounds. To use these high intensities, above 10^{14} particles per second, it is necessary to develop a new device able to separate the interesting nuclei (down to one per month!) from the majority of beam ions that are transmitted after the thin production target.

We will present here the new opportunities that S^3 will open in several physics domains and the latest technical developments in the design of the spectrometer itself. Details about other aspects may be found on the S^3 website.

1.1 Physics objectives

The pioneering capability of LINAG opens unique opportunities for the production of rare isotopes. Using fusion-evaporation reactions with these high-power beams on thin targets, coupled to the large acceptance recoil spectrometer S^3, will yield unparalleled intensity in the regions far from stability best fed by this reaction mechanism. Transfer or deep-inelastic reactions might also be used to produce secondary radioactive beams which could also be used at the intermediate focal plane of S^3 to initiate secondary reactions. Of particular interest are the isotopes close to the proton-drip line and the superheavy elements.

[1] http://pro.ganil-spiral2.eu/spiral2/letters-of-intent/letters-of-intent-list/texts-of-loi-for-spiral2/s3-the-super-

1.1.1 Superheavy elements

In the physics case of the SPIRAL2 white book, the field of superheavy element research was identified as one of the major subjects which can be addressed by the stable beam part of the facility, most notably the fundamental question *"Is there a limit, in terms of number of protons and neutrons, to the existence of nuclei?"*

The main goal, the synthesis of ever heavier new elements until the "island of stability" is eventually reached, will be driven by applying the most modern existing—or yet to be developed—techniques of nuclear spectroscopy, reaction mechanism studies and even chemistry of heavy and superheavy nuclei. The highly intense stable beams available at SPIRAL2, together with a highly efficient separator and/or spectrometer such as S^3, are an ideal combination for low cross section experiments.

The present status of the field is summarized in Figure 2. One of the major open questions is the connection of the decay patterns observed in ^{48}Ca induced reactions on actinide targets at the gas-filled separator of the FLNR, Dubna (brown framed region). In contrast to the decay chains leading to the heaviest nuclei in reactions with ^{208}Pb and ^{209}Bi targets, first observed at the velocity filter SHIP of GSI (green framed region) and later at the gas-filled separator GARIS of RIKEN, these are not connected to isotopes with known α decays that would settle their unambiguous identification. Instead they all end in fission assigned to unknown isotopes. First attempts to reproduce the data for ^{48}Ca + ^{238}U and ^{48}Ca+^{248}Cm have been successfully performed at GSI, and impressive progress has also been made for the Z assignment by a group of chemists from the PSI in Switzerland.

The setup proposed here has the capability to contribute significantly to the solution of this puzzle. Nuclear structure studies, in terms of in-beam and decay spectroscopy, have almost reached the heaviest known nuclei. They have provided the first information on the structure of actinides and trans-actinides. The nuclides studied by decay spectroscopy at the velocity filter SHIP at GSI, for example, are marked in blue in Figure 2. The development of single-particle levels towards high Z and A is a major ingredient in the localization of the next shell gap in Z and N. To pursue this task the trends of the first excited states have to be followed into the red circled region in Figure 2. As a start, a series of reactions has been defined as first-day projects for the combination of LINAG and S^3. As the A/Q of the heavy-ion linac will be limited in the first phase to 3, reactions with relatively light projectiles (A<50) on actinide targets are the natural choice. Reactions of various silicon, sulfur, argon and calcium isotopes will offer exciting opportunities to perform forefront experiments in the context of superheavy element synthesis, reaction mechanisms, nuclear spectroscopy and even chemistry studies.

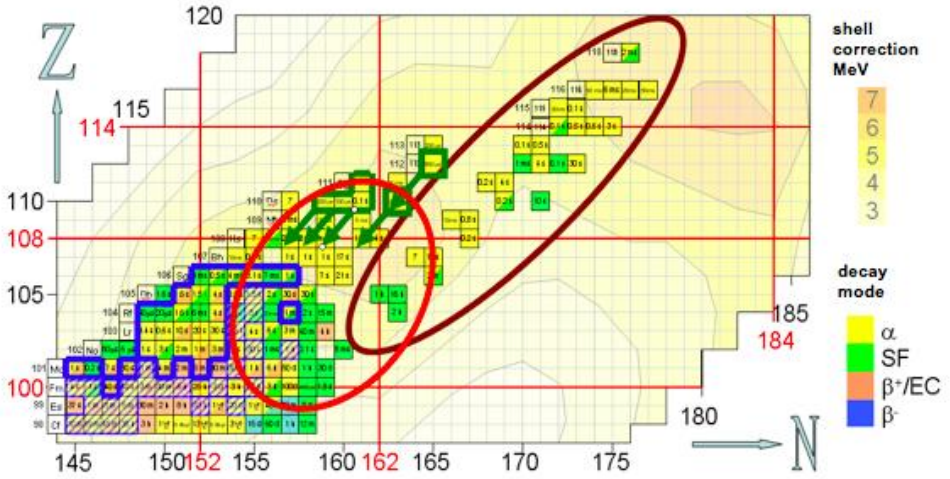

Figure 2: Excerpt of the chart of nuclides in the region of superheavy elements. Indicated regions: Green: decay chains of the heaviest elements synthesized at SHIP (Z=110-112). Brown: decay patterns observed at Dubna for 48Ca-induced reactions on actinide targets. Blue: isotopes for which nuclear structure data has been collected at SHIP (bold line: new or improved data, hatched area: reproduced or confirmed data). Red: region of interest

for near future investigations. The background color shows shell correction energies according to R. Smolanczuk et al. Phys. Rev. C 52, 1871 (1995).

Precise measurements of decay properties, as a first step, will clarify discrepancies in calculated values of the shell correction energies for heavier superheavy elements. For example, the $^{40}Ar+^{238}U$ fusion reaction will produce nuclei around the N=162 deformed sub-shell closure and alpha decay spectroscopy will give important information about this region. Using ion traps foreseen with the S^3 low energy branch, Mass spectrometry of trans-uranium nuclides will give a direct observation of the binding energy, providing critically needed experimental tests of theoretical mass models, which often vary by about 1 MeV in this region. Together, these will help refine predictions of the position of the island of stability and improve our understanding of the effects of deformation.

Requirements

This physics program requires the following experimental conditions:

- The highest intensities of beams, especially for masses around 50 (^{48}Ca is of particular importance, heavier beams are required to go to the heaviest elements)
- A wide range of targets, including actinide targets that are necessary for all hot fusion reactions
- Large angular and Bρ acceptance, due to the large emittance of the nuclei produced and their charge state distributions
- High reaction channel selectivity, to have a background rate at the focal plane as low as possible. This includes physical m/q selection to exclude high rates of adjacent masses.
- In-flight mass resolution. The mass determination of the produced superheavy element appeared as critical to validate the production of new elements. This would be a unique property of S^3.
- A detection system for alpha, electron, and gamma spectroscopy at the focal plane and a gas catcher system to transfer ions to traps.

1.1.2 Neutron-deficient nuclei

Fusion-evaporation reactions can also produce a wide range of neutron-deficient nuclei with a variety of interesting properties: proton emission, super-allowed beta decay, shape coexistence, and isomerism giving information on single particle states and correlations between nucleons. New isotopes with masses around 100 or higher could be produced. Masses of these nuclei are of interest for the study of the rp-process. Current facilities can fill in some of the gaps in mass measurements, but a facility like S^3 would have a unique ability to reach nuclei such as $^{99,100,101}Sn$, $^{98,99}In$, and $^{95,96}Cd$.

The self-conjugate, doubly-magic nucleus ^{100}Sn is one of the "holy grails" of nuclear structure far from the line of stability. The ^{100}Sn region of the nuclear chart is the stage for many phenomena (see Figure 3), which are currently the subject of intense research. The large difference in binding energy between the valence protons and neutrons might make ^{100}Sn significantly different from ^{40}Ca or ^{208}Pb, the best studied doubly-magic nuclei to date, both of which are located at the bottom of the valley of stability.

Studies of nuclei around ^{100}Sn are hampered by small cross sections and large backgrounds from less exotic reaction channels. In fact, even single-particle energies and two-body matrix elements in ^{100}Sn, which are essential ingredients for the description of multi-nucleon structures around ^{100}Sn within the shell-model framework, are poorly known. The energy splitting between the $d_{5/2}$ and $g_{7/2}$ single-neutron states in ^{101}Sn has been measured only recently. Studies of excited states and masses of nuclei with one and two nucleons outside of the ^{100}Sn core will provide the basis for understanding nuclear structure in intermediate mass nuclei.

The ^{100}Sn region is an ideal place to study the distribution of the $\pi g_{9/2} \rightarrow \nu g_{7/2}$ Gamow-Teller β-decay strength. Near a major shell closure the strength should be concentrated in a single analog state, while

the fractionation of the strength provides a stringent test of the shell-model description of the nuclear wave functions, particularly the size of cross-shell excitations. The ^{100}Sn nucleus is located at the proton drip line. The proximity of the proton drip line manifests itself through the presence of spontaneous ground-state and isomer proton emission and β-delayed proton emission. Also, an island of alpha radioactivity is located just above ^{100}Sn, including predicted "super-allowed," N=Z α emitters, which could exhibit enhanced α-decay rates due to very favorable α pre-formation probability. The astrophysical rp-process is expected to terminate just above ^{100}Sn in the Sn-Sb-Te cycle for long, hydrogen burning scenarios. Ground-state properties of isotopes in this region, in particular masses from which Q values are determined, would be most useful.

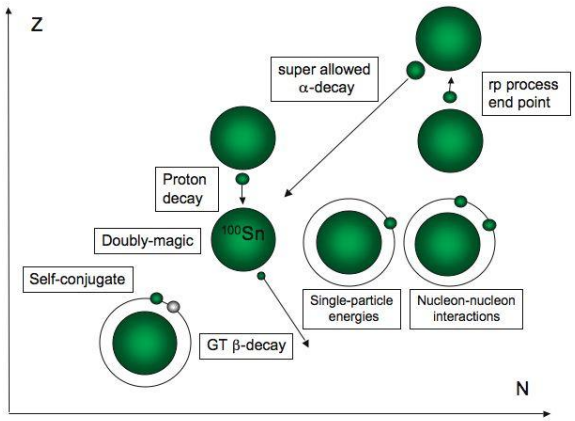

Figure 3: The ^{100}Sn region is of great interest with respect to a variety of physical phenomena, both well established unanswered questions and recently emergent topics.

Requirements

The requirements for such studies are the following:

- The highest intensities of beams, especially for masses greater than 50. The most interesting nuclei are produced with symmetric reactions, implying heavy-ion fusion (primary beams of ^{58}Ni and heavier)
- Large angular and Bρ acceptance, since few particle evaporation increases the angular distribution of the nuclei
- In-flight mass resolution of 1/300. Due to the high fusion cross section of medium mass nuclei, it is absolutely required to have at least an A/q separation of reaction products, to limit the final counting rate to less than 10^9 pps (for a gas catcher) or 10^6 pps (for secondary reactions).

1.1.3 Neutron-rich nuclei

Very high primary beam intensities open also the possibilities of producing neutron rich exotic nuclei in large numbers, either through the transfer of few nucleons on light nuclei, or with massive transfer for heavier ones. The physics topics addressed here have been largely presented and discussed in the SPIRAL2 project. Among the open questions of special interest are the evolution of the nuclear effective interactions in the monopole and multipole terms, the quenching of the known shell gaps and development of new ones, the evolution of nuclear collectivity (onset of deformation in light neutron-rich nuclei, shape coexistence, etc.) and the onset of exotic shapes.

Undoubtedly, the neutron rich beam intensities produced by SPIRAL2 through U fission will be much higher in all the regions covered by the fission peaks, but it could be possible with S³ to produce nuclei outside these zones, either lighter or heavier. For examples multiple nucleon transfer in a ^{136}Xe+^{208}Pb reaction can produce neutron rich nuclei on the ^{208}Pb region and with ^{48}Ca+^{208}Pb reaction,

neutron rich nuclei can be significantly produced in the N=28 region. On the light side, reaction like $^{12}C(^{13}C,2p)^{11}Be$ can give high yields of exotic nuclei with energies from 6-14 MeV/u, competitive for some cases with an ISOLDE type facility.

The very high intensities on S^3 targets will prevent any kind of prompt spectroscopy of these nuclei – which is the "traditional" method to study them. However, it could be possible to study them in additional reactions with a secondary target and perform a high cross section reaction like nucleon transfer or Coulomb excitation.

Requirements

Such reactions have very specific requirements, significantly different from the fusion-evaporation reactions.

- Very large angular and momentum acceptance. Reaction products have a very large angular and momentum distribution, much bigger than the fusion-evaporation reactions.
- For most reactions, the production cross sections are not necessary peaked at 0°.
- High magnetic and electric rigidity. Reaction products have rather large energies (10MeV/n or more), and Bρ of 1.5Tm and Eρ>30MV are required, the later being the most difficult to reach while still retaining good separator properties for the fusion-evaporation studies described above.
- Nuclei selection. A large number of exit channels are open and the contaminants closer to the stability are most of the time overwhelming. This requires a very high selectivity. A pure momentum selection may be sufficient for the lightest nuclei but perhaps not for heavier species. A mass selection is very challenging due to the high electric rigidity required. One possible solution is to have two interchangeable electric dipoles, one with a large gap for fusion-evaporation studies and one with a small gap for transfer and DIC studies.

As described previously, the Super Separator Spectrometer S^3 will produce proton-rich radioactive beams and heavy elements by means of fusion-evaporation reactions and modestly neutron-rich nuclei outside the fission peaks by deep-inelastic collisions. In particular, the low-energy branch of S^3 will allow the production of beams of refractory elements as well as very short-lived isotopes at ISOL energies. Basically all ISOL-type experiments could be performed with these isotopes. It is therefore foreseen to link the S^3 cave to the DESIR hall so that low-energy beams from S^3 can be fed into the DESIR facility.

2 Scientific and technical considerations

In order to define the required characteristics and performances of the separator, the collaboration has defined two key experimental cases and simulated their kinematical characteristics. The goal is to determine the performances (mainly transmission and mass resolution) that should be reached in an optimized system. We computed:

- The production rates of the nuclei. The primary beam is the major contaminant following the production target. Nevertheless, fusion-evaporation reactions have different channels that can contaminate the interesting nuclei with others of similar A and Z.
- The coupled angular and momentum distributions of the reaction products, including straggling in the target and in-flight nucleon evaporation.
- The charge state distribution of the reaction products.

In addition to the two key experiments we also considered a very asymmetric fusion-evaporation reaction to test the system performances for cases with very large angular divergences (Section 2.2.3). We also take into account the requirements of the other reactions requested in the LoI's, such as two-step reactions induced by secondary beams and the atomic physics cross section measurements.

2.1 Simulation method

S3Fusion is a Monte Carlo program developed in a C++ and ROOT framework to simulate the fusion-evaporation process at random depths within the target and to deduce the energy spread and angular straggling induced by multi-scattering processes.

We start with LINAC beam properties, considering an energy spread of 0.2% and an angular spread of about 1mrad. Then for each beam particle a random depth is generated at which the fusion-evaporation reaction will occur, so that the beam energy at that position and the associated excitation and recoil energy of the reaction product can then be computed. The excitation energy gives a temperature used to evaporate randomly—assuming a Maxwellian energy spectrum—a chosen number of neutrons. This evaporation induces a consequent energy and angular straggling.

At each interaction point, the angular straggling that is induced by the target is added randomly from a Gaussian distribution—for the beam in the full target and for the recoil in the remaining part of the target. The angular straggling is calculated from the Meyer model [2]. This model has been computed to find the mean full width at half-maximum of the angular distribution arising from multiple scattering at a specific incident energy and target reduced thickness. It is used and validated by the simulation of experiments at Dubna.

For each particle trajectory through a different material thickness, we are able to build an energy profile using the stopping power and range library computed by Jan-Olov Liljenzin and bring C language by Ricardo Yanez, based on Northcliffe-Schilling [3] and Hubert-Bimbot-Gauvin [4] correlations, valid respectively at the low (E/A < 10 MeV) and intermediate (10 < E/A < 150 MeV) energy regimes.

Step by step, the angular straggling induced by the different layers (including the carbon stripper) is added to each particle. This approach has the advantage that it gives the individual influence of each component, allowing them to be compared, for example the evaporation part of the straggling or the non-negligible influence of the stripper thickness at low recoil energy.

The following assumptions and references have been considered in these calculations:

[2] L. Meyer, Phys. Stat. Sol. B 44 (1971) 253
[3] C. Northcliffe, R.F. Schilling, Nucl. Data Tables A7, 233 (1970)
[4] F. Hubert, R. Rimbot and H. Gauvin, Atomic Data and Nuclear Data Tables 46, pp. 1-213 (1990)

- Mass excesses: P. Moller, J.R. Nix, and W.J. Swiatecki, Atomic Data Nucl. Data Tables **59**, 185(1995) ; Masses from the Finite-Range Droplet Model http://ie.lbl.gov/txt/m20.txt
- Charge state distribution: calculated after Eric Baron 1991 (GANIL), not valid for such high Z. Charge states are given after a carbon foil for equilibration.
- The beam spot is considered to be "LINAC like" with a given initial energy and angular spread.
- In the following, tables will be used to conveniently display the important parameters. The following symbols have been used:

E	average kinetic energy after target
<Bρ>	average magnetic rigidity
<Eρ>	average electric rigidity
<Q>	average charge state
<V>	average velocity
Δθ	angular spread (assuming a Gaussian shape)
dQ	charge state spread
dp/p	momentum spread

2.2 Benchmark reactions

2.2.1 Direct kinematics reaction: ^{48}Ca+ ^{248}Cm → ^{292}116 + 4n

The aim of this reference reaction is the synthesis of the superheavy nuclides with Z=116, of which only 10 nuclei have been produced to date. With S^3, several tens of atoms per week could be produced. This will allow for a deeper understanding of the properties of this element (α decay scheme, life time, etc.) as well as an insight into the production mechanism of superheavy elements (SHEs) through a possible measurement of the excitation function. The kinematics of this reaction are characteristic of many of the experiments that aim to produce superheavy elements, including those that attempt to synthesize new superheavy elements. The large emittance is partly due to the 4 neutron evaporation, but angular straggling in the target also contributes significantly. Experimental conditions are from [5].

For this reaction, the requirements are the following:

- **Total transmission: 50%**. Transmitting 50% of the full charge state (and angle and energy) distribution produced in the target will allow S^3 to compete—in terms of efficiency—with gas filled separators.
- **Beam rejection: 10^{13}**. The counting rate on the implantation detector must be less than 10Hz.
- **Mass resolving power: > 300**. Due to the very low fusion cross sections and sharp excitation functions, the counting rate of the evaporation residues is very low and limited to only a few neutron evaporations. Ideally, a mass resolution of 1/300 would allow some discrimination of these channels and some physical separation to permit chemistry studies.
- **Final focal plane size: < 10×20 cm²**. This is the largest reasonable size of the implantation detector that would preserve adequate gamma detection efficiency.

Reaction ^{48}Ca + ^{248}Cm → ^{292}116 + 4n	Target: 1 µm of Ti + 0.3 mg/cm² of ^{248}Cm.
Central E_{inc} = 4.97 MeV/u 4.92 MeV/u after the target	Angular straggling:

[5] Yu. Oganessian & al., PRC 63 (2000) 011301.

Central E* = 32.13 MeV Central E_{ER} = 0.1301 MeV/u after evaporation 0.1187 MeV/u after the stripper Energy spread at the entrance of the separator : σE/E= 3.14 % ➔ σp/p = 1.57 %	σ_θ (n evaporation) = 12.56 mrad σ_θ (target) = 10.45 mrad σ_θ (total) = 20.89 mrad

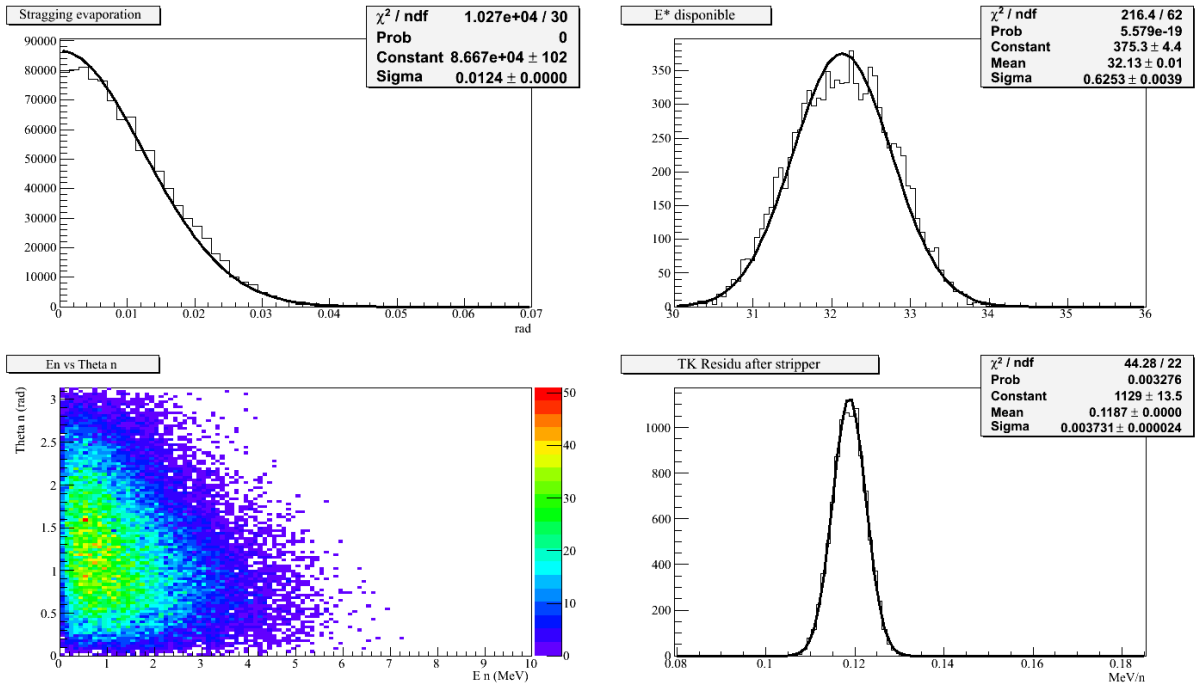

Figure 4: Upper left: angular distribution (dσ/dΩ [arb. units] vs θ [rad]) purely from evaporation
Upper right: excitation energy distribution [MeV] of compound nuclei due the random reaction depth
Lower left: angle [rad] vs energy [MeV] of emitted neutrons
Lower right: kinetic energy distribution [MeV] of evaporation residue after the stripper.

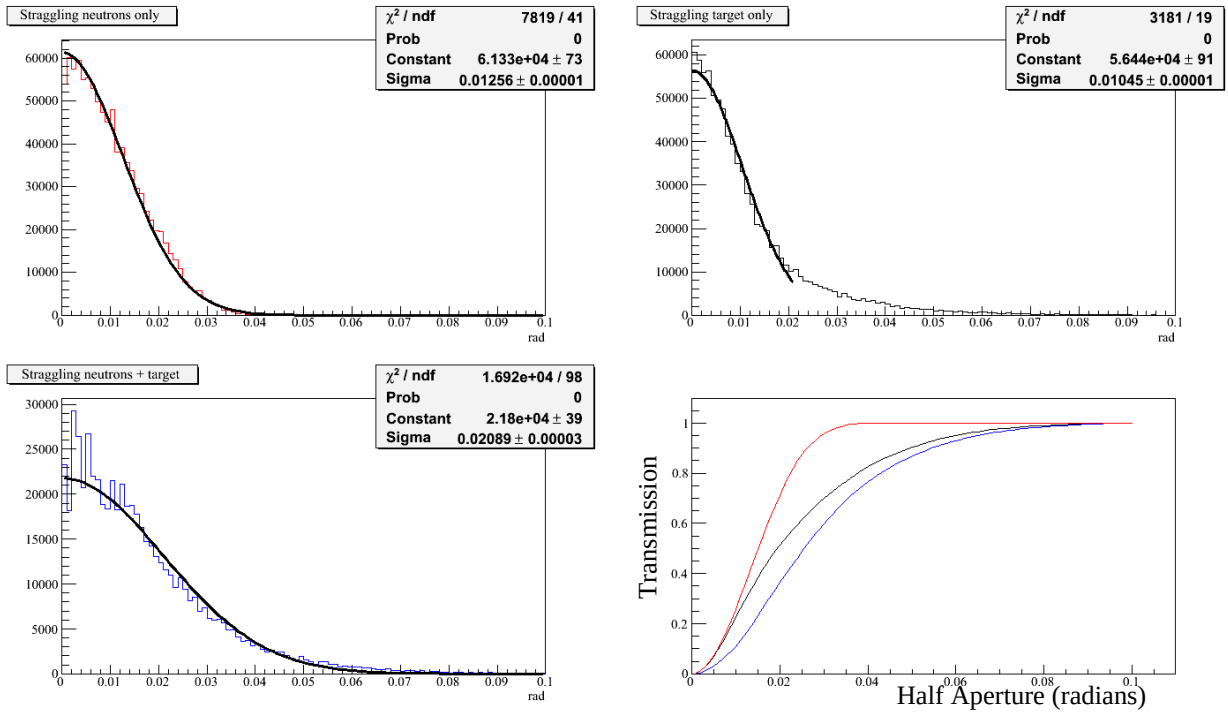

Figure 5: Angular spread due to neutron evaporation (upper left), interaction with target atoms (upper right), and total (lower left), with the Gaussian fit parameters in each case. Finally, the predicted transmission vs. geometrical half aperture, in radians, is shown at lower right.

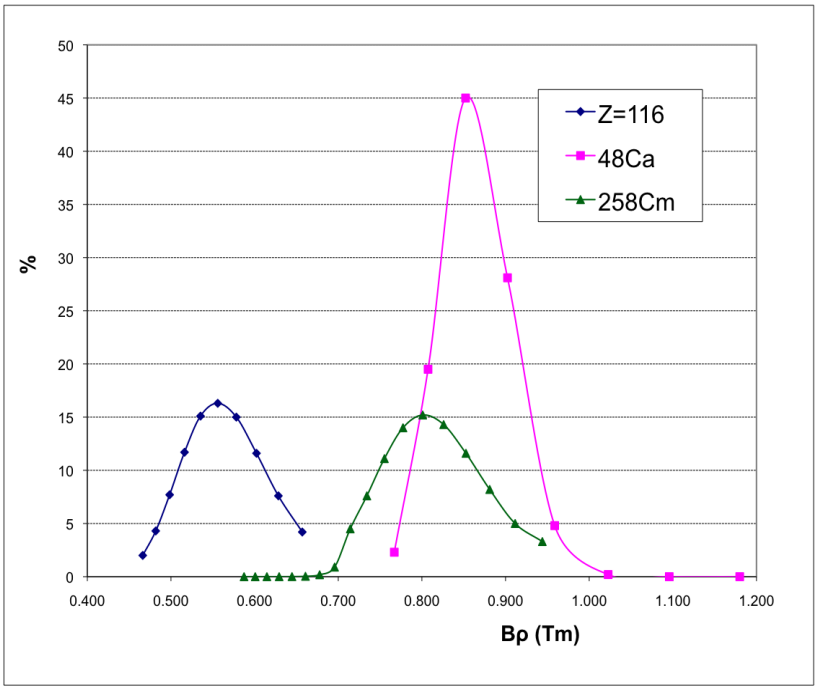

Figure 6: Magnetic rigidity of charge state distributions for evaporation residues (Z=116), primary beam particles (^{48}Ca) and backscattered target atoms (^{248}Cm) for $^{48}Ca + ^{248}Cm \rightarrow ^{292}116 + 4n$.

From these analyses, we can calculate the kinematics data for the transmitted primary beam and the evaporation residue:

	E [MeV/n]	<Bρ> [Tm]	<Eρ> [MV]	<Q>	<V > [cm/ns]	Δθ (±2σ) [mrad]	dp/p (±σ) [%]	dQ
Beam parameters ^{48}Ca	4.92	0.88	27	+17	3.0	± 2.3	±0.2*	± 2
Recoil parameters $^{292}116$	0.119	0.286	3.96	+26	0.5	± 41.8	±1.57	± 2

Table 1: Kinematics data for $^{48}Ca + ^{248}Cm \rightarrow ^{292}116 + 4n$.

Main issues:

- *Evaporation residues are kinematically clearly separated from the beam. The rejection is therefore easier, but since this is the case where rejection efficiency must reach a very high value of 10^{13}, even very improbable charge states or extreme tails of the beam distribution have to be carefully considered.*
- *Large angular and charge state acceptances are required; these will put strong constraints on the size of the magnetic elements.*

2.2.2 Symmetric systems: $^{58}Ni + ^{46}Ti \rightarrow ^{100}Sn + 4n$

We have performed similar calculations for the fusion of a ^{58}Ni beam on a ^{46}Ti target.

Reaction: $^{58}Ni + ^{46}Ti \rightarrow ^{100}Sn + 4n$	Target: 0.5 mg/cm^2 of ^{46}Ti
Central E_{beam} = 3.71 MeV/u 3.48 MeV/u after the stripper Central E^*_{CN} = 59.34 MeV Central E_{ER} = 1.12 MeV/u after evaporation 0.991 MeV/u after the stripper Energy spread at the entrance of the separator: σE/E= 5.3 % ➔ σp/p = 2.65 %	Angular straggling: σ_θ (n evaporation) = 17.01 mrad σ_θ (target) = 4.82 mrad σ_θ (total) = 18.01 mrad

One major difference as compared to the previous case is the much larger fusion cross section of the system. Hence, the counting rates will be much higher and will include a large number of nuclei around ^{100}Sn produced at much higher rates than ^{100}Sn itself (see Table 2).

With a beam intensity of I(^{58}Ni) = 6 × 10^{13} pps (A/q = 3), we can estimate:

- Total fusion cross section ~0.6 barn ➔ 2.5 × 10^{8}pps
- Fusion cross section for evaporation residues with A = 140 mbarn ➔ 5.7 × 10^{7} pps
- **Production cross section for ^{100}Sn: 5 nb ➔ 2 pps**

In this case, the requirements are:

- **Total transmission: 50%**
- Beam rejection: 10^{7}. The limiting factor then will be the isobaric contamination.
- Mass resolving power: > 200. Necessary to eliminate nearly all residues with A ≠ 100.
- Isobaric identification. Must distinguish ^{100}Sn from the other nuclei with the same mass.
- Final focal plane size: 10 × 20 cm

Z	N	A		events	percent	σ (mb)	rate (pps)
49	52	101	In	6	0.60%	3.72	1.52E+06
48	53	101	Cd	3	0.30%	1.86	7.61E+05
47	54	101	Ag	2	0.20%	1.24	5.07E+05
49	51	100	In	6	0.60%	3.72	1.52E+06
48	52	100	Cd	100	10%	62	2.54E+07
47	53	100	Ag	105	10.50%	65.1	2.66E+07
46	54	100	Pd	18	1.80%	11.2	4.58E+06
48	51	99	Cd	4	0.40%	2.48	1.01E+06
47	52	99	Ag	67	6.70%	41.5	1.70E+07
46	53	99	Pd	26	2.60%	16.1	6.58E+06
45	54	99	Rh	1	0.10%	0.62	2.54E+05
48	50	98	Cd	1	0.10%	0.62	2.54E+05
47	51	98	Ag	13	1.30%	8.05	3.29E+06
46	52	98	Pd	15	1.50%	9.29	3.80E+06
47	50	97	Ag	37	3.70%	22.9	9.37E+06
46	51	97	Pd	224	22.40%	139	5.68E+07
45	52	97	Rh	122	12.20%	75.6	3.09E+07
46	50	96	Pd	19	1.90%	11.8	4.83E+06
45	51	96	Rh	49	4.90%	30.4	1.24E+07
44	52	96	Ru	7	0.70%	4.34	1.77E+06
46	49	95	Pd	1	0.10%	0.62	2.54E+05
45	50	95	Rh	12	1.20%	7.44	3.04E+06
45	49	94	Rh	7	0.70%	4.34	1.77E+06
44	50	94	Ru	130	13%	80.5	3.29E+07
44	49	93	Ru	2	0.20%	1.24	5.07E+05
43	50	93	Tc	23	2.30%	14.3	5.85E+06
total				1000	100%	620	2.54E+08

Table 2: Production cross-sections taken from PACE V for the ^{58}Ni + ^{46}Ti fusion reaction.

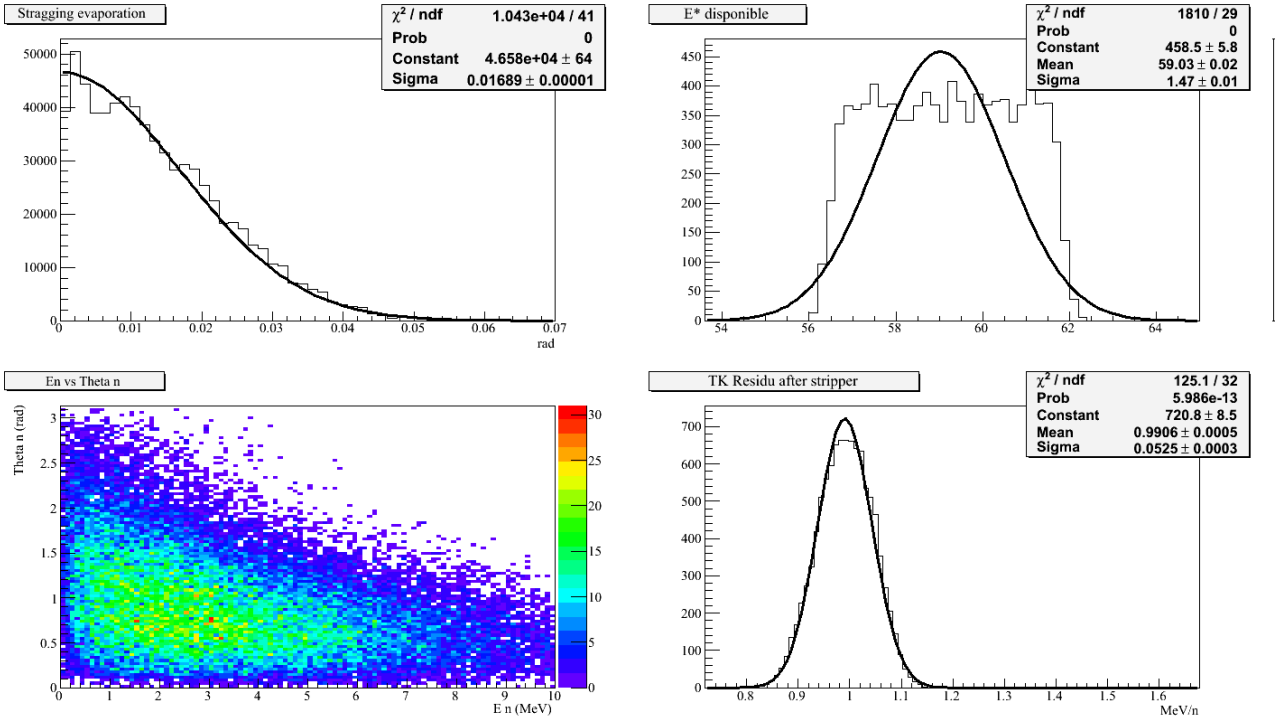

Figure 7: Upper left: angular distribution ($d\sigma/d\Omega$ [arb. units] vs θ [rad]) purely from evaporation
Upper right: excitation energy distribution [MeV] of compound nuclei due the random reaction depth
Lower left: angle [rad] vs energy [MeV] of emitted neutrons
Lower right: kinetic energy distribution [MeV] of evaporation residue after the stripper.

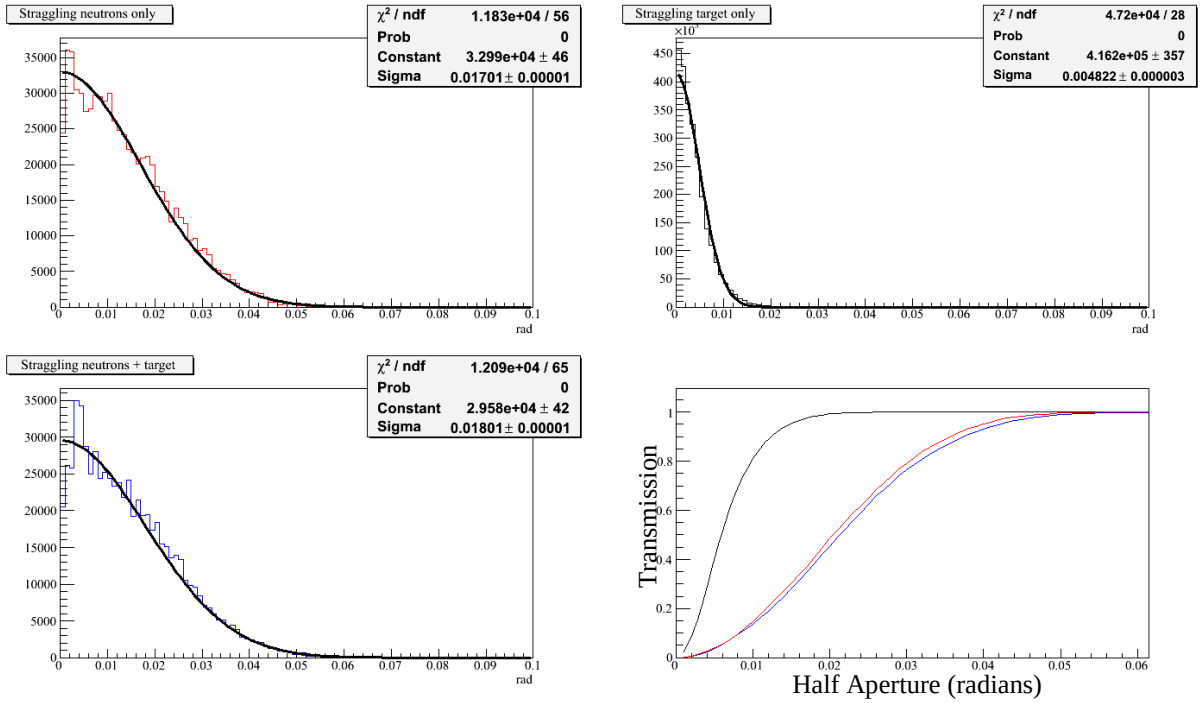

Figure 8: Angular spread due to neutron evaporation (upper left), interaction with target atoms (upper right), and total (lower left), with the Gaussian fit parameters in each case. Finally, the predicted transmission vs. geometrical half aperture, in radians, is shown at lower right.

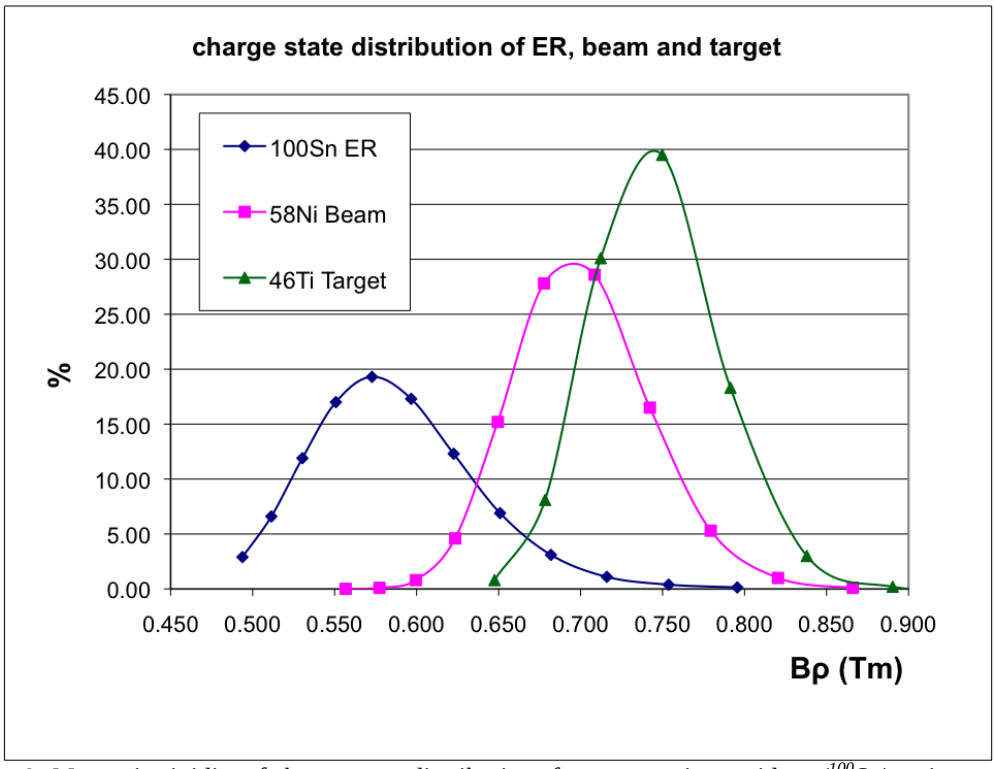

Figure 9: Magnetic rigidity of charge state distributions for evaporation residues (^{100}Sn), primary beam particles (^{58}Ni) and backscattered target atoms (^{46}Ti) for the reaction ^{58}Ni + ^{46}Ti → ^{100}Sn + 4n.

The kinematics parameters are the following:

	E [MeV/n]	<Bρ> [Tm]	<Eρ> [MV]	<Q>	<V > [cm/ns]	Δθ (±2σ) [mrad]	dp/p (±σ) [%]	dQ
Beam parameters ^{58}Ni	3.48	0.556	14.39	22+	2.58	± 5	±0.2*	
Recoil parameters ^{100}Sn	0.991	0.286	3.96	24+	1.38	± 36	±2.65	±2

Table 3: Kinematics data for ^{58}Ni + ^{46}Ti → ^{100}Sn + 4n.

Main issues:

- *Separation of beam and evaporation residue is much less than with more asymmetric fusion. There is an overlap in the magnetic rigidity distributions but the velocity difference is still large. Primary beam counting rates that are 1% of isobaric counting rates are acceptable (i.e. 10^6 pps).*
- *Angle and charge state distributions are large.*
- *Mass resolution is critical in this case to eliminate the very high counting rate of other evaporation residues.*
- *Isobaric selection must be reached. Due to the low energies, it is impossible to do it in-flight with a degrader. A gas catcher with laser ionization selection or a very high resolution mass separator (for reaccelerated beams) could provide the additional selection necessary at the end of S³. This will be the perfect device to study nuclei in the region of ^{100}Sn with a high-resolution ion trap, for mass charge radius or spectroscopy measurements.*

2.2.3 ^{22}Ne + ^{238}U → ^{255}No + 5n

Reaction ^{22}Ne + ^{238}U → ^{255}No + 5n	Target: 0.17 mg/cm^2 of ^{238}U + 0.2 µm of ^{12}C

Central E_{beam} = 5.45 MeV/u 5.43 MeV/u after the stripper Central E^*_{CN} = 54.1 MeV Central E_{ER} = 0.039 MeV/u after evaporation 0.032 MeV/n after the stripper Energy spread at the entrance of the separator : σE/E = 10.37 % ➔ σp/p = 5.18 %	Angular straggling: σ_θ (n evaporation) = 41.63 mrad σ_θ (target) = 34.28 mrad σ_θ (total) = 55.11 mrad

Neutron emission

Five neutrons are emitted by the excited compound nucleus.

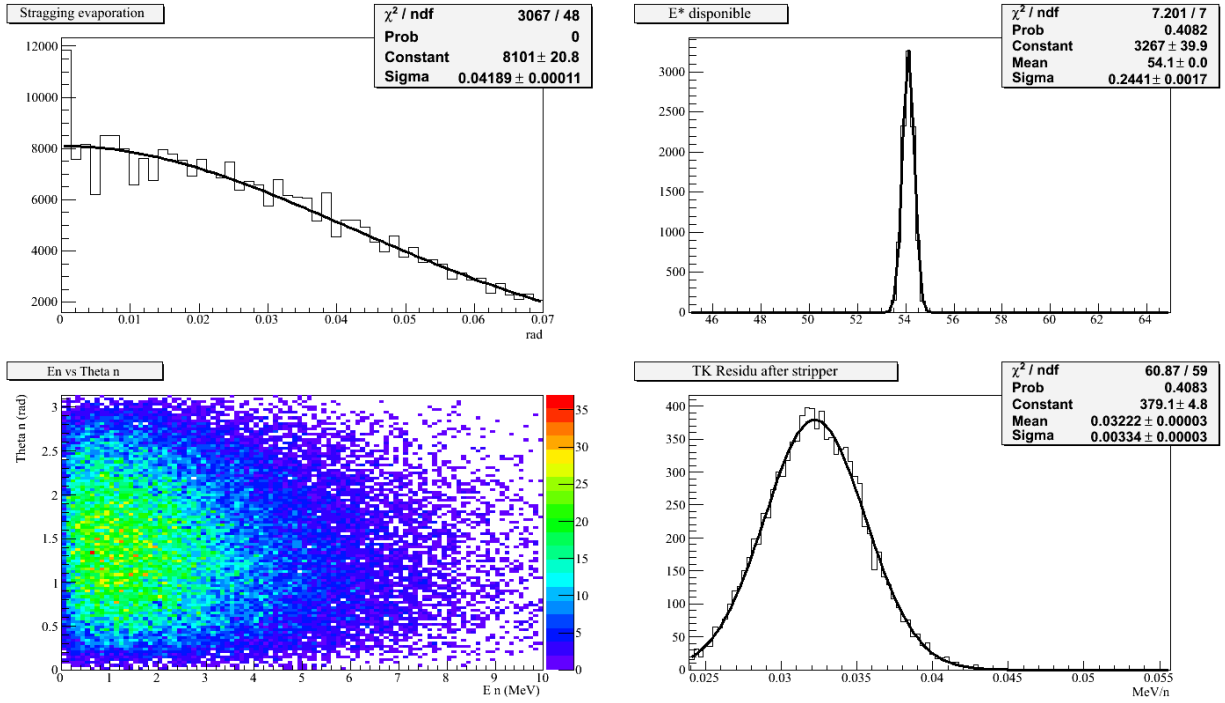

Figure 10: Upper left: angular distribution ($d\sigma/d\Omega$ [arb. units] vs θ [rad]) purely from evaporation
Upper right: excitation energy distribution [MeV] of compound nuclei due the random reaction depth
Lower left: angle [rad] vs energy [MeV] of emitted neutrons
Lower right: kinetic energy distribution [MeV] of evaporation residue after the stripper.

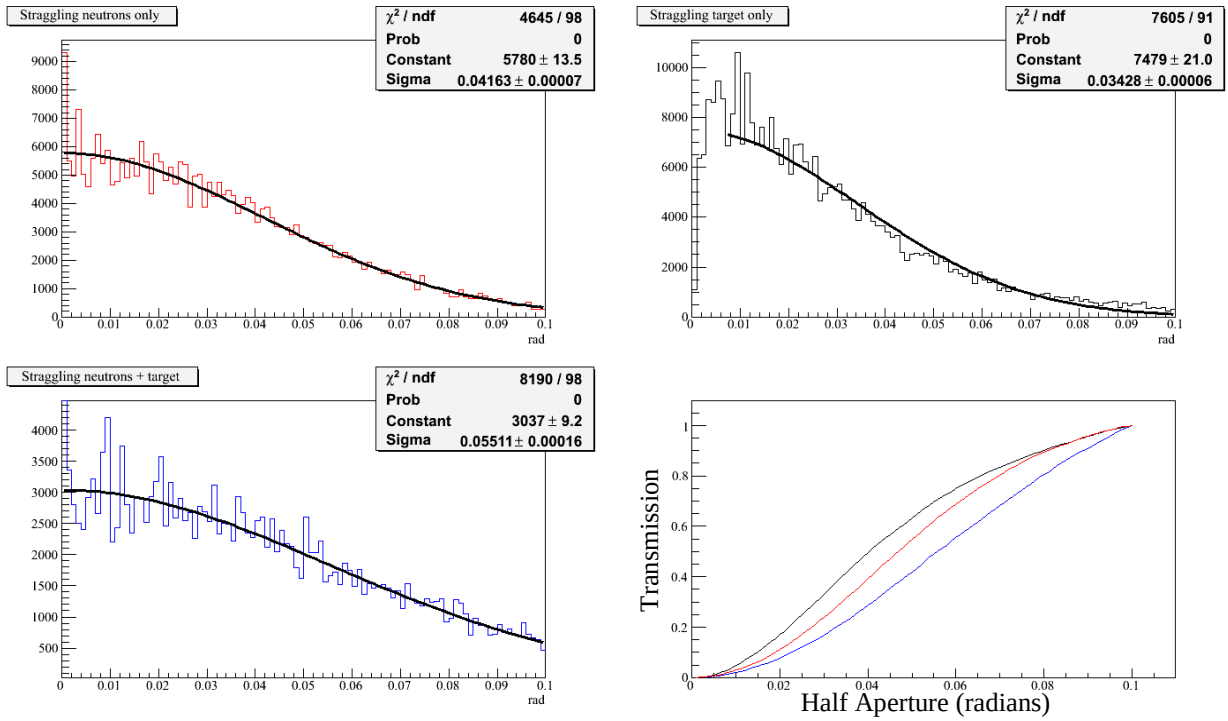

Figure 11: Angular spread due to neutron evaporation (upper left), interaction with target atoms (upper right), and total (lower left), with the Gaussian fit parameters in each case. Finally, the predicted transmission vs. geometrical half aperture, in radians, is shown at lower right.

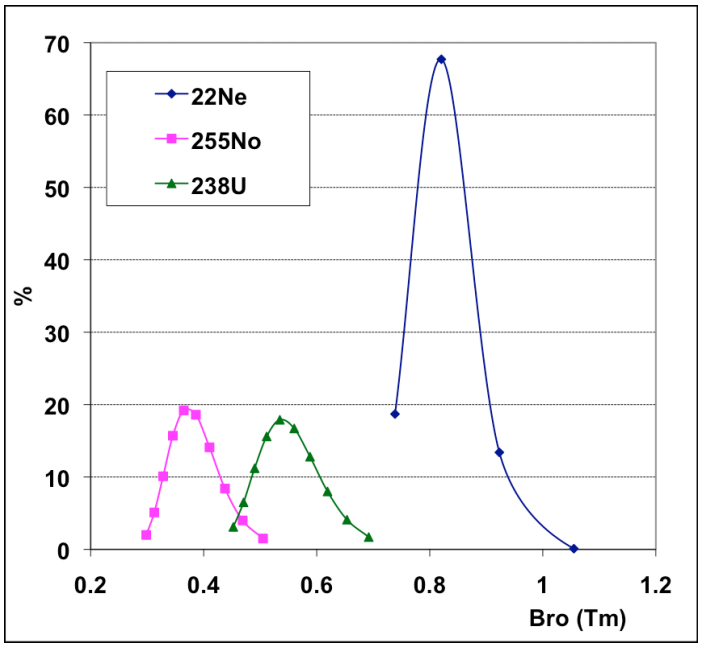

Figure 12: Magnetic rigidity of charge state distributions for evaporation residues (^{255}No), primary beam particles (^{22}Ne) and backscattered target atoms (^{238}U) entering the spectrometer.

	E [MeV/n]	<Bρ> [Tm]	<Eρ> [MV]	<Q>	<V > [cm/ns]	Δθ (±2σ) [mrad]	dp/p (±σ) [%]	dQ
Beam parameters ^{22}Ne	5.433	0.739	23.86	10+	3.22	± 1.44	± 1.8	
Recoil parameters ^{255}No	0.032	0.064	0.16	18+	0.24	± 110	± 5.18	±2

Table 4: Kinematics data for $^{22}Ne + {}^{238}U \rightarrow {}^{255}No + 5n$.

Performances

This experiment is not a "reference" experiment in the sense that its parameters are not used to directly constrain the characteristics of the spectrometer; the very large angular and momentum distribution of the products make it impossible to efficiently transmit them and significantly degrade the mass resolution. Nevertheless, it gives a good insight on the performances of the spectrometer for such extreme emittance cases of whose study S^3 may still be well capable.

2.3 Spectrometer requirements

After consideration of many alternatives, a very flexible layout has been devised for a new vacuum separator with large acceptance in a combination of angular range and both momentum and charge state range—while also providing a powerful primary beam suppression and physical separation of isotopes by m/q at the final focal plane. A vacuum separator has been selected because gas-filled devices do not provide sufficient physical separation of isotopes by m/q. There are also practical constraints that will limit design choices. For example, the object point at the target for the optics has to be 1-cm tall to accommodate high power beams on a rotating target wheel. The spot will remain narrow in the horizontal direction (~1 mm) to preserve momentum and mass resolution in the dispersive plane. The tall beam spot together with the large angular and momentum acceptance present serious challenges, with optical aberrations resulting in the need for at least third order corrective elements. There is also a need to maintain relatively large open spaces following the target, at the intermediate achromatic focal plane, and at the final focal plane to accommodate auxiliary detectors and meet other mechanical requirements. This is essential also to maintain flexibility for presently unforeseen physics studies. It is a challenge to keep good acceptance with the larger drift spaces required to maintain this flexibility. With these various constraints in mind, the specifications of the spectrometer are optimized based on detailed simulations for the two fusion-evaporation reactions detailed above, for studies of superheavy elements and isotopes near ^{100}Sn.

In summary, the design of the spectrometer should satisfy the following characteristics:

- **Excellent primary beam suppression (10^{13} in most cases) at 0°**
- **Total transmission better than 50% for the two selected experiments**

  As a guideline this corresponds roughly to:

  - *charge state acceptance of ± 10%, typically 5 charge states with <Q> ≥ +20*
  - *momentum acceptance for each charge state of ± 10%*
  - *large angular acceptance in both planes of +/- 50 mrad*
- **Maximum magnetic rigidity $B\rho_{max}$ = 1.8 Tm** *(momentum achromat)*
- **Maximum electric rigidity $E\rho_{max}$ = 12 MV** *(±300 kV for a 20 cm gap electric dipole with ρ = 4 m)*
- **Mass resolving power of at least 300 (FWHM) for physical separation in m/q**
- **Beam spot on the production target of S^3 of either:**

- σ_x = 0.5 mm (Gaussian) × σ_y = 2.5 mm (Gaussian) *or*
- σ_x = 0.5 mm (Gaussian) × Δy = 10 mm (uniform)

  (where 'x' denotes the horizontal direction and 'y' the vertical direction)

- **Final focal plane size depending on the experiment**
  - *200 x 100 mm (maximum for high resolution mode, e.g. SHE synthesis)*
  - *100 x 100 mm (delayed gamma spectroscopy)*
  - *50 x 50 mm (low-energy branch gas catcher, GS properties)*

The vast array of different physics studies that could be possible with S^3 implies that it should be compatible with various detection settings (an implantation/decay detector, a gas catcher followed by an ion trap for laser spectroscopy and high resolution mass measurements, a transfer/Coulex measurement set-up). Special modes are considered to accommodate some physics cases. For example, some light ion reactions and atomic physics studies use beams with very high electric rigidity which are not compatible with the electric dipole to be used. In these cases the electric dipole can be replaced by a magnetic dipole and the optical tune adjusted accordingly. Similarly, for some inverse kinematics cases an alternate version of the electric dipole with a smaller gap and higher electric field could be used to achieve a higher electric rigidity, possibly up to 24 MV. In such cases the angular acceptance requirement would be relaxed so that the smaller gap would remain compatible with reasonable overall acceptance.

2.4 Previous separators for high intensity beams

Separators dedicated to high intensity beams are most commonly used for the study of superheavy or heavy elements. Classical separators combine magnetic and electrostatic deflection (e.g. SHIP at GSI) or use gas-filled magnetic dipoles (e.g. RITU at Jyväskylä University and the DUBNA gas-filled separator). New separators are currently at various stages of development, like TASCA (GSI) or the superconducting gas-filled separator at Berkeley. It is possible to combine several complementary stages of separation. The VASSILISSA separator (at Dubna) is a succession of a triplet of electrostatic dipoles followed by a final magnetic dipole which enhances the rejection by a factor of 100, and the RMS at HRIBF/ORNL is a momentum achromat followed by a mass separator.

Nevertheless, no device has a rejection factor much above 10^{12}; that is for 10^{12} unwanted ions after the target, only one reaches the detection plane (*). **S^3 must have a rejection power better than 10^{13}, an order of magnitude better than what is presently achieved.**

(*)This has to be considered for the energy and mass region we are interested in. Rejection can be better for light (A<20) ions at lower energies (E<1A.MeV), like the ERNA separator in Bochum.

Two Existing Separators

We studied vacuum separators presently in operation at different laboratories, and also looked at different on-going projects. The two examples below have been strong inspirations for the preliminary design of S^3.

SHIP Separator (GSI)

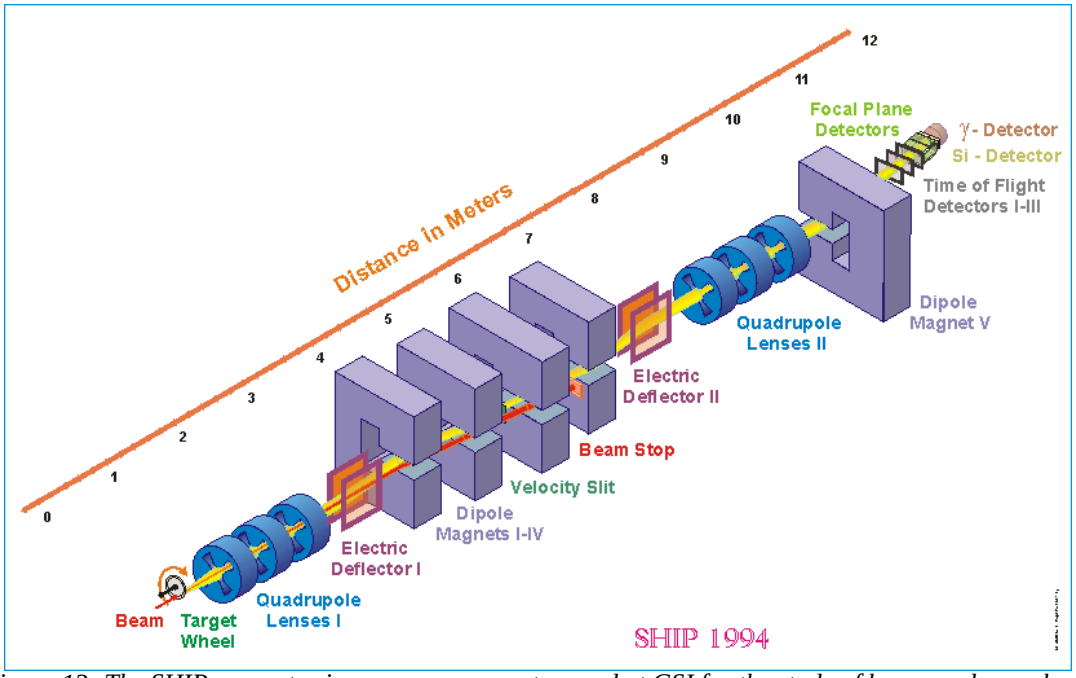

Figure 13: The SHIP separator is a vacuum separator used at GSI for the study of heavy and superheavy elements produced by fusion reactions. It has a very good rejection power of 10^{11} and an acceptance of 2.7 msr. It has a low dispersion, which gives large energy (±10%) and charge state (±10%) acceptances, and provides an m/q resolving power of ~100 for the transmitted nuclei.

References

- G. Munzenberg & al, Nucl. Inst. Meth. 161, 65-82, 1979
- G. Munzenberg *et al.*, *NIM B* **26** (1987), p. 294.
- http://www.gsi.de/forschung/kp/kp2/ship/index_e.html

The RMS (Oak Ridge)

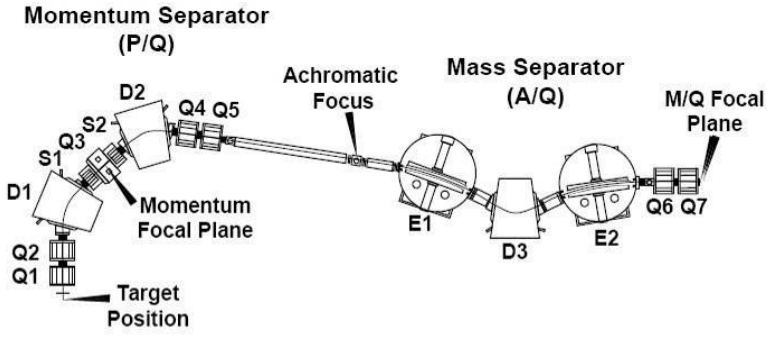

Figure 14: The RMS is a two step separator used for the production of medium-heavy nuclei using fusion-evaporation reactions. It has a very high rejection power, even for symmetric or inverse kinematics reactions. It has also a good mass resolution (1/450 at the final focal plane). Its acceptance is 13msr in angle and ±5% in m/q.

References

- J.D. Cole & al. NIMB70 (1992) pp343
- C.J. Gross & al NIMA 450 (2000) pp12

Updated references for present separators, spectrometers and associated techniques can be found in the two last EMIS (International Conference on Electromagnetic Isotope Separators and Techniques

related to their Applications) conference proceedings:

- Nuclear Instruments and Methods in Physics Research B 126 (1997)
- Nuclear Instruments and Methods in Physics Research B 204 (2003)

And also in the 2006 EcoS Report:

- http://www.nupecc.org/ecos/ECOS_Report_20060912.pdf - F. Azaiez & al.

2.5 The S^3 baseline concept

The S^3 group considered all existing or proposed separators as starting points for the present instrument. No existing devices can presently achieve all the above objectives. Due to the high intensity and the low energy of the primary beam, conventional high-energy fragment separator techniques such as intermediate absorbers cannot be used to aid the separation of the primary and recoil beams. The requirement of physical separation of isotopes via m/q dispersion at the final focal plane implies that electrostatic devices, either a Wien filter or an electric dipole must be used. Because of the high primary beam intensities available at SPIRAL2, substantial suppression of the primary beam must be accomplished before entering the region of the electrostatic element. Hence, we have chosen a next-generation separator built on the principles of the Texas A&M MARS [6] and the Oak Ridge RMS [7] separators. The basic principle is to first suppress primary beam by at least a factor of 1000 with a pre-separator (momentum achromat) and then further suppress the beam and give physical mass channel selection using a mass separator. This device would have the capability to fulfill the requirements described above and is well suited for direct and symmetric kinematics fusion-evaporation reactions.

As a result of these considerations the Momentum Achromat Mass Separator (MAMS) concept—detailed below—was chosen by the collaboration in 2008 as the S^3 basic optical design. The baseline optical solution of the MAMS concept was highly symmetric and used magnetic quadruplets before and after each dipole. This was a very robust design that enabled point-to-point and parallel to parallel optics for each stage and included sextupole and octupole correction coils in each magnet of the quadruplets. The MAMS concept—first presented at the Third S^3 Collaboration Meeting by J. Nolen and S. Manikonda [8]—is an evolution of a fragment separator study [9] that showed the benefits of telescopic imaging on highly symmetric focusing cells. However, practical considerations required revision of this initial concept, and the revised layout is described in detail below.

The Argonne, GANIL, and Saclay ion optics groups have iterated the initial basic layout in search of an optimized solution that meets all the physical and optical requirements spelled out above. Optics solutions have been constrained by the necessity of using certain magnet designs (i.e. open-sided focusing magnets after the first dipole) that are compatible with a well shielded beam dump and the desire to include increased drift spaces at the target and intermediate and final image positions, while still fitting within the final vault interior dimensions of 16 x 36 m^2 and leaving adequate space at the final focal plane region for various detectors, the isobar separator, and the gas catcher apparatus.

In the following, the details are given of the resulting S^3 baseline design composed of just such a two-stage separator. An overview of the most recent version of the layout is shown in Figure 15.

[6] R.E. Tribble, R.H. Burch, C.A. Gagliardi, Nucl. Instr. and Meth. A 285 (1989) 441.
[7] J.D. Cole, T.M. Cormier, J.H. Hamilton, and A.V. Ramayya, Nucl. Instr. and Meth. Phys. Res. B 70 (1992) 343.
[8] http://pro.ganil-spiral2.eu/spiral2/instrumentation/s3/meetings-and-workshops/third-collaboration-meeting/presentations
[9] B. Erdelyi, J. Maloney, J. A. Nolen, *Phys. Rev. ST Accel. Beams* **10**, 064002 (2007)

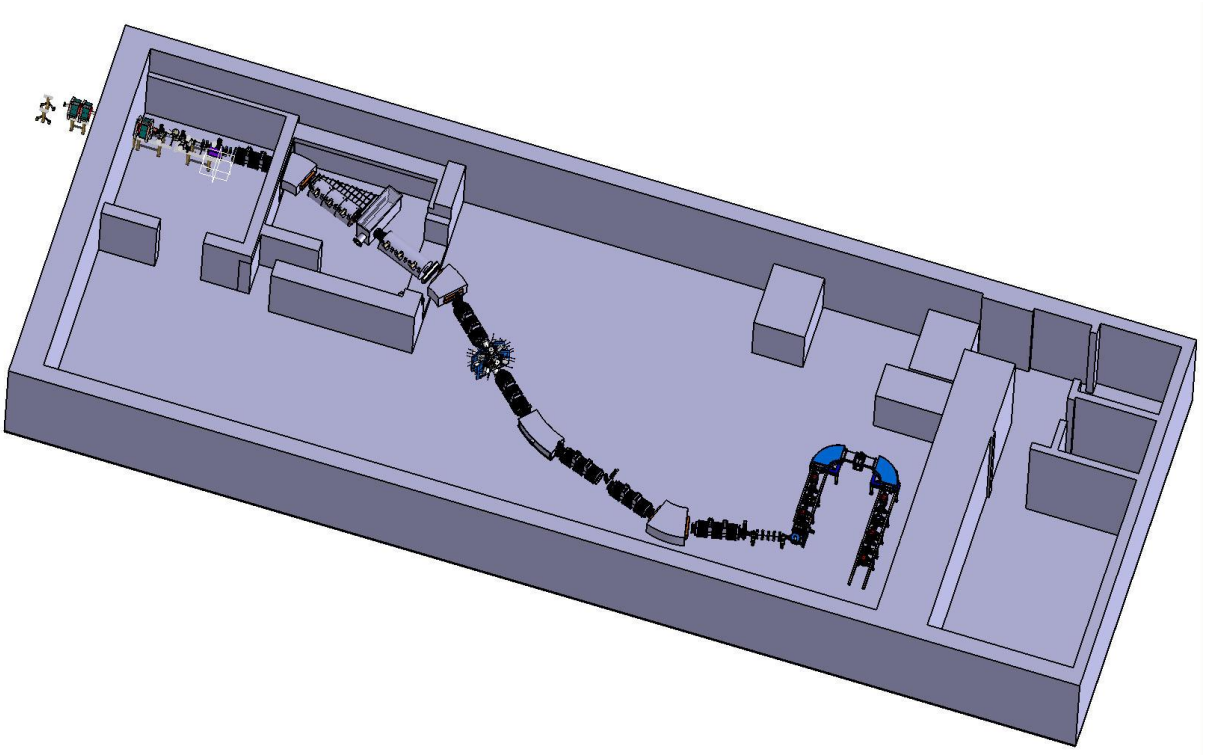

Figure 15: MAMS layout in the S³ experimental vault

Summary of the adopted concept

First stage: Pre-separator based on a momentum achromat to suppress the primary beam by at least 1:1000.

a. The momentum achromat includes two cells—each containing a magnetic dipole between two magnetic triplets—with momentum dispersion at the center (nearly unit magnification in both planes) and producing an achromatic focus at the end. Optical symmetry is used as much as possible to suppress higher-order effects. The magnetic triplets will contain sextupole and octupole correction coils as necessary to achieve the overall specifications, including aberration correction at the dispersive image and the final achromatic image of the first stage.

b. Charge states of the beam which enter the momentum acceptance are "blocked" with adjustable beam stoppers at the dispersive focal plane as required.

c. The magnetic triplet following the first dipole is "open-sided" so that the beam dump can be located outside the magnets in a well shielded area.

d. The final image is fully achromatic with unit magnification in both planes and also has zero mass and charge dispersion, reproducing the object exactly to first order. A small aperture is located at the achromatic image to suppress scattered beam and reaction products that arrive at this point but outside the dimensions of the image.

Second stage: Further beam suppression and mass channel selection by a mass separator stage which is fully achromatic in momentum for each m/q value.

a. The first half contains an electrostatic dipole that creates an energy-dispersive focal plane. Because of the initial beam suppression in the momentum achromat, the intensity of any residual beam hitting the electric dipole plates will be tolerable. The electric rigidity limit of this dipole will be large enough for direct kinematics and symmetric fusion reactions, and the gap and height of the dipole plates will be large enough to ensure high transmission.

b. The second half consists of a magnetic cell similar to those of the momentum achromat stage. The complete second stage is also fully achromatic, providing separation purely according to m/q ratio of the transmitted ions.

c. The final focal plane is dispersive in m/q and has resolving power and acceptance such that at least 5 charge states are transmitted through a set of independently adjustable slits for physical mass channel selection, giving excellent selectivity of reaction channels as well as a very high degree of beam rejection. The m/q focal plane is sized such that the five central charge states can be transmitted to a detector array or gas catcher of reasonable size. (There is no isobar filtering in any of these schemes, so isobars of the residue of interest will also pass the mass selection slits).

2.6 First day experiments

The Scientific Advisory Committee (SAC) of SPIRAL 2, in agreement with the Management of the project and Directorate of the GANIL facility, launched in 2009 a call for Letters of Intent (LoIs) for the Day 1 SPIRAL 2 Phase 1 facility (LINAC and associated experimental area with S^3 and NFS experimental halls).

The LoIs will define the physics program at the start-up of the S^3 facility in 2013 and will set the technical specifications of SPIRAL2 Phase 1.

2.6.1 S^3 Letters of Intent in numbers

A total of 13 LoIs for day-one experiments were submitted by the S^3 collaboration and were presented in open sessions of the SAC in September 2009 and June 2010. These LoIs were signed by 170 physicists and represent collectively 380 days of requested beam time.

2.6.2 List of LoIs

- **LoI_Day1_1: Fast ion-slow ion collisions (FISIC) project** (E. LAMOUR)
- **LoI_Day1_2: Production and spectroscopy of heavy and superheavy elements using S^3 and LINAG** (P. GREENLEES)
  - Neutron deficient nuclei around Z = 92, N = 126
  - K-isomerism studies in the Z = 100–110 region
  - Study of neutron rich isotopes produced by asymmetric reactions
  - Production of SHE with Z = —106 to 112 with Uranium target.
- **LoI_Day1_3: In-source resonant laser ion spectroscopy of ^{94}Ag** (I. G. DARBY)
- **LoI_Day1_4: In-source resonant laser ion spectroscopy of the light Sn isotopes A = 101–107** (I. G. DARBY)
- **LoI_Day1_5: In source resonant laser ion spectroscopy of Z >= 92** (I. G. DARBY)
- **LoI_Day1_6: Single particle states and proton-neutron interaction in the ^{100}Sn region** (L. CACERES, F. Azaiez)
- **LoI_Day1_7: In-beam gamma spectroscopy of neutron-rich nuclei studied with PARIS at the intermediate focal plane of S^3** (I. STEFAN, B. Fornal)
- **LoI_Day1_8: Shell structure, isospin symmetry and shape changes in N = Z nuclei** (G. DE ANGELIS, B. Wadsworth)
  - Coulomb excitation of ^{104}Sn: probing large scale shell model calculation
  - Coulomb excitations of the T = 1 bands of the odd-odd ^{62}Ga, ^{66}As and ^{70}Br nuclei
- **LoI_Day1_9: Quadrupole Moments of isomeric states using the tilted-foils technique at S^3** (G. GEORGIEV, M. Hass)
- **LoI_Day1_10 : Precision study of the superallowed beta decay of heavy odd-odd N = Z nuclei** (B. BLANK)

- **LoI_Day1_11 : ^{100}Sn factory – studies of the structure of nuclei in the ^{100}Sn region** (D. SEWERYNIAK)
- **LoI_Day1_18 : The evolution of Z = 40 sub-shell while approaching the proton-dripline** (B. BASTIN)
- **LoI_Day1_17 : Detailed spectroscopy of proton-rich nuclei around N = 82 through emission from isomeric states** (C. PETRACHE, Ph. Woods, D. Seweryniak)

Figure 16 below summarizes all the different regions in the nuclear chart that may be studied at the start-up of the S³ facility.

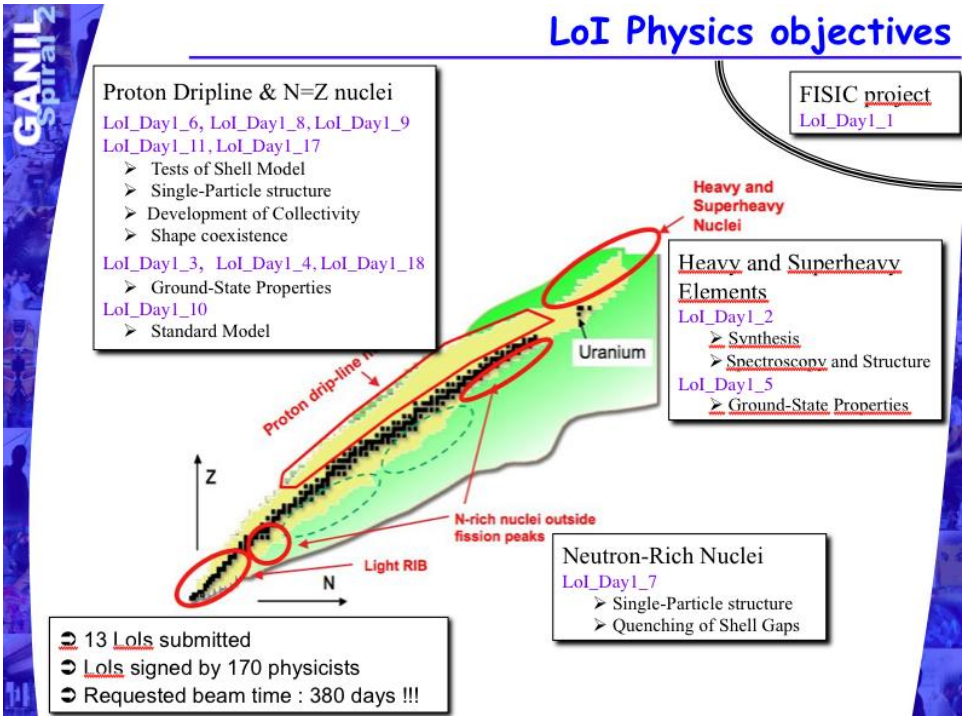

Figure 16: LoI physics objectives

2.6.3 S³ operation modes

The wide range of reactions described in the previous section (decay spectroscopy studies at the focal plane, secondary reactions at the intermediate and final focal plane and in-source spectroscopy studies in a gas cell) implies working in different modes as described in the following table.

Letter	Momentum achromat	Mass Separator	Low Energy Branch	Spectrograph
LoI_Day1_1	■			■
LoI_Day1_2	■	■		
LoI_Day1_3	■	■	■	
LoI_Day1_4	■	■	■	
LoI_Day1_5	■	■	■	
LoI_Day1_6	■	■		
LoI_Day1_7	■			■
LoI_Day1_8	■	■		
LoI_Day1_9	■			
LoI_Day1_1	■	■	■	

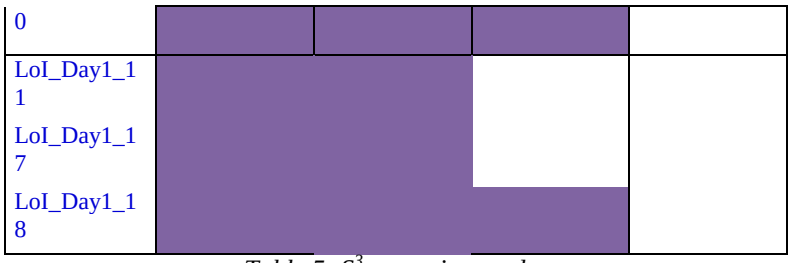

Table 5: S^3 operating modes

- The *momentum achromat* goes from the production target up to the intermediate achromatic image. The dispersive plane holds the lateral beam dump and interceptive fingers and slits. Separation is limited to momentum over charge only.
- The *mass separator* goes from the intermediate achromatic image up to the final mass dispersive plane. The products are also separated in mv^2/q at the middle energy dispersive plane. The electric dipole limits the use of the mass separator to low energy ($mv^2/q < 12MV$) ions.
- The *low energy branch*—when in use—continues beyond the mass dispersive plane and includes a gas catcher, to stop the selected products, coupled to either an RF extractor followed by a high resolution mass separator (fast extraction), or a laser ionization extractor (high selectivity). After this branch, an additional detection set-up is needed (e.g. beta-gamma decay station).
- The *spectrograph* is an alternative configuration where the electric dipole is replaced by a magnetic dipole. The first half of the mass separator is now a momentum spectrometer. The energy dispersive plane becomes a momentum dispersive plane where a detection set-up is installed. The second half is not used since the alternative magnetic dipole has a different angle than the last dipole.

2.7 LINAC beams for the Day 1 SPIRAL2 Phase 1 experiments

Based on the recommendations of SPIRAL2 SAC for the LoIs, a list of Heavy Ions beams, for the startup-up of the LINAC, has been established by the SPIRAL2 management. This list is not exhaustive, and new beams can be added depending on requests of prospective users.

Ion(s)	Energy Range (MeV/nucleon)	Maximum Intensity (pμA)	Date of availability***)	Remarks
$^{12}C^{4+}$	5-7	≥10**)	February 2013	S^3 beam line
$^{18}O^{6+}$	5-7	≥10**)	February 2013	S^3 beam line
$^{22}Ne^{8+}$	5-7	≥10**)	February 2013	S^3 beam line
$^{40}Ar^{14+}$	4-5	≥10**)	February 2013	S^3 beam line
$^{28\text{-}30}Si^{10+}$ or $^{32\text{-}36}S^{12+}$	5-7	≥10**)	November 2013	S^3 beam line
$^{40}Ca^{14+}$	5-7	≥10**)	November 2013	S^3 beam line
$^{48}Ca^{16+}$	5-7	≥10**)	November 2013	S^3 beam line
$^{58}Ni^{18+}$	4-14	≥1**)	November 2013	S^3 beam line

Table 6: List of heavy ion beams for the startup-up of the LINAC.

Remarks:

Beam time structure: acceleration (or bunch) frequency is 88 MHz, with Δt for each bunch typically 1 ns (depends on beam energy and target position).

*) The parameters indicated in this table are the first and the best approximations that can be made today. They may be different from those available in reality at the beginning of operation of SPIRAL2. User's request of different beams and specifications supported by recommendations of the Scientific Advisory Committee for the Day 1 SPIRAL2 Phase 1 experiments might be taken into account. The SPIRAL2 project will update the list of parameters periodically.

**) Based on the order of magnitude of the expected best currents extracted from a high performance, fully operational, 28 GHz ECR Ion source.

***) These dates assume that: installation of equipment in the NFS and S^3 areas can start in July 2011, commissioning of the LINAC can begin in the first quarter of 2012 and commissioning of the instrumentation in the S^3 and/or NFS halls with the LINAC beam(s) would begin in September 2012.

2.8 Operating scenarios

As an envelope, hypothetical case we may suppose that 31 weeks of beam will be available at S^3. Then we can divide that "typical" year among the different physics programs, each with their specific beam. These programs are based on the letters of intent proposed by the collaboration. This is naturally not fully realistic, since most of these programs would be pursued in continuous campaigns of at least one year, but, in the long term, this is a reasonable picture of the different beams and operating conditions of the spectrometer.

Scientific program	Beam time (Weeks)	Ions	Mass A	Intensity (pμA)	Energy (MeV/u)	Bρ (T.m)	Eρ (MJ/C)	Total ng of Ions 1E26	Beam dump(4) zone	Power (kW)
VHE/SHE	4	12C	12	30.00	7	0.4	1.16	4.53	HMR	2.52
VHE/SHE	4	22Ne	22	30.00	5	0.37	0.94	4.53	HMR	3.3
VHE/SHE	6	48Ca	48	20.00	5	0.8	5.1	4.53	HMR	4.8
N=Z	5	58Ni	58	10.00	5	0.6	8.6	1.89	HMR	2.9
N=Z	4	58Ni	58	10.00	10	1.0/0.65(1)	8.6	1.51	HMR+AZ	5.8
Neutron-rich	4	48Ca	48	10.00	10	1.4/1.4(2)	NR	1.51	HMR+AZ	4.8
FISIC	2	20Ne	20	25.00	14	1.2/NR(3)	NR	1.89	SAZ	7
FISIC	2	36Ar	36	20.00	14	1.4/NR(3)	NR	1.51	SAZ	10.08

Table 7: S^3 operating scenario

(1) Different magnetic rigidities for the two parts of the spectrometer

(2) Magnetic dipole in place of the electric dipole

(3) Specific layout for atomic physics

(4) Beam dump zones:

a. HMR: High magnetic rigidity

b. AZ: Acceptance zone

c. SAZ: shutters of the acceptance zone

This operating scenario is used for the estimation of the induced radiological activation for one given program on the short term, and for the global activation on the long term (10 "typical" years of operation).

3 Ion optics of the spectrometer

3.1 Technical constraints

The design of the spectrometer will also be tailored to the room layout and the interfaces to other systems (target box, beam dump, focal plane detection, low-energy branch, etc.). The associated constraints will be described in the following sections.

3.1.1 Room layout and annex facilities

The SPIRAL2 Phase 1 building has been defined since the end of 2009 (Figure 17). All the active elements of the accelerator are located underground, at a level of -9.5 m, in order to comply with safety requirements. The S^3 room is located in the AEL (Aire Expérimentale LINAG) between the LINAG and the production building, in order to minimize the distance to the DESIR facility.

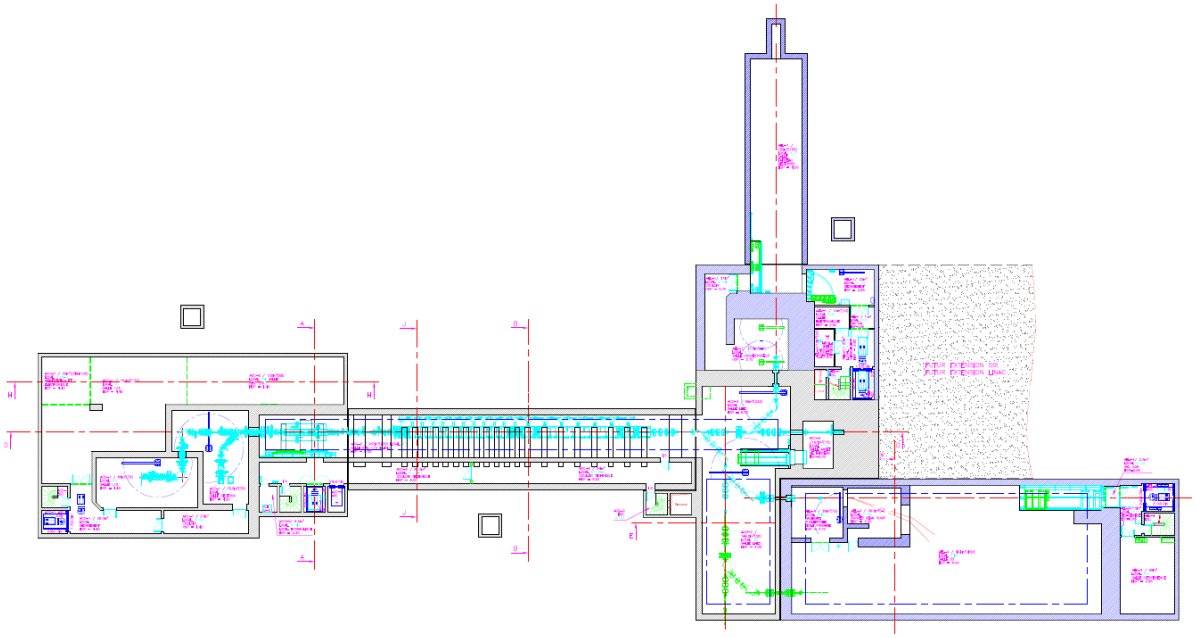

Figure 17: Full map of the lower (-9.5 m) level of the SPIRAL2 Phase 1 buildings, including the accelerator (cyan).

Figure 18 gives a functional representation of the S^3 facility.

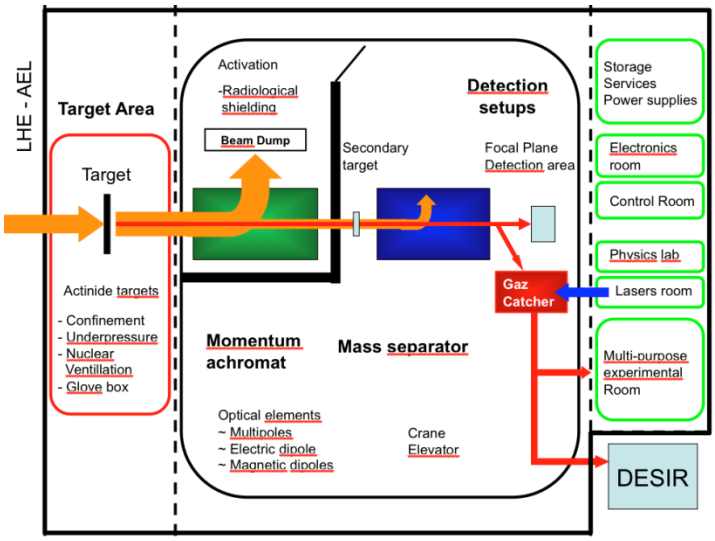

Figure 18: Schematic drawing of the S³ experimental area.

The S³ beam line layout must take into account the size and encumbrance of different equipments. The physical dimensions of the room and the entry position of the beam line are fixed. The experimental hall is 15 m wide and 36 m long. Objects up to 2.7 m high and up to 6 tons can be moved with standard technical infrastructure equipment through the elevator—heavier elements can be loaded in the S³ cave with a crane. Two beam line entrances are possible. S³ will use the north one with the beam entering travelling parallel to the long wall at a distance of 1.321 m from it. The height of the beam line is fixed at 1.5 m. The target position is 3.150 m from the entry point, leaving a usable space beyond the target of 32.850 m by 13.679 m.

For safety and radioprotection issues, the S³ cave will be divided into 3 main sections:

- The primary target area, a "nuclearized" area that allows the use of actinide targets or, more generally, can confine any potentially activated target material
- The beam dump area (after the first dipole), which is physically enclosed by concrete walls in order to minimize the transmission of neutrons produced in the beam dump and the associated material activation outside of this zone
- The rest of the separator-spectrometer, with the focal plane detection area at the east end

This last section will host different detection configurations for individual experiments. Three main classes of experiments have been identified:

- Implantation-decay correlations at the final focal plane
- In beam spectroscopy around a secondary target at the intermediate achromatic point
- Ground state property measurements, with the ions selected by a gas catcher and ion guide system coupling to a high-resolution mass separator (the low energy branch) and subsequently transported to a multipurpose experimental room adjoining the S³ experimental hall (Access to this room is possible even when the beam is present in the spectrometer hall)

The wall, floor and ceiling thicknesses are designed to limit outside irradiation and soil activation (see Chapter 6 on "Nuclear safety").

At an intermediate level (-6 m), on top of the multipurpose experimental room are located additional laboratory rooms and the laser system. The power supplies for the magnets, electronics and data acquisition rooms are on the above floor (level 0m). And finally, a room for storage and supplies is also located on the first floor.

The following sketch shows a layout of the different S³ areas by level (Figure 19).

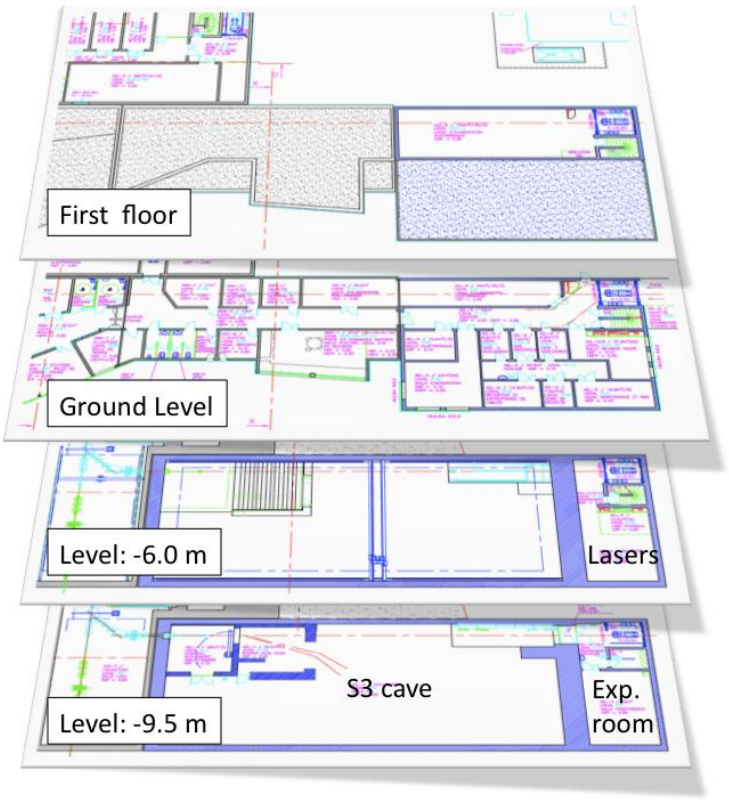

Figure 19: S^3 experimental area and auxiliary spaces.

It is expected that the ions selected by the low energy branch will also be able to be transported to the DESIR hall, where experimental setups will be installed for decay studies, moments and mass measurements as well as fundamental, weak-interaction studies. Therefore a dedicated beam line will connect the S^3 and DESIR buildings. Still, the DESIR and S^3 areas will be independent so that S^3 can remain in operation during the construction of the DESIR facility.

The S^3 experimental area will be accessible independently of operation of other LINAG beam lines (i.e. studies in NFS or deuteron beams being delivered to the production building). The vacuum in the experimental areas will need to be decoupled from the ultra-high vacuum of the accelerator. In addition, fast-acting valves will have to be installed.

Access has been studied to bring in large and heavy equipment. Partly, large experimental equipment would be installed later, after the first period of commissioning and the first physics experiments.

3.1.2 Upstream beam line

The roughly three meters of space between the last primary beam focusing quadrupole (before the production target) and the first multipole of S^3 will be principally occupied by beam diagnostic detectors; magnetic steerers and beam raster dipoles; standard and fast-acting vacuum isolation valves; and the high-velocity, rotating target box. All of this equipment is essential to the efficient operation of S^3.

Beam diagnostic detectors will determine the intensity, profile, and direction of the incoming primary beam. It is presently foreseen to have both non-intercepting and intercepting detectors to allow continuous beam monitoring both at standard operating currents ($I > 1$ nA) and more precise monitoring at low beam currents ($I < 1$ nA). Three non-intercepting wire detectors (EMS) will be positioned roughly 2.4 m before, 1.5 m before and at the target position (the latter together with a low power Faraday cup). Two position-sensitive ionization chambers (GAZ)—for low current measurements—will be located together with the two upstream EMS detectors. Two perpendicular, one-dimensional residual gas detectors (MIGR) will be positioned roughly 1.2 m before the target

position to allow intensity measurements and rough profile measurements in both the horizontal and vertical planes.

The beam spot on target is assumed to be 1-cm tall by 1-mm wide in the optics simulations. High intensity beams require a combination of target rotation and a tall beam spot. The beam can be narrow in the direction of target rotation, but must be expanded vertically by either a magnetic magnification via beam line quadrupoles or by rastering the beam at a high frequency.

A raster can consist of two rapidly variable vertical steerers, separated by a drift. The oscillation rate should be very high, possibly as high as 100 kHz, coupled with the high angular velocity of the target rotation. A high frequency raster is in used to produce a highly uniform 2D rectangular beam distribution for cryogenic targets at Jefferson Lab [10]. It uses low-inductance air-core dipoles and a special driver circuit to achieve a triangular wave pattern with rapid turn-around in both horizontal and vertical directions. The final choice of a beam magnification system vs. a high frequency raster system depends on the results of further studies. A combined vertical and horizontal magnetic steerer will be placed immediately following the last primary-beam quadrupole to allow the beam to be centered on the target. Additional steering may be built into one or more of the raster dipoles to allow adjustment of both the spot position and angle on the target within the same beam line space.

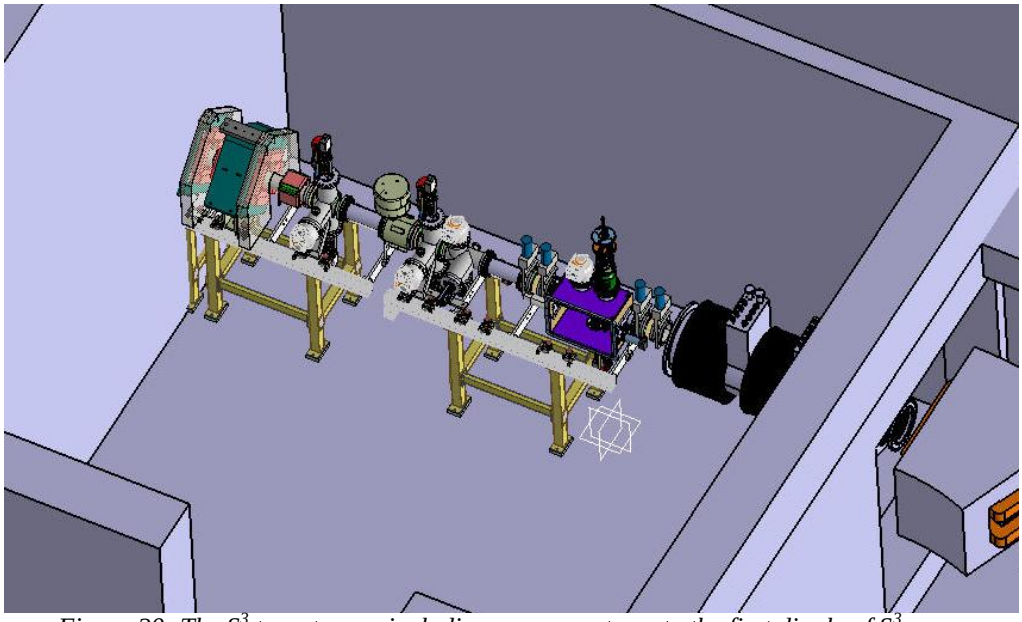

Figure 20: The S^3 target cave, including components up to the first dipole of S^3.

Two valves will be placed on each side of the target box to allow easy isolation, removal and exchange, while keeping all components under vacuum. There will be at least two target boxes, one for stable targets and one specially designed for actinide targets. A fast-acting valve will be placed roughly 1.5 m upstream of the target to allow for the rapid isolation of the S^3 cave from the accelerator lines in the event of an incident.

The present configuration would allow less than the present 0.8 m drift space between the target wheel and the entrance effective field boundary of the first quadrupole of S^3, if desirable. Optimizations of the target box design are expected to further reduce the required space. Minimizing this initial drift space from S^3 to the target will help improve the transmission of the system (see Section 3.2.3.4.2), particularly for products with large angular divergences from the target, such as the ^{255}No case discussed in Section 2.2.3.

[10] Yan, C., N. Sinkine and R. Wojcik. "Linear beam raster for cryogenic targets." NIM A (2005): 1-15.

3.1.3 S3 beam line

Within the S3 beam line, space must be reserved among the optical elements to allow for the placement of necessary vacuum and diagnostic components, along with bellows between elements to allow independent alignment of the individual optical elements. Beam diagnostic detectors will be placed both at the intermediate achromatic image (Image 2) and at the energy dispersive image (Image 3). Depending on the particular magnet technology to be used, some alignment may be possible without moving the beam line (e.g. by adjusting support links in the case of superconducting multipoles), while in other cases, alignment may be needed even within each multiplet (e.g. in the case of the room-temperature, closed sextupole option, the coils would be placed directly on the beam pipe). Fixed and movable shielding will also be necessary in various locations both for radiation safety to allow human intervention and to protect sensitive experimental equipment from radiation damage or excess background.

The beam dump is in multiple parts, both stationary and adjustable, extending from the first dipole to the first image (Image 1), where a momentum dispersed focus will be produced. More detail on particular constraints arising from the mechanical and other requirements of the beam dump will be given in the following section, 3.1.3.1. Considerable space will also be provided about the intermediate achromatic image (Image 2), particularly for the placement of photon or charged-particle detection arrays when operating S3 in spectrograph mode with a secondary reaction target placed at Image 2.

Special care must be taken to isolate the electric dipole from the remainder of the system. Valves will be placed at the entrance and exit of the electric dipole to preserve the vacuum in the rest of the system in the event of discharge induced degradation in this element. Limited, fixed lead shielding may also be indicated to shield other parts of the system or experimental apparatus from x-rays produced during such discharges.

Roughly 35 cm will be required between the effective field boundaries (EFB) of the magnetic dipole and a neighboring superconducting AML multipole triplet, including: 11 cm from the EFB to the flange of the AML multiplet, 7.5 cm from the EFB to the flange of the magnetic dipole, and 15 cm for bellows sufficient to allow 5 mm transverse alignment in both planes. This assumes that the adaptation between the shape of the multiplet exit and the dipole entrance can be accomplished in a very small space. If a valve is to be placed between the elements (as may be desirable after the second dipole) this would take an additional 12 cm, bringing the total to roughly 47 cm. The drift space within the superconducting triplet is set at 20 cm between neighboring EFBs.

Roughly 30 cm will be required between the effective field boundaries (EFB) of a magnetic dipole and a neighboring room-temperature multipole triplet, including: 6.5 cm from the EFB to the flange of the room-temperature multipole, 7.5 cm from the EFB to the flange of the magnetic dipole, and 15 cm for bellows to allow 5 mm transverse alignment. In the case of room-temperature elements, where the sextupole component is built onto the beam pipe, bellows will be needed between each element of a multipole triplet to allow individual alignment. This will increase the intra-triplet drift space required by roughly 15 cm.

Roughly 45 cm will be required between the effective field boundaries (EFB) of an electric dipole and a neighboring superconducting AML multipole triplet, including: 11 cm from the EFB to the flange of the superconducting multipole, 6.0 cm from the EFB to the flange of the electric dipole, 15 cm for bellows to allow 5 mm transverse alignment, and 12 cm for a valve.

Diagnostic detectors will be placed at image points throughout the system. At Image 1 these will be integrated into the design of the beam dump. At Image 2 the space requirement is more critically set by the large experimental detector arrays to be located there, but some thought should be given to possible interference between these experimental detectors and any simultaneously needed diagnostic equipment. A high-power faraday cup will also be placed at Image 2. Image 3 should provide sufficient space to locate a position sensitive micro-channel plate detector and a silicon detector, as well as a simple slit system.

Because of limited space among the optical elements of the spectrometer, vacuum pumping capacity will have to be located opportunistically. Pumps can easily be placed on the target box, the beam dump box, the Image 2 box, the electric dipole chamber, the Image 3 box, and the Image 4 box. To provide an optimum pumping capacity, the magnetic dipoles should be designed to allow pumping capacity to be added there as well. So far no place has been left along the S^3 line for magnetic steerers. The need for small corrections will be studied based on experience at comparable devices, and based on this, small steerer coils can be incorporated into the design at appropriate locations, either within the multipoles, the dipoles, or both.

3.1.3.1 Beam dump area

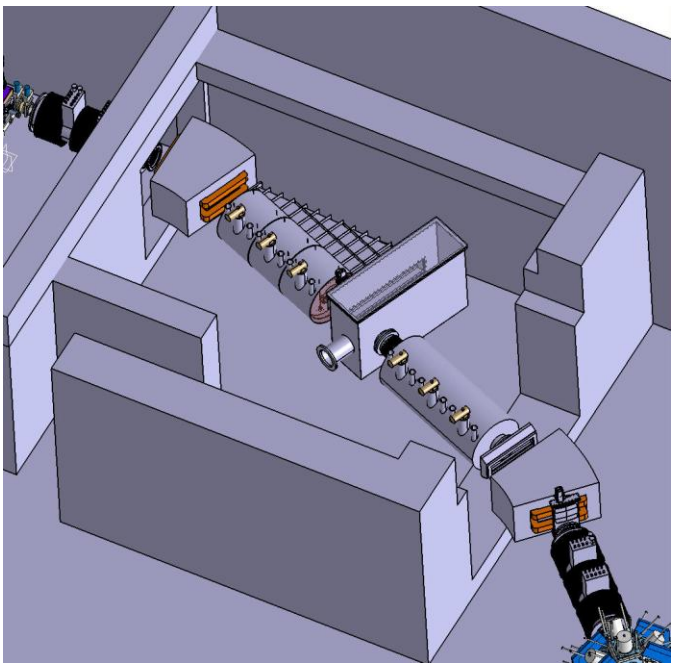

Figure 21: Beam dump cave.

The detailed design of the multi-finger high-power beam dump and the necessary fixed and movable shielding are still under study at CEA/IrFU. The amount of free space needed about the first dispersive image (Image 1), therefore, has yet to be determined. The present optical lattice provides roughly 0.8 m of usable space between the second and third multipole triplets.

Higher-energy experiments using S^3 in a two stage configuration, with a production target at the object and a reaction target at the intermediate achromatic image could benefit from the ability to place a very thin wedge degrader foil at Image 1. The effective wedge angle and the second half of the momentum achromat would be tuned to preserve achromaticity for the desired products, while contaminants with more or less specific energy loss would be displaced from the acceptance at the Image 2 aperture. Particular care will be needed in the mechanical design if the degrader and the movable beam dump fingers are to be usable simultaneously.

3.1.3.2 Achromatic point area

It has been proposed that some experiments will make use of a secondary reaction target and high-efficiency γ-ray or charged particle detector arrays at the intermediate achromatic image in S^3 for two-step reaction studies. The baseline design provided less than one meter of usable space along the beam line at this point. Longer drifts at this point would be highly desirable for these experiments. The full EXOGAM array, for example, would need a clear space as long as 1.54m, depending on the radial size of the beam line magnets before and after the intermediate image. Very long drifts, such as might be necessary to accommodate AGATA in a standard configuration, would unfortunately not be compatible with the basic design goals of the system. It is also important to verify that the beam dump

cave wall does not interfere with the free space about the intermediate image where experimental systems might be placed.

The current designs all provide at least 1.6 meters of drift space at Image 2, measured between the effective field boundaries of the preceding and following magnetic multipoles. This translates into roughly 1.4 meters of usable space between the neighboring triplet flanges, with the exact value dependent on the particular first-order optical lattice and the specific designs of the magnetic elements to be used. The actual usable space will also depend on the mechanical design of the particular detector mounts, the sensitivity of detectors to stray magnetic fields produced in the nearby multipoles, and the radial extent of the nearest multipole element. Superconducting multipoles, for example, are far more compact about the beam line and would thus more easily allow detectors placed about Image 2 to overshoot the flange position and make use of space even beyond whatever fully clear space is provided. The current layout does accommodate EXOGAM at this position when using superconducting triplets.

3.1.4 Downstream beam line

The spectrometer must leave sufficient space downstream of the final focal plane to allow placement of the wide variety of focal plane detectors and other devices to be coupled to S^3. The arrangement and support structure of the various devices to be used downstream of S^3 should be constructed to be compatible with each other in addition to any outside interfaces. Specifically, the gas stopping station and at least the first components of any high-resolution mass separator system will have to be dismountable to provide space for the standard S^3 implantation detection system, the EXOGAM/AGATA array, etc. Lasers for a LISOL type gas cell implementation will be brought in from the adjacent laser spectroscopy room. A compact implantation and decay station is planned for the end of the low energy line, and the reaccelerated beams will also be transported to the DESIR facility.

The most demanding device in terms of downstream space is the ANL style gas stopping station, which will couple to a high-resolution mass separator immediately downstream. This ensemble is estimated to require at least 6.5 m of free space between the final focal plane of S^3 and the downstream wall. One sample implementation using a separator similar to the DESIR HRS is shown in Figure 22. The AGATA array is likely the most demanding device in terms of lateral space, and would require more than 2 meters of free space on each side of the final focal plane. Additional space will be needed—beyond the physical size of any experimental system to be implemented here—to provide easy access to the entire room through the single entry door. Space requirements of necessary auxiliary systems (e.g. AGATA electronics racks) must also be taken into account.

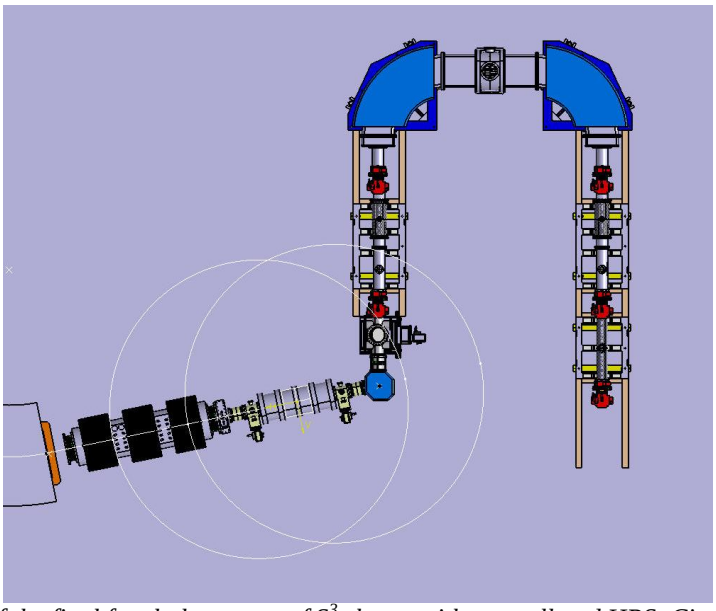

Figure 22: Top view of the final focal plane area of S³ shown with gas cell and HRS. Circles give regions of two meter radius from the beam line to indicate the approximate space required to place AGATA, and therefore what portion of the HRS may need to be displaced.

3.1.4.1 Detection system

3.1.4.1.1 Footprint

The spectrometer must leave sufficient space downstream of the final focal plane to locate a gas stopping station, including a high-resolution isobar separator, which requires at least 6.5m downstream and a similar transverse free space. There should also be adequate space between the final unit of S^3 and the side wall to provide easy access to the entire room through a single entry door and to allow the placement of large detector arrays at the final focal plane.

3.1.4.1.2 Standard detection

The "standard" detection of the spectrometer is an implantation-decay station with the following capabilities:

- Located on the mass focal plane in order to measure the mass of the incoming ions
- Energy and time of flight measurements for an additional selection of the ions scattered in the spectrometer, and hence an improved rejection
- Spatial and time correlation of the event, to detect charged particle (alpha, proton, electron…) decay chains
- Gamma detection for the spectroscopy of the daughter nuclei.

These properties are obtained by a combination of several detectors:

- Emissive foil tracking detectors for measuring the trajectories and time of flight
- Implantation silicon detector for energy and time measurement as well as space-time correlation
- "Tunnel" silicon detector for the detection of charged particle decays
- Germanium detectors for gamma spectroscopy

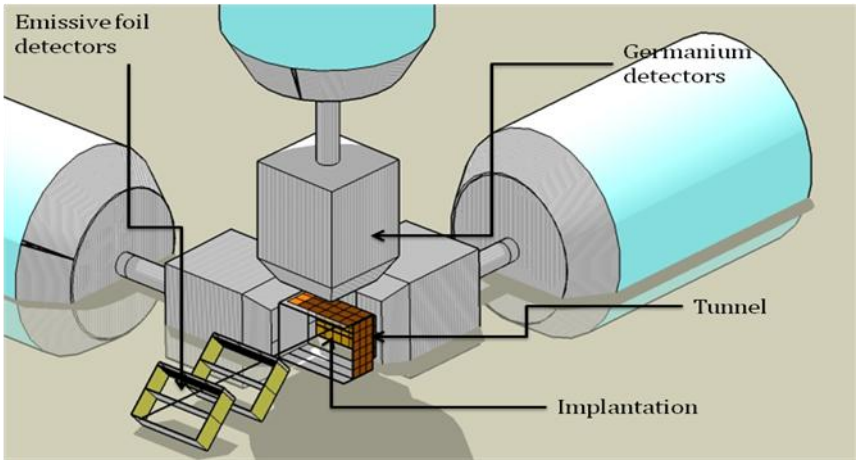

Figure 23: Sketch of the implantation-decay station components

According to the physics constraints, the following performances are required for this detection system:

- Emissive foil detectors
  - Large size (200 x 100 mm^2)
  - Very thin material
  - Time resolution < 1 ns
  - Position resolution ≈ 1 mm
  - Counting rate 1 kHz / channel and 1 MHz full detector with 10 kHz trigger
- Implantation
  - Large size (100 x 100 mm^2 or 200 x 100 mm^2)
  - Position resolution < 1 mm
  - Windowless
  - High energy: 10 MeV to 500 MeV (dynamic 50) Resolution FWHM 1 %
  - Low energy: - 7.5 MeV to - 250 keV FWHM TBD
  - Low energy: 100 keV to + 15 MeV FWHM < 2 x 10^{-3} WITH 15 keV @ 8 MeV
  - Timing resolution 1 ns with emissive foil
  - Counting rate 1 kHz / channel, 10 kHz on whole detector
  - Ability to detect the high energy pulse (> 50 MeV) quickly (≈ 10 µs) followed by a low energy pulse (< 15 MeV).
  - No dead time to detect short lived decay chains.
- Si Tunnel
  - Large size (60 x 100 mm^2)
  - 0 to 15 MeV for electrons and escaped alpha FWHM < 5 keV
  - Time resolution: 10 ns
- Gamma detection
  - Low Range: 0 to 4 MeV FWHM < 2 keV @ 1.3 MeV TR: 10 ns

    - or -

- High Range: 0 to 20 MeV (TBC)

3.1.4.1.3 Impact of the spectrometer optics

The interface between the detection system and the optics of the spectrometer lies in the image of the interesting reaction products at the final detection plane. The following picture shows a simulation of the focal plane image of A = 291, 292, and 293 ions for five charge states from q = 22+ to 26+. The population of the three masses and five charge states are artificially equivalent for the purpose of the representation. The mass resolving power in this case is around M / dM = 300 (FWHM).

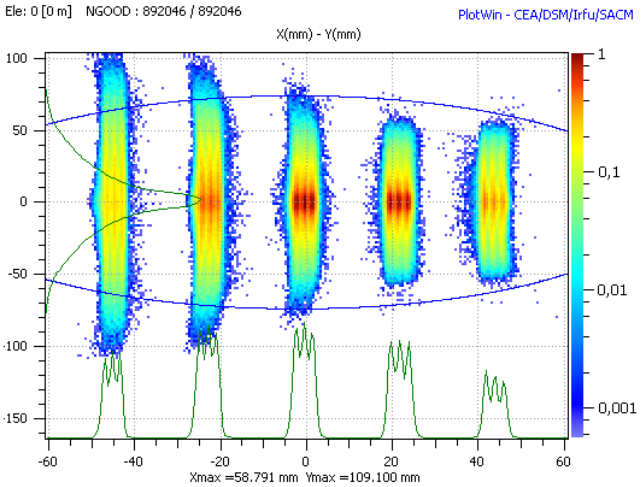

Figure 24: Simulation of the image at the detection plane of A=291,929,293 ions with q=22 to 26+. Mass resolving power here is around 300 (FWHM).

The main features of this distribution are:

- The position in the dispersive horizontal direction is directly linked to the mass over charge ratio of the ions. The detector spatial resolution must be fine enough to discriminate adjacent masses.
- The ion distribution has an extension in both directions (due to the mass dispersion in the horizontal plane and optical aberrations in the vertical plane), and the detector must be large enough to accept the majority of the ions.
- The density is highly heterogeneous, and the detector should be able to handle the highest counting rates.

As a first statement, we can say that these features depend very little on the optics configuration or the magnet technology used.

3.1.4.1.3.1 Mass resolution

The final dispersion on the focal plane detector is determined largely by the electrostatic dipole deflection angle, which is set to provide the desired resolving power in the presence of optical aberrations. The detector should have a position resolution in the dispersive plane better than the resolved spot size of the optical system, in this case about 1mm, in order not to impair the mass measurement. For this reason, we have considered using a stripped silicon detector with a 780µm pitch. This detector is similar to the one already used in the MUSETT project.

3.1.4.1.3.2 Size

The current technology of silicon detectors enables the construction of 100 x 100 mm^2 detectors out of 6" wafers. Considering a more physical charge state distribution than the flat distribution shown above, a single detector would be able to accept well over 80% of the ions transmitted to the focal plane. The size on the implantation detector naturally has an impact on the tunnel detector. If tunnel detectors are to have the same size as the implantation detector, we could reach 24% detection efficiency for backscattered alpha particles and conversion electrons. For the latter, thick (up to 2mm) large size silicon detectors are available today.

The size of the focal plane also has an impact on the gamma detection efficiency, which critically depends on the distance from the impact point to the germanium detector. Simulations show that with a ring of eight EXOGAM clovers, plus one at the back of the implantation detector, 10% efficiency is reached at 1 MeV.

3.1.4.1.3.3 Counting rates

The mass over charge resolution creates "hot spots" on the detector. These localized high counting rates may cause several problems:

- Dead time for the electronics. The S^3 electronics will have very low dead time, in order to accommodate the fast decays (down to 10 µs) that should be detected in the same pixel. This aspect is a more stringent constraint than the counting rate and is dealt with through fast, triggerless electronics.
- Damage to the detector. We are currently investigating "p-type" silicon detectors that are recently available in a large size and that have a high tolerance for radiation damage. In practice, localized deterioration of the detector can be overcome by slightly shifting the detector when a given area suffers heavy damage.

Note that the highest counting rates will be reached when medium mass nuclei (A<200), with high production cross sections, are detected. In this case, it could be possible to shift the silicon detector away from the focal plane. The distributions are then widened and the peak local counting rates reduced. Slits can be set at the focal plane to select only the interesting isobars (and consequently reduce the counting rate on the silicon detector) or the position at the focal plane could be measured with an emissive foil detector, which is more tolerant of higher counting rates. With such alternative methods, the mass resolution is degraded, but the maximum value of 1/300 is not always needed. It is really required primarily in the case of superheavy elements studies, when the counting rates are very low.

3.1.4.2 Low energy branch

The low-energy branch of S^3 will provide additional selection of the most exotic species that can be produced with the LINAG beams and will deliver these isotopes as a 50 keV beam to low-energy experiments located in the S^3 hall or the adjacent DESIR experimental area, once available. The approach proposed is to install a high-intensity gas catcher at the focal plane of the S^3 spectrometer, form a high-quality low energy beam from the recoils, and mass separate them with a compact high-resolution isobar separator. The figure below (Figure 25) shows a possible layout for the gas catcher and isobar separator system with its implantation at the S^3 focal plane. The high-voltage platform is about 1.7 meters long and the whole assembly fits in a footprint of 6.5 meters by 7.0 meters.

In cases where the laser spectroscopy can most advantageously be done directly at the source, the gas catcher could be replaced by the Leuven laser ion source. The advantage of using a laser ion source, apart from being element selective, is that it allows in-source or LIST laser spectroscopy measurements on exotic isotopes (e.g. around ^{100}Sn or in the VHE regions).

For ionization inside the gas cell, the Leuven laser system could be installed on the upper level of the multipurpose experimental room.

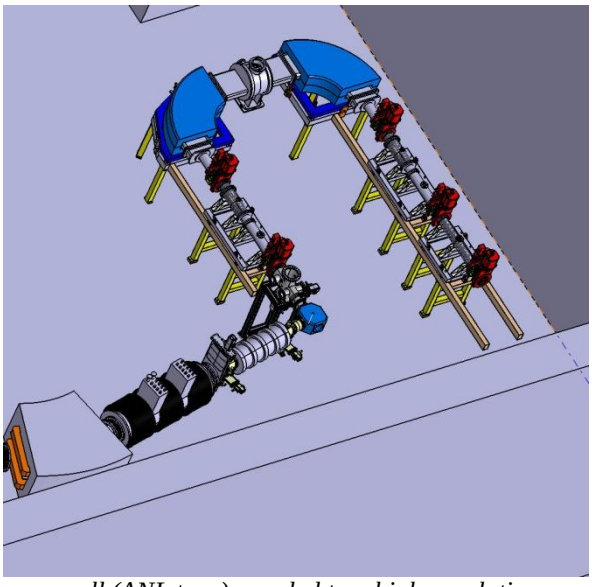

Figure 25: Fast extraction gas cell (ANL type) coupled to a high-resolution mass separator (DESIR type) following the M/Q dispersive image of S^3.

3.2 Ion optics studies

The ultimate goal of the ion optical studies presented in this report is the production of a detailed design of the high-resolution, large-acceptance, multi-mode mass separator and spectrometer, S^3. The starting point of this design study was the highly-symmetric MAMS baseline lattice discussed in the previous chapter, consisting of three identical momentum-dispersive ion-optical units, and one similar unit with the magnetic dipole replaced by a cylindrical electric condenser.

The S^3 optical design study has now reached the point to enable detailed comparison of different hardware options for the system components and now also includes detailed mechanical constraints. Field properties and field maps produced from preliminary magnet designs have been used in the optical models and their performances will be discussed below among other results of the design studies.

3.2.1 - Reaction Input files

The optical properties of S^3 have been selected to allow the study of a very wide range of fusion products, from heavy and superheavy elements to proton rich species in the region of ^{100}Sn. The breadth of these capabilities is represented in the optical design study by two specific experimental cases of asymmetric and symmetric fusion:

$$^{48}\mathrm{Ca} + {}^{248}\mathrm{Cm} \rightarrow {}^{292}116 + 4\mathrm{n}$$

and

$$^{58}\mathrm{Ni} + {}^{46}\mathrm{Ti} \rightarrow {}^{100}\mathrm{Sn} + 4\mathrm{n}$$

The characteristics of these reactions have been detailed in Chapter 2. In summary, kinematic calculations of these reactions have been carried out to produce realistic input distributions, including charge state distributions, as well as coupled angular and energy distributions. The spatial distribution on the target is set by the optical system leading up to the target and will be determined by the thermal properties of the target material. The values used here are taken from preliminary results of ongoing thermo-mechanical studies of the performance of high-velocity rotating production targets. The horizontal distribution is taken—identically to the target simulations—to be a Gaussian distribution with a standard deviation of 0.5 mm. For the vertical distribution, both uniform and Gaussian distributions have been considered as options, with a full height of 1cm in either case. In this study we use a uniform distribution, the option with poorer optical performance.

The optical system will be sufficiently flexible to be used for a wide variety of experiments, for example on the products of transfer reactions, deep-inelastic scattering, or even secondary reactions in a target at the achromatic image. Some specific demands of these other types of experiments will be discussed in the following sections. Optical simulations of other particular experimental cases can be carried out if input distributions are available. One additional reaction will be considered here to test the system performance for input distributions with comparatively large angular spreads.

$$^{22}\mathrm{Ne} + ^{238}\mathrm{U} \rightarrow ^{255}\mathrm{No} + 5\mathrm{n}$$

3.2.2 Methods for ion optical calculation,

Parallel modeling efforts have been undertaken at GANIL and at SACM to consider various optimized systems to meet the design requirements, to test individual design principles, and to consider the efficacy of preliminary designs for the various magnetic and electric elements to be used in the system. The details of the modeling and optimization methods used are discussed in the following sections, along with the performances of specific optimized optical lattices produced in each code. Discussion of more general results and conclusions of the optical studies follow in Section 3.2.3. Further details of the magnetic elements of which the system is composed are given in the following chapter on Hardware Designs, Chapter 4.

3.2.2.1 Map method

Optical simulations of S^3 have been performed at GANIL using the arbitrary order Taylor expansion method in the COSY Infinity code (version 9.0 [11]). This code has been used extensively in previous similar studies (e.g. the St. George recoil separator at the University of Notre Dame). Realistic magnetic dipole and multipole elements were approximated with Enge function fringe fields based on preliminary S^3 multipole designs for various orders and magnet technologies (room-temperature and superconducting). It should be noted that Enge fringe field models include only the principle multipole term, though weak higher order harmonics are known to exist in the various physical multipole elements (see Figure 26 and Figure 27).

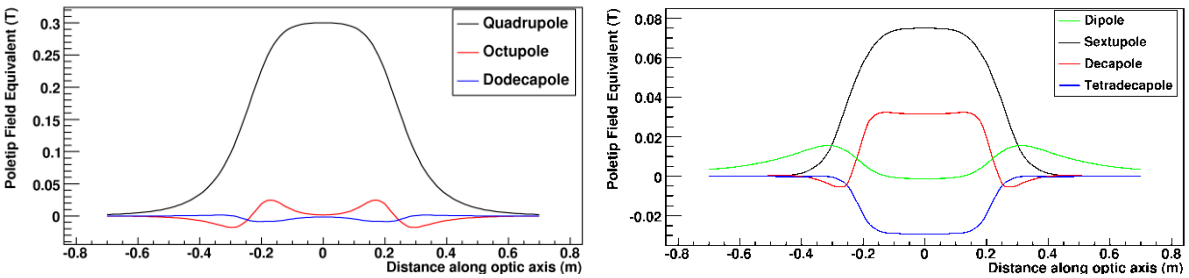

Figure 26: Dominant terms in the multipole expansion of the room-temperature quadrupole (left) and sextupole (right) field versus distance along the optic axis, based on an analysis of midplane field data. The Enge parameter fringe field approximation neglects all but the principle order.

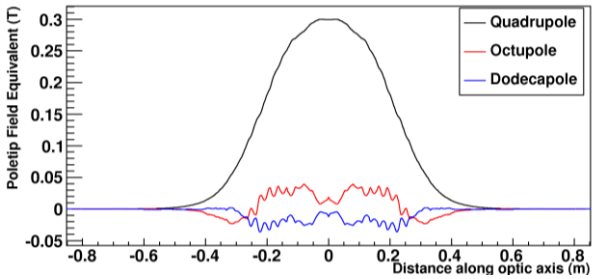

Figure 27: As in Figure 26, but in this case for the superconducting quadrupole, based on a simple flat coil model by S. Manikonda. The sextupole and octupole components of the superconducting multipoles were modeled using the same shape.

[11] K. Makino, M. Berz, Nuclear Instruments and Methods A558 (2005) 346-350

For the systems optimized with higher-order corrections, room-temperature multipoles were used for the momentum achromat and superconducting multipoles for the M/Q separator, in both cases iron-dominated elements. More recent calculations to re-optimize the first order lattice use superconducting air-core elements throughout, except for the triplets before and after the beam dump, where room-temperature, iron-dominated elements were used. Standard Enge shape fringe fields cannot be used for air-core elements, so a modified function was used which includes the characteristic undershoot in the fringe field region, following the method used at RIKEN to model their air-core multipole triplet. The electric dipole used a hard-edge approximation.

First-order system configurations were generated by Simplex minimization based on Monte Carlo generated initial conditions within S^3 design requirements. Second- and third-order optimizations were then carried out sequentially. Optimizations considered the size of aberrations for primary-beam-like particles at the beam dump location (Image 1) and the size of aberrations for product-like particles at both the intermediate achromatic image (Image 2) and the M/Q dispersive final focal plane (Image 4). Second-order optimizations (sextupole tuning) were conducted first, minimizing a weighted sum of second- and third-order aberrations at the multiple points of interest (using a combined Monte Carlo and Simplex minimization method); then third-order optimizations (octupole tuning, minimizing in the same way as before) were conducted, while considering the system performance at the image points, again, including terms up to third-order in the Taylor expansion.

Since S^3 is a large acceptance system, its performance is a high-order phenomenon, which depends critically on the particular multi-dimensional distribution of the input particles. Performances were verified—subsequently to minimizing the aberrations in COSY calculations—by mapping simulated, fully-coupled particle distributions through transfer maps, at first including terms up to third-order. The results of the Monte Carlo calculations of third-order optimized systems will be discussed below, but to summarize, the system requirements detailed in Chapter 2 for the two baseline experimental cases were generally satisfied in third order.

The results of simulations of the third-order optimized system when including aberration terms up to fifth-order were promising, though somewhat degraded from those produced when only including terms up to third-order. Fifth-order optimizations in COSY—that is tuning sextupoles and octupoles while including aberration terms up to fifth-order in the optical calculations—are more than an order of magnitude slower than third-order optimizations, due to the much larger number of non-zero Taylor coefficients in the transfer maps. In addition, this more complex treatment suffers increasingly from the reality that the desired system performances are not necessarily guaranteed simply by minimizing aberrations at the image locations.

While M/Q resolving power is very closely linked to the size of optical aberrations at the image locations, angular acceptance and overall transmission efficiency are much less so. In reality the system resolution is a higher order phenomenon depending delicately on the interaction of the specific multi-dimensional input distribution with the higher-order transfer map; meanwhile the transmission efficiency may suffer due to large aberrations at any point throughout the full system, regardless of well managed aberrations at selected image locations. For these reasons, a true optimization of second- and third-order corrections in S^3, while including aberration terms up to fifth-order, must include a Monte Carlo calculation at each optimization step. This further increases the time necessary for system optimization.

The optimizations were then parallelized and made external to COSY to allow several necessary improvements: to continue rapid simulations including terms up to fifth-order; to allow optimizations using a wider variety of minimization algorithms, which are also more flexible than those built into COSY (e.g. they allow minimizations including more variables simultaneously); and to allow optimizations based on direct Monte Carlo analysis of system performance, rather than minimizing aberrations at the images and only afterward verifying acceptance, transmission and resolving power.

Preliminary fifth-order optimizations were then performed in a few different ways, but all based on a single selected third-order optimized lattice taken from the results of the previous optimization step. Thus the results do not necessarily represent a global optimum. In fact, following the results of

optimizations at lower orders, it may be better to include higher order aberration terms at an earlier stage—when first tuning the octupole corrections for example—rather than re-optimizing a corrective tune generated while truncating the calculations at a lower order.

Since the angular acceptance had not yet been included in the optimization, there was some question as to how to include it. Analytically calculating the angular acceptance based on Taylor coefficients becomes progressively more difficult and less meaningful as calculation order increases. Thus, angular acceptance was calculated based on Monte Carlo methods, defining it simply as the largest initial angle for a transmitted ray. Some fifth-order optimizations were performed that considered only angular acceptance and transmission, while others also included M/Q resolution.

The ideal way to optimize the angular acceptance is to optimize the transmission for a particular, coupled Monte Carlo input distribution that is characteristic of experimental cases motivating the large acceptance requirement. The ^{255}No production case was calculated specifically for this purpose. Preliminary results for this case will be given below (Section 3.2.2.1.3). The calculated transmission is promising even though the recently developed high-acceptance tune was not used and no specific optimizations have been performed yet for this input distribution.

The different criteria included had to be reweighted for the new optimizations. As noted previously, in the parallelized optimizations Monte Carlo calculated resolution is used directly as a quality factor at Image 4 rather than the more indirect aberration minimization. At Image 2, transmission through a 1 cm x 3 cm aperture is the only requirement rather than a weighted aberration sum. The spot size of primary-beam-like particles at Image 1 is not yet included in these optimizations and neither are the losses from beam dump fingers at Image 1 included in the net transmission calculations.

The results of the COSY calculations will be discussed according to topic in the following sections. Except where noted otherwise, a 1 cm wide by 3 cm high aperture was placed at the intermediate achromatic image for the COSY based Monte Carlo calculations.

3.2.2.1.1 $^{48}Ca + ^{248}Cm \rightarrow ^{292}116 + 4n$

The desired performances have been achieved in third-order COSY calculations for the superheavy element production case, using sextupole corrections throughout the system and octupole corrections in the M/Q separator. The first-order lattice used is that shown in Figure 46. Transmission of all produced particles of mass 292 is 62%, and the resolving power—calculated based on the full-width at half-maximum—is above 300 for all five charge states within the acceptance.

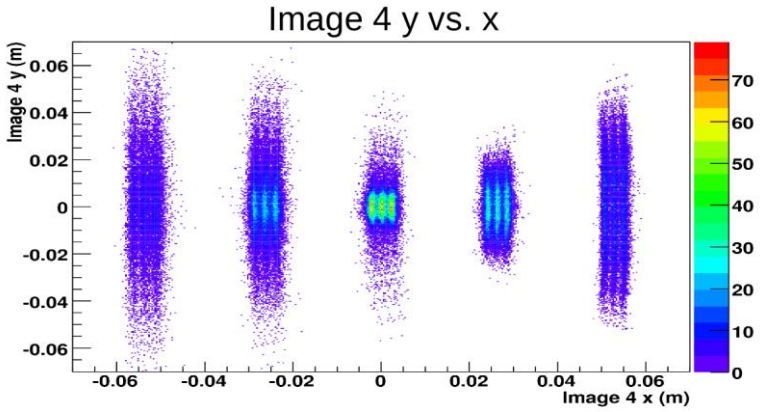

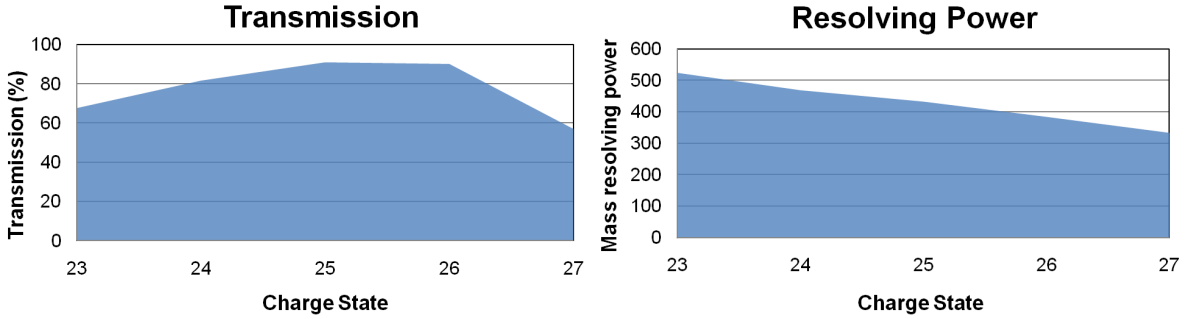

Figure 28: Distribution at the final focal plane (top), transmission (bottom-left) and resolving power (bottom-right), calculated for the full-width at half-maximum, for five charge states and three masses centered on $^{292}116^{25+}$ taken from a Monte Carlo calculation using a third-order COSY map. Note that the x-space in the top plot presents species of decreasing Q from left to right.

Third-order COSY calculations including only sextupole correction elements throughout the system were unable to reach the desired M/Q resolving power.

3.2.2.1.2 $^{58}Ni + ^{46}Ti \rightarrow ^{100}Sn + 4n$

The same third-order optimized COSY model of S^3 used above (in Section 3.2.2.1.1) was used in calculations for the proton-rich, ^{100}Sn production case. Transmission of all produced particles of mass 100 is 56%, and the resolving power—calculated based on the full-width at half-maximum—is above 300 for all five charge states within the acceptance.

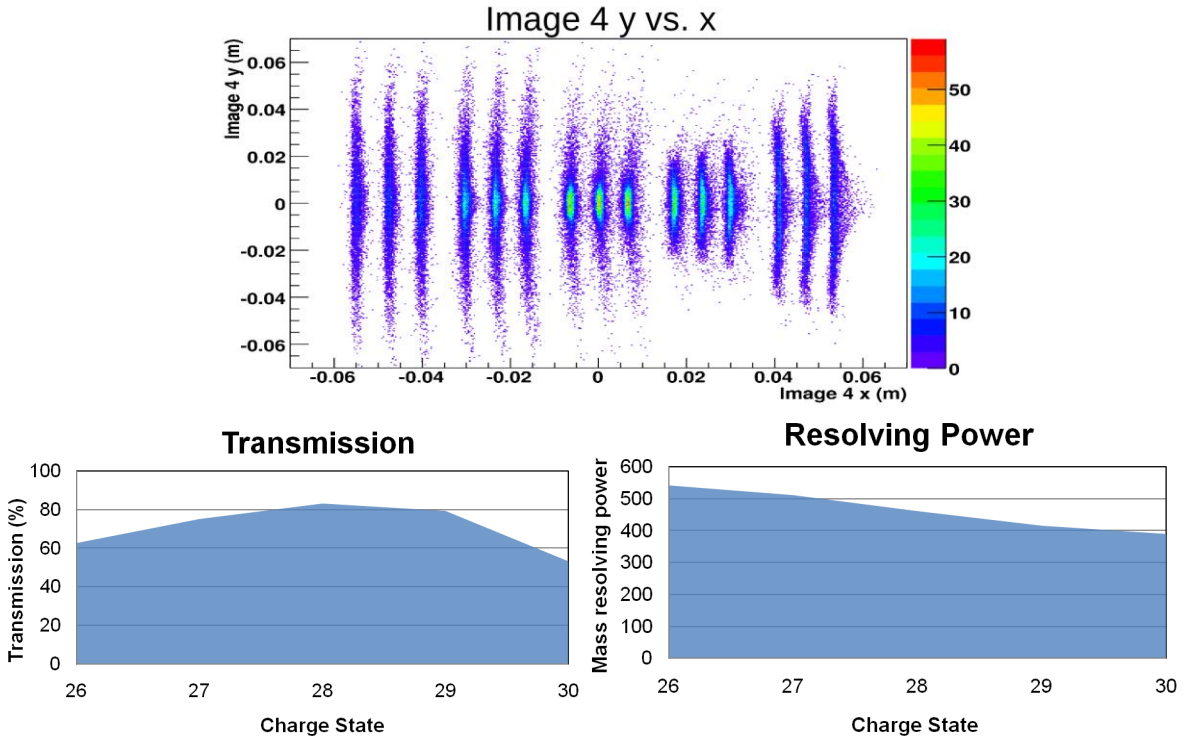

Figure 29: Distribution at the final focal plane (top), transmission (bottom-left) and resolving power (bottom-right) for five charge states and three masses centered on $^{100}Sn^{28+}$ taken from a Monte Carlo calculation using a third order Taylor map method. The folded transmission of the full charge state distribution (taken from the ETACHA code) is 56%, and the resolving power is calculated based on the full-width at half-maximum. Note that the x-space in the top plot presents species of decreasing Q from left to right.

Fifth-order calculations based on this third-order optimization—which was performed including map coefficients up to only third order—yield degraded transmission and M/Q resolving power (Figure 30). Using the exact same Monte Carlo apertures provides a transmission of only 45% of all mass 100 products. To get a more realistic estimate of the achievable transmission, we remove the aperture at Image 2. While this may overestimate the achievable transmission, it will much more closely

approximate the true performance of an optimized system than will a calculation including a small Image 2 aperture without first re-optimizing the image at that point. Unoptimized fifth-order calculations with no Image 2 aperture (*Figure 30*) provide a transmission of 59% of the full charge state distribution. On the other hand, M/Q resolving power remains near or above 300 for only the central three charge states.

Comparing Figure 30 to previous third-order calculations (Figure 29), it seems that some fourth- and fifth-order aberrations are cancelling second- and third-order vertical aberrations, resulting in a smaller overall vertical spot size. The sextupole and octupole correctors do couple strongly to fourth- and fifth-order map terms, thus re-optimizing these corrective elements in view of the full fifth-order behavior should improve the system performance significantly.

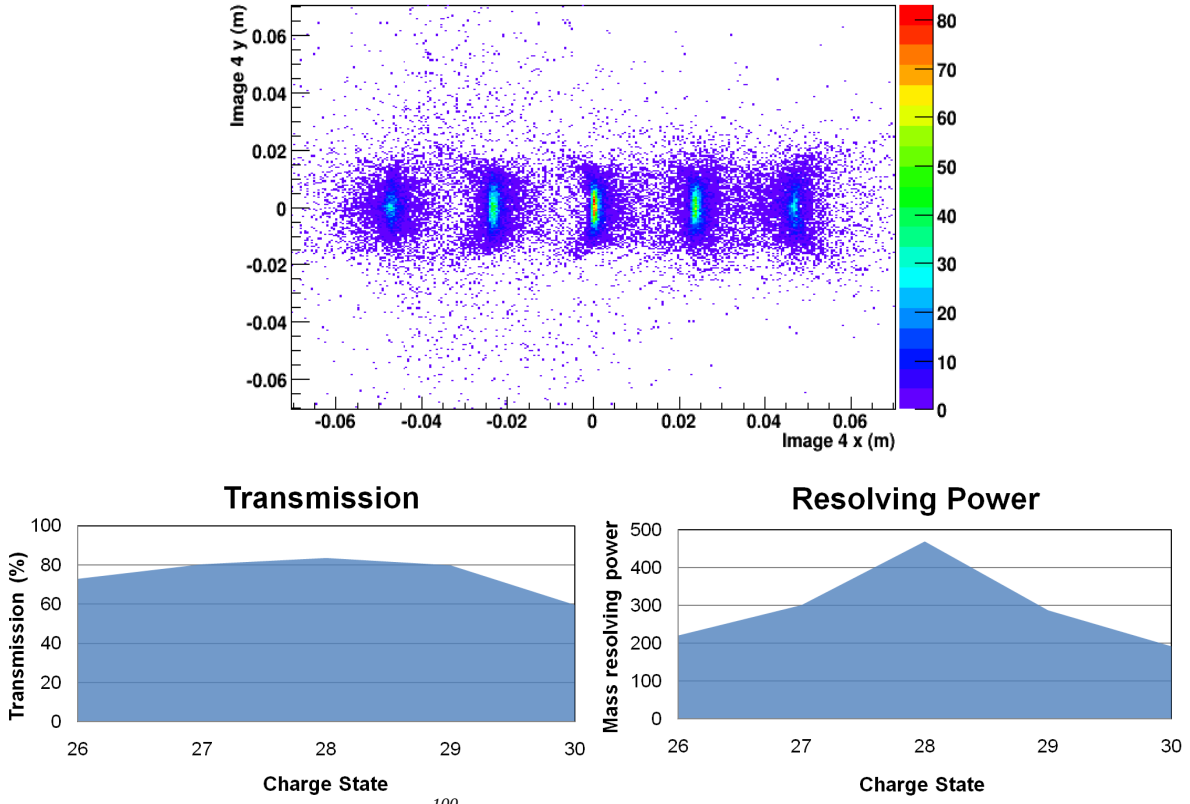

Figure 30: Monte Carlo simulation for ^{100}Sn production setting based on a fifth-order Taylor expansion, with corrections fit considering aberrations only up to third order. The focal plane spatial distribution for five charge states, centered on 28+, is shown at top. No aperture was placed at Image 2 in this simulation, resulting in improved transmission (bottom-left), while resolving power (bottom-right) is degraded for non-central charge states.

3.2.2.1.3 $^{22}Ne + ^{238}U \rightarrow ^{255}No + 5n$

Third- and fifth-order Monte Carlo calculations, again based on the third-order optimized COSY model of S^3 used above (in Section 3.2.2.1.1), were performed for the production of ^{255}No. The Image 2 aperture was removed for these calculations, since the system has not so far been optimized for a particle distribution with such a large angular spread. Surprisingly, fifth-order Monte-Carlo calculations produced better angular acceptance than third-order calculations, even though no additional optimization was performed based on the fourth and fifth order terms. Delving into the Monte Carlo calculation results reveals that large aberrations near the dipoles producing reduced transmission in third-order calculations are being partially cancelled by higher order aberrations present in the fifth-order calculations.

For selected studies of superheavy element properties, M/Q resolution may be of lesser importance than transmission and primary beam rejection efficiency, in which case the system's higher order

corrections may be optimized primarily to increase angular acceptance while minimizing aberrations at Image 2, in order to allow a very small Image 2 aperture to minimize transmission of scattered beam particles from the first half of the system. Additional first order tunes, particularly if the target could be moved closer to the first multipole of S^3, would even more dramatically increase the angular acceptance of the system (see Section 3.2.3.4).

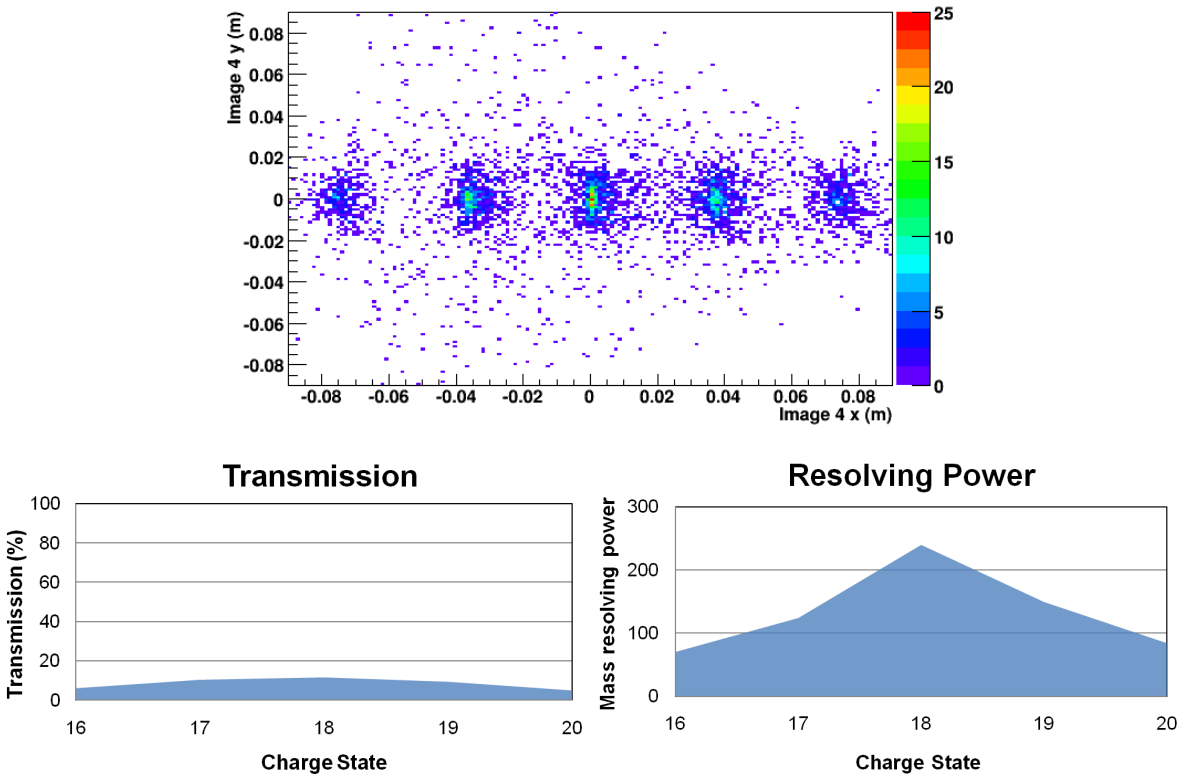

Figure 31: Distribution at the final focal plane (top), transmission (bottom-left) and resolving power (bottom-right) for five charge states centered on $^{255}No^{18+}$ taken from a Monte Carlo calculation using a fifth-order Taylor map method. The folded transmission of the full charge state distribution is 7.0%, and the resolving power is calculated based on the full-width at half-maximum.

3.2.2.1.4 $^{58}Ni + ^{50}Cr \rightarrow ^{99}In + 3p + 4n$

This particular experimental case was selected from among the submitted LoIs to give some idea of a typical focal plane distribution of fusion evaporation products that might be observed in S^3 (in this case, for a one-step production, N = Z study). Cross sections for all products were calculated in PACE4. Coupled angle-energy distributions and charge state distributions were taken from calculations for ^{100}Sn production used as the baseline case for S^3. Rays were mapped in third order through the full system and those transmitted to the focal plane are shown below (Figure 32).

In this case, isobar contaminants are produced at a rate of roughly two orders of magnitude more than ^{99}In, all of which will naturally pass the final M/Q selection slits. At roughly one tenth the level of the isobar contaminants, other residues with close lying M/Q ratios will also pass the selection slits. It should be noted that fifth order calculations indicate the vertical extent of the distribution may be exaggerated in third order calculations (see Figure 30).

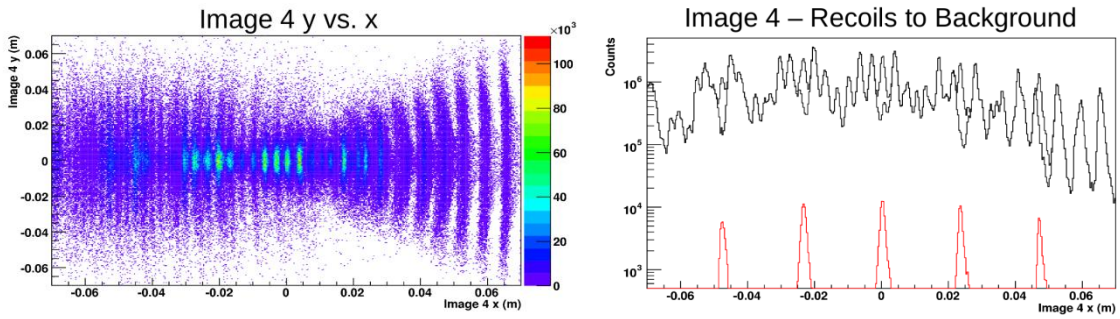

Figure 32: Production setting for ^{99}In including background rates. A third-order Monte Carlo simulation was performed based on PACE4 estimated cross sections. Shown are the focal plane spatial distribution of all products (left) and the horizontal distribution of the recoil of interest versus background counts (right), with the ^{99}In products given by the red curves, total contaminants given by the upper black curve, and non-isobar contaminants given by the lower black curve.

3.2.2.2 Ray tracing with TraceWin

The Saclay optical group has been in charge the evaluation of the 4-fold symmetric lattice type. The main feature of the 4-fold symmetric lattice is that it consists of basic cells that are reproduced throughout the system. Each cell is composed of a multipole triplet (for beam focusing in the horizontal and vertical planes), and a half-dipole (to induce dispersion). Two cells form a dipolar stage, four cells form a separation stage (either in mass or momentum), and eight cells form the full spectrometer. In the mass separator, the two dipoles are not of the same type (one electric and one magnetic), and the symmetry is therefore not perfect.

For each cell, the goal is to obtain—in first order—a transfer matrix with diagonal elements equal to zero. This is done by adjusting the magnetic field of the three quadrupoles and the distance between the last quadrupole and the dipole. The transfer matrix of two cells, neglecting dispersion, is the unitary matrix [-I], and similarly the transfer matrix for one separation stage is the unitary matrix [I]. Such an optical design insures the cancellation of certain geometrical second order matrix elements for each separation stage. The complete spectrometer is achromatic, as is each separation stage. The optical functions are displayed in Figure 33. The beam envelope of the first order optics is shown in Figure 34a.

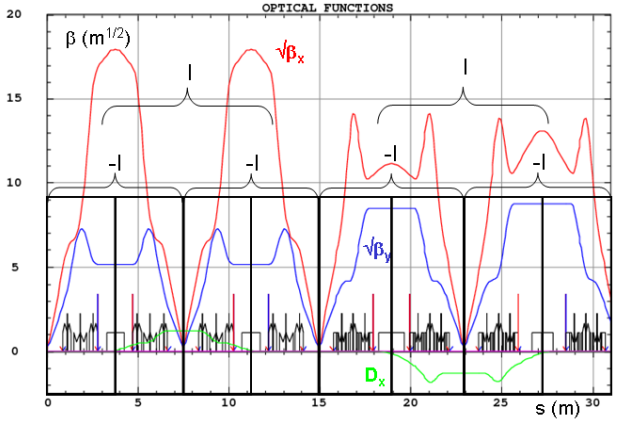

Figure 33: Optical functions of the spectrometer, horizontal beta function (red line), vertical beta function (blue line), and dispersion function (green line). The basic cells defined in the first order optics are indicated with square black boxes, and labels indicate the combinations producing unitary transfer matrices.

A first order lattice satisfying the geometrical and the optical requirements was produced with the Beta code. That lattice was built with a theoretical description of the magnets (quadrupole, sextupole, magnetic dipole and electrostatic dipole), without taking into account the fringe fields. In addition to the first order optics requirements, other constraints were to keep the first order beam envelope within the specified system apertures (see Figure 34b), to limit the magnet strengths in order to avoid iron saturation, to preserve enough free space around the intermediate focal planes for the placement of

several diagnostic and/or other equipment (fixed and movable finger beam dump, profile monitors, tracking detectors, etc.) and to keep the total dimensions of the system inside the imposed limits (see Figure 34a).

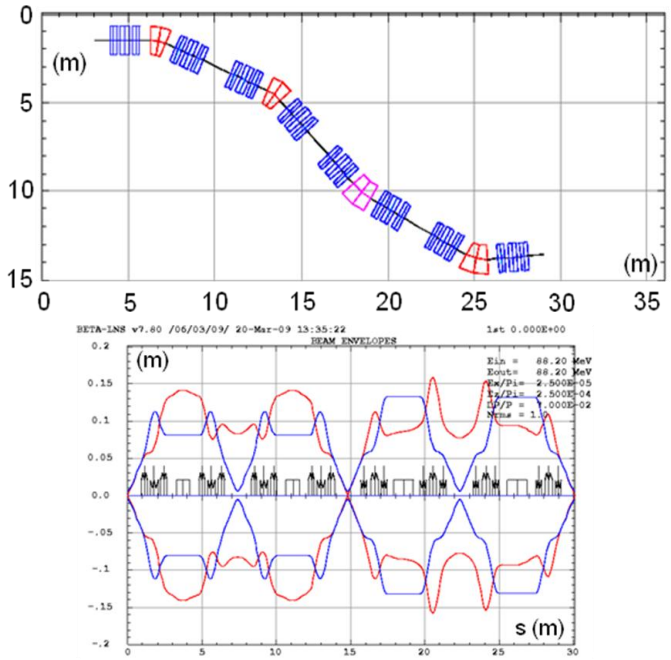

Figure 34: (a) S^3 layout from the first order calculation performed in the Beta code. The spectrometer has to fit into an area of (26 x 12) m^2. (b) ^{100}Sn first order beam envelopes, in the horizontal (red line) and the vertical (blue line) planes.

This lattice model was imported into the tracking code TraceWin. The TraceWin code transports, taking into account all orders, a cloud of particles which has the same kinematic distribution as the recoil products after the target. The distribution of the ^{100}Sn reaction products after the target, which was used in the TraceWin optimizations discussed here, is shown in Figure 35. Different optimization constraints and methods have been experimented with in order to reach the mass separation requirement at the final focal plane. The optimization method finally chosen uses as variables all the sextupoles, all octupoles wherever they are inserted, and the last quadrupole triplet in order to maximize the resolution of three different particle beams transported to the final focal plane (Image 4) of the spectrometer.

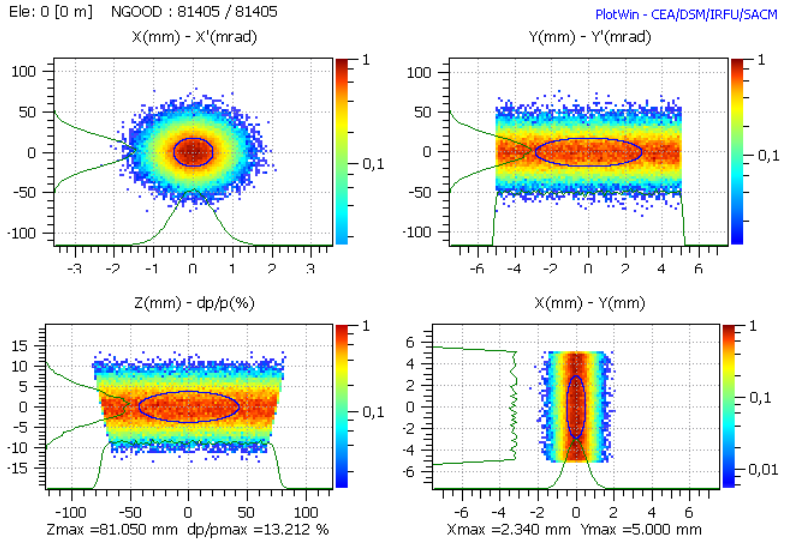

Figure 35: Initial distribution of the ^{100}Sn reaction products after the target. The standard deviations are: $\sigma(x)$ = 0.5 mm, $\sigma(x') = \sigma(y')$ = 17.8 mrad, Δy = +/- 5 mm (uniform distribution), $\sigma(\delta p/p)$ = 3.7 %.

The TraceWin code was modified in order to track three charge states of the same particle distribution successively, which then cover the useful final focal plane area (± 50 mm in the horizontal plane). Once the optimization process converged, the magnet setting was adapted to the ^{292}116 superheavy element reaction case (^{48}Ca + ^{248}Cm -> 4n + ^{292}116). The spectrometer mass separation power was then calculated from the beam FWHM sizes and positions at Image 4, using the distribution of the ^{292}116 reaction products. The same first-order lattice is employed for all the following optimizations, in order to compare the different magnet technologies for each combination of multipoles. Each higher-order multipole component can be optionally inserted in each separator stage, and in each magnet type (closed or open).

The first simulations were performed using hard edge models for the magnetic elements. These simulations have shown that, to obtain the required resolution (as seen in Figure 36), a sextupole component is needed in *all* quadrupole magnets located in the dispersive regions. These are necessary to correct the chromatic aberrations. The compensation of the geometrical aberrations introduced by these sextupoles has to be done with other sextupoles in the non-dispersive part of the beam line. The simulations also show that octupole corrections in the mass separator strongly improve the mass resolution (Figure 37). The insertion of octupole components in a magnetic multipole implies the use of superconducting technology for that element.

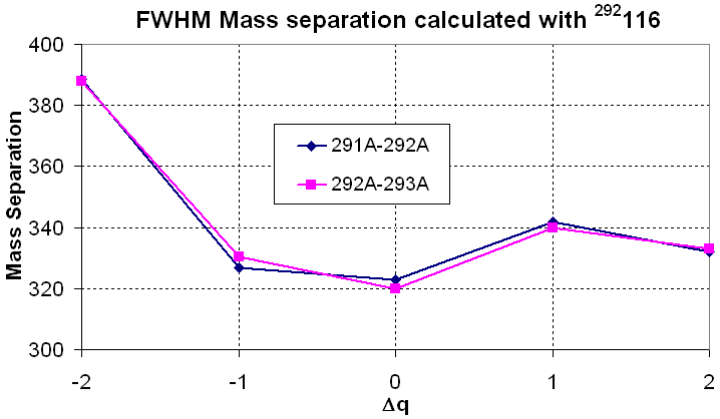

Figure 36: Mass resolving power in the hard edge case with only sextupole correction components. Δq represents the charge compared to the reference charge-state (<q> = 26+ for ^{292}116).

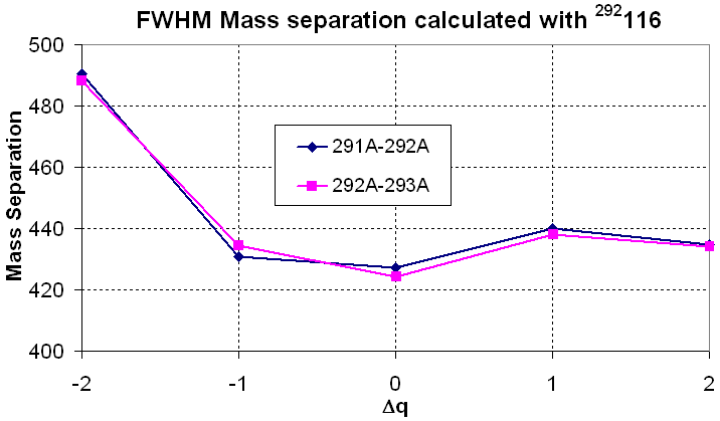

Figure 37: Mass resolving power in the hard edge case with sextupole and octupole correction components (octupoles only in the mass separator). Δq represents the charge compared to the reference charge-state (<q> = 26+ for ^{292}116).

Afterwards, the quadrupole, sextupole and octupole theoretical magnets were replaced by realistic field maps provided by the Opera3D code. It must be noted that the TraceWin code does not yet implement magnetic and electrostatic dipole field maps, which means the fringe field contributions for these elements are not taken into account. At first, field maps of room temperature closed magnets were used for all elements, including the second triplet which has to be "opened" (see section 4.5).

The closed magnets used for the simulations are: iron-dominated type for the room temperature quadrupoles (section 4.1.1), air core coils proposed by GANIL for room temperature sextupoles (section 4.1.1), and flat race track multipoles developed at Saclay for the superconducting magnets (section 4.2.3). As the magnet apertures are large compared to their length, the perturbations due to the magnetic fringe fields are significant. One of the disturbing effects of the quadrupole fringe field is to create an octupole-like effect on the beam, which deteriorates the previous optimization results. Figures Figure *38*, Figure *39*, and Figure *40* show the results obtained for different corrections with or without octupoles. Octupole corrections were needed in the mass separator stage to achieve the desired resolving power (Figure 38 and Figure 39). Moreover, simulations also showed that the introduction of octupole correction in the closed quadrupole magnets of the momentum achromat significantly improves the final mass resolution (Figure 40).

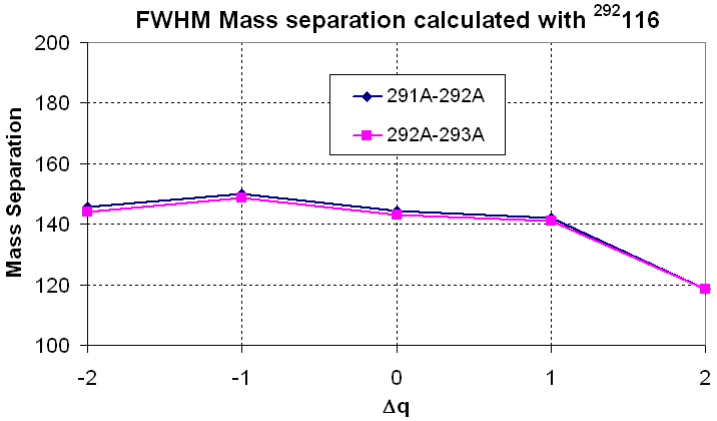

Figure 38: Mass resolving power in field map based calculations, without octupoles.

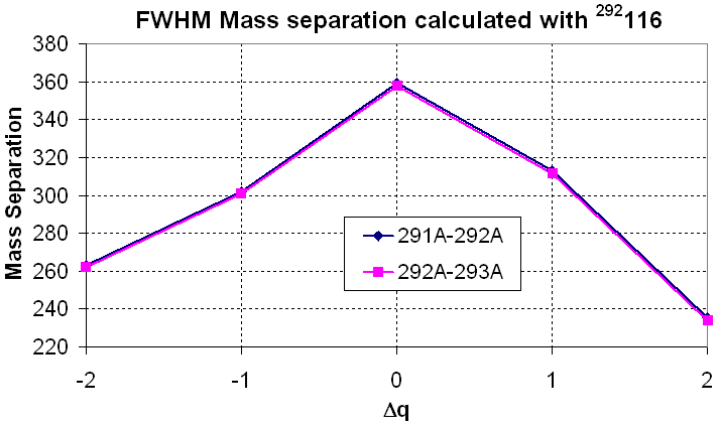

Figure 39: Mass resolving power, again using field maps, now with octupoles in the mass separator.

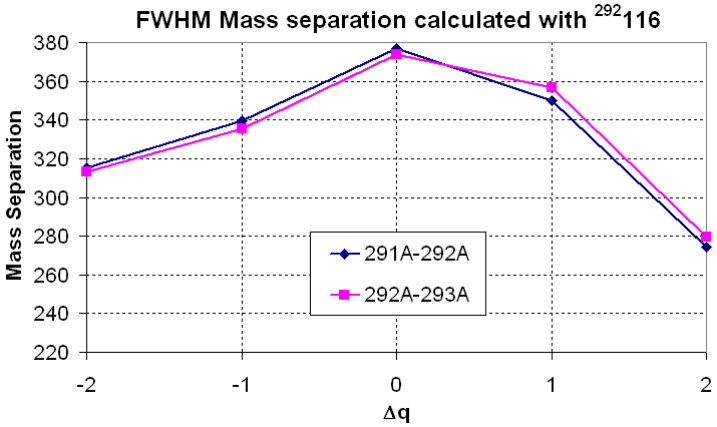

Figure 40: Mass resolving power, again using field maps, now with octupoles in the mass separator and the momentum achromat.

Open multipole field maps (quadrupole and sextupole) were then introduced at the position of the second multipole triplet. Two different types of open multipole magnets were designed and tested at Saclay, an open multipole working at room temperature and a first design of an open superconducting multipole (MOSAR, see Section 4.2.4). For both multipoles the sextupole component is obtained by the subtraction of two dipole fields of different transverse extension. The main dipole component is cancelled and the higher harmonics, mainly the sextupole, remain. In both cases the spectrometer performances were reduced (see Figure 41 and Figure 42) and are comparable, on average, though they exhibit different behavior. Compared to the designs with closed multipoles, the main difference comes from the sextupole component. Since the dipolar coils do not have the same transverse extent, a dipole component remains in the region where the dipole fields are not overlapping (see Figure 79, Section 4.2.4). Therefore the residual dipolar field varies in the transverse direction, and the particles which propagate at different transverse positions don't feel the same dipolar field integral. For these particles the system is no more a first order achromat and the chromatic correction doesn't work efficiently. This effect is difficult to correct in the warm magnets. On the other hand, a new design of the MOSAR magnet gives a sextupole component of similar quality as a closed sextupole magnet, without the unwanted dipole component (see Figure 80). The resulting mass resolving power of the spectrometer with the new MOSAR magnet design is still undergoing optimization, but a preliminary result is shown in Figure 43.

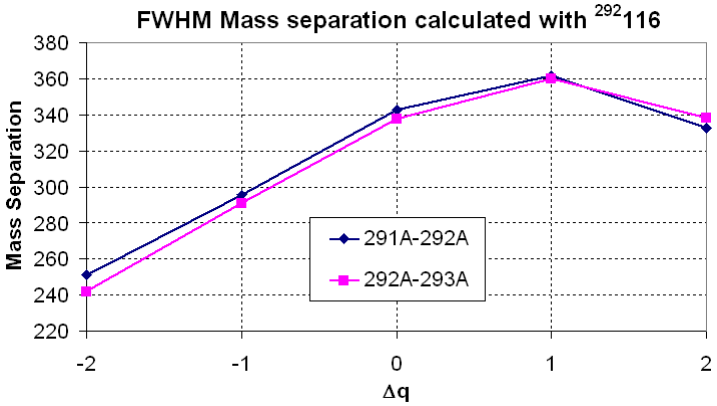

Figure 41: Mass resolving power using field maps of room temperature open multipoles, octupoles in the mass separator and the momentum achromat.

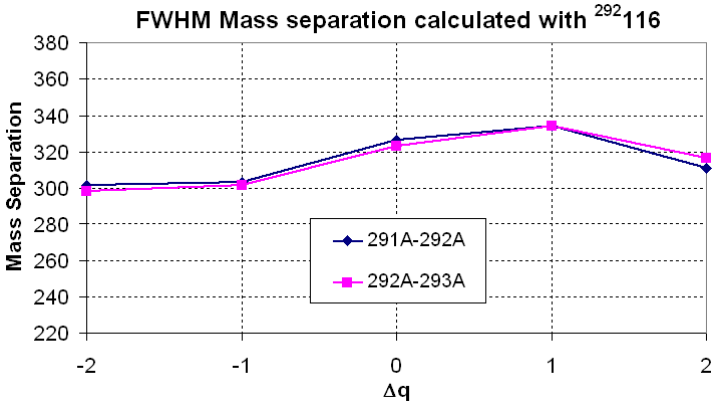

Figure 42: Mass resolving power using field maps of MOSAR open multipoles, octupoles in the mass separator and the momentum achromat.

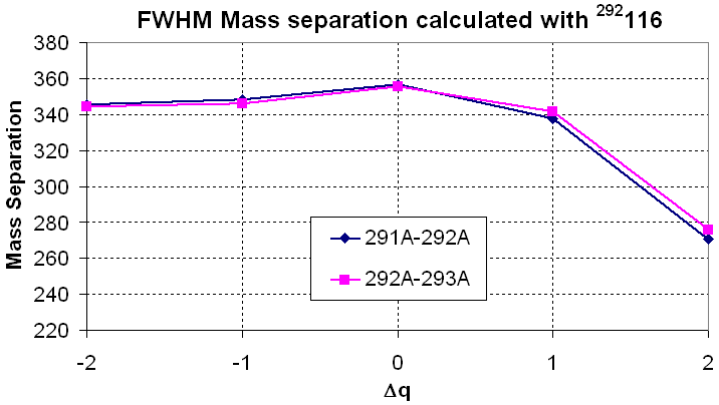

Figure 43: Preliminary mass resolving power using field maps of the new design of the MOSAR open multipoles, octupoles in the mass separator and the momentum achromat.

The 4-fold symmetry was relaxed for some of the latest calculations, substantially improving both the transmission and the mass resolving power achieved. The mass resolving power is now on the level of that previously achieved in TraceWin for hard edge element calculations.

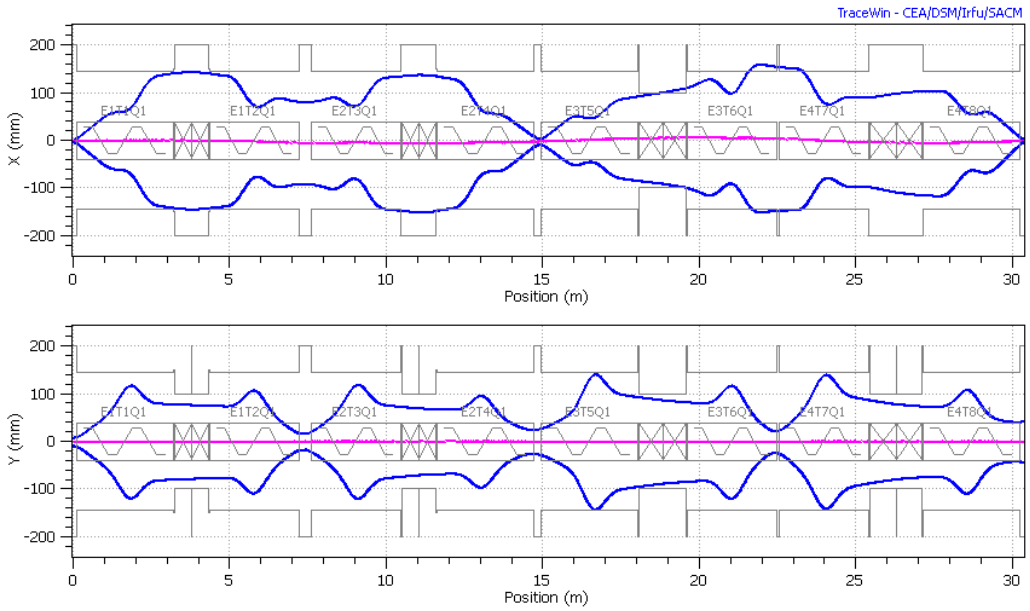

Figure 44: *^{100}Sn first order beam envelopes, in the horizontal (top) and the vertical (bottom) planes for a 2-fold symmetric lattice.*

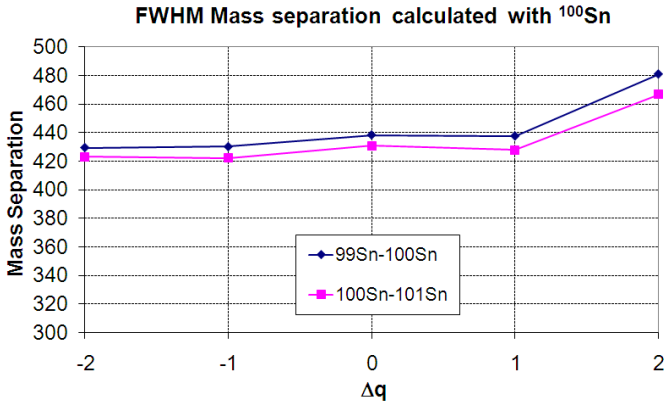

Figure 45: Mass resolving power using the latest MOSAR designs in a lattice preserving only 2-fold symmetry.

3.2.2.3 Ray tracing with Zgoubi

In order to avoid some of the limitations of the COSY map method and the ray tracing code TraceWin, additional optical simulations of S^3 have been performed using the ray-tracing code Zgoubi. This code has been used previously for the design of the large-acceptance VAMOS spectrometer presently in operation at GANIL. The all-order, experimental performance of VAMOS observed at commissioning was very close to that produced in the Zgoubi optical simulations during the design study. Zgoubi allows the use of realistic elements by including up to 3D field maps for all magnetic elements and 2D field maps for electric elements. In these models, magnetic dipole elements were approximated with Enge function fringe fields based on preliminary S^3 dipole designs, while other magnetic elements use 3D field maps (2D for first order calculations) and the electric dipole used a 2D midplane field map. Field maps from preliminary designs of the AML superconducting air-core multipole were used in triplets T1, and T4 through T8, while the GANIL room-temperature, open multipole field maps were used for triplets T2 and T3.

While the use of air-core elements results in non-standard fringe fields, it also produces a much more realistic optical model, since the necessary scaling and superposition of field maps of the various multipole orders is very close to reality, while a linear combination treatment is more approximate in the case of iron-dominated elements.

First-order system configurations were generated starting with Monte Carlo generated initial conditions. As in the fifth-order, parallelized COSY implementation used above, the optimization algorithm is a separate code using the MINUIT2 minimization package within the ROOT data analysis framework, which runs Zgoubi independently to calculate the system. The particular optimization method most used was the "Combined" method, which uses a combination of the Simplex and Migrad minimization algorithms.

So far only first-order calculations—full ray-tracing including only dipole and quadrupole elements—are being carried out in Zgoubi, in order to produce an optimized first-order lattice, taking into account the latest element field maps and mechanical design constraints. Once a first order system is optimized, field maps from correction elements will be superimposed and again optimized similarly to what was done in COSY and TraceWin.

The eight principal elements (four from each plane) of the first order transfer map generated by a single quadrupole magnet have been compared between Zgoubi—using a full 3D field map treatment—and COSY—using a symplectically scaled Enge or modified Enge function fringe field. The comparison was performed to gauge the ease of transition from COSY calculations to full field map calculations, and it provides a measure of the similarity of the COSY approximated elements to the true behavior observed in a full ray tracing treatment. The greater the difference between the first order behavior in the two models, the less dependable are the predictions of the COSY model: for quadrupole field settings, for acceptance and transmission calculations, and for aberration calculations and multipole correction tunes; note that all of the forgoing depend on the location of the first order rays in the system.

A comparison between Zgoubi and COSY was performed for both room-temperature iron-yoke quadrupoles and for superconducting air-core quadrupoles. It was found that the behavior of the room-temperature elements was reproduced much more accurately by the scaled Enge function fringe fields than was that of the superconducting air-core elements, notwithstanding the use of modified Enge functions for the air-core elements that reproduced well the quadrupole field strength along the element. So while the superposition of higher order elements is generally more correctly treated in ion optical models for air-core multipoles, the principal multipole—of fundamental importance in determining the system performances—is reproduced more accurately in COSY for iron-dominated elements. Thus the results of a COSY optimization based on the air-core elements considered here is generally less reliable—and therefore of less use in setting initial conditions for a Zgoubi calculation—than a COSY calculation based on iron-dominated elements.

The precision offered by Zgoubi calculations is rewarding, but also places higher demands on the quality of the field maps on which the calculations are based, by fully taking into account any field

uniformity issues or the presence of higher order harmonics in the current element designs. Zgoubi would be the first model yet to consider the effects of the electric dipole fringe fields in S^3. Presently, improvements are underway in the design of this element, what might be called a third generation preliminary design, to allow the S^3 model in Zgoubi to be developed further.

3.2.2.4 Method comparison

Of the codes used, Zgoubi allows the system to be treated with the greatest level of reality. The fieldmap based methods in general provide a far more realistic treatment of the optical elements, since field homogeneity over the full active volume of the elements is correctly treated and all harmonics present in real-world elements are included. This realistic treatment is especially important when considering the efficacy of various open multipole element designs to be used in the beam dump and boundary conditions of element designs, such as the plate edges of the electric dipole. Zgoubi allows all-order ray tracing through 3D field maps for magnetic elements but is presently limited to only 2D field maps for electric elements. Thus issues of field uniformity in the vertical plane arising from the upper and lower plate boundaries cannot be considered in the electric dipole. Ray tracing, by nature, is easily parallelizable and such a framework can be created for Zgoubi to speed system optimizations.

TraceWin is also a ray tracing code and thus has several of the advantages of Zgoubi. Having been originally produced for accelerator design applications, however, it has some limitations, which are inconvenient for modeling large-acceptance spectrometers. In particular, it does not treat the dipoles by ray tracing a magnetic fieldmap, which produces an incomplete picture of higher order behavior. Also, TraceWin includes space-charge effects and beam acceleration, which are incompatible with the use of negative drifts and forces the truncation of the fringes of field maps used to calculate the system.

COSY is capable of calculating systems at an arbitrary order of Taylor expansion and can include at least 2D field maps for realistic optical elements. In practice however, using ever increasing expansion order and more precise descriptions of optical elements—from Enge coefficient fringe fields, to z-dependent all-order multipoles, and finally to 2D field maps—results in prohibitively long map computation time. For example, calculating a fifth-order transfer map for a single quadrupole element using a symplectically scaled Enge function fringe field takes less than one second, while the same map calculation based on a 2D quadrupole field map takes more than 20 minutes.

In addition to generating the transfer maps, calculating the system performances in the Taylor expansion method requires evaluating the result of a large number of rays acted on by the system. At some point, after adding successively higher orders to the Taylor expansion, the mapping of a single ray through the Taylor expansion begins to take a comparable amount of computation as a full ray-tracing treatment. For example, a fifth-order COSY transfer map might have roughly 4000 non-zero coefficients, as compared to a 2D midplane fieldmap which might have roughly 6000 field values on a one-centimeter grid for a single magnetic multipole element. Also, the map method is more difficult to parallelize, since the computation is of a coarser granularity. Thus COSY is well suited to early stages of the design project, where higher order behavior is important (up to about fifth order), but before detailed element designs are being considered.

3.2.3 Ion-optical results

3.2.3.1 Description of the first-order lattices

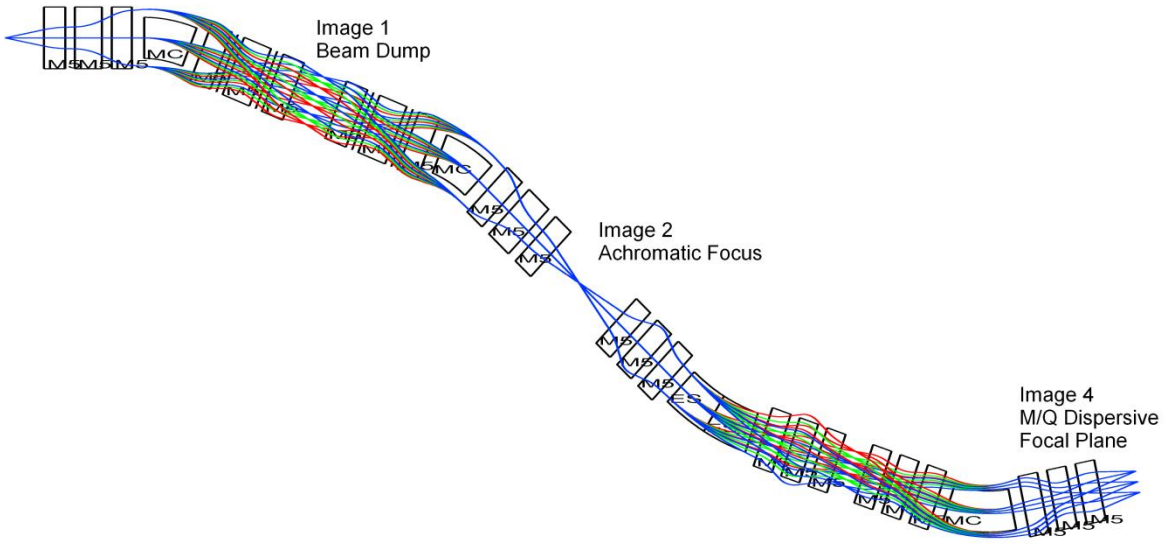

Figure 46: The room layout of an optimized S^3 lattice, overlaid with first order rays showing three horizontal angles, three charge states and three momenta (colors). The horizontal extent of the envelope is magnified by a factor of 4 from the actual size for the sake of visibility. In this case, room temperature elements—including a combined multipole triplet in the beam dump region—are used before Image 2 and superconducting elements after Image 2. This is the reduced symmetry version, with shorter drifts at Image 1 and Image 3 of roughly 1 m and 60 cm respectively.

Several first-order configurations of the MAMS concept were considered, motivated by mechanical space requirements at the object and image locations; the desired first order angular acceptance; the effects of magnification on resolution and transmission; practical issues of magnet technology; and some higher order phenomena. The system now consists of eight multipole triplets (T1 through T8), three magnetic dipoles and one electric dipole (D1 through D4). Multipole triplets were selected over quadruplets to preserve angular acceptance while increasing the drift space at some of the object and image locations.

Superconducting multipoles must be used in the second half of the system (triplets T5 through T8) because of the need for octupole correctors in these elements to achieve the desired M/Q resolving power. In the system shown above, which has been optimized with higher order corrections in COSY calculations, room-temperature elements have been used for the multipoles in the first half of S^3—the momentum achromat (triplets T1 through T4). Multipole field strengths used in the focusing and higher order correction of the system are consistent with the desired maximum magnetic rigidity of S^3 and the design limits of the elements themselves, according to ongoing consultations with the magnet design groups.

Minor changes to the first order lattice considered in higher order optimizations have been made to meet the mechanical requirements of the complete system. In particular, drift spaces about the electric and magnetic dipoles have been expanded to accommodate bellows and valves (see Section 3.1.3). Intra-triplet drifts of 20 cm between effective field boundaries have been used throughout the system, except in the case of room-temperature multipoles, where additional space would be needed—according to current room-temperature sextupole designs—to accommodate bellows to independently align the three sextupoles. The latest such updated designs use air-core, saddle coil superconducting triplets of AML type throughout (triplets T1 and T4 through T8), the open triplet (T2) of either room-temperature GANIL design or a superconducting MOSAR design, and the following triplet (T3) of either AML type, or symmetric to T2. In all cases considered, the momentum dispersion at Image 1 is 1.2 cm/% and the charge dispersion at Image 4 is 0.65 cm/%.

All of the first order lattices considered here are consistent with the physical constraints of the S3 room and the smaller production and beam dump rooms, including the need for space at Image 4 to place the low energy branch beam lines. One possible exception could be the separated sextupole solutions, which have so far been modeled only up to Image 2 and thus have not been considered as full systems in mechanical studies.

3.2.3.1.1 The beam dump - open multipole multiplet

The open multipoles to be used in the beam dump region (immediately before Image 1) present a particular challenge to the magnet designers. In any case, non-standard coil configurations will have to be used to allow the high-rigidity side of the triplet to be open to the beam dump. The non-standard coils will produce unwanted harmonic terms in the multipole field, whose effect on the beam dynamics may be difficult to quantify or control. In the case of superconducting elements, the open-sided cryostat and mechanical support structure of the coils will be additional difficulties. For room-temperature elements, the desired aperture and field gradient will put the elements already very close to the design limit for this technology, with the additional requirement of an open sided element exacerbating any existing saturation issues and creating additional field uniformity issues.

Much of the difficulty of open-sided elements could be avoided by separating the two multipole components, i.e. following the first dipole with a pentuplet or sextuplet consisting of alternating pure quadrupole and sextupole elements rather than a triplet with quadrupole and sextupole components superimposed in each element. The open sextupoles in this case would have better field uniformity. Saturation issues would be eliminated entirely for the separated sextupole solution since the separation between quadrupoles reduces the field strength necessary to achieve the first order focus at Image 1, while the sextupole field would be spatially separated from the nearly saturated quadrupole iron (for high rigidity settings).

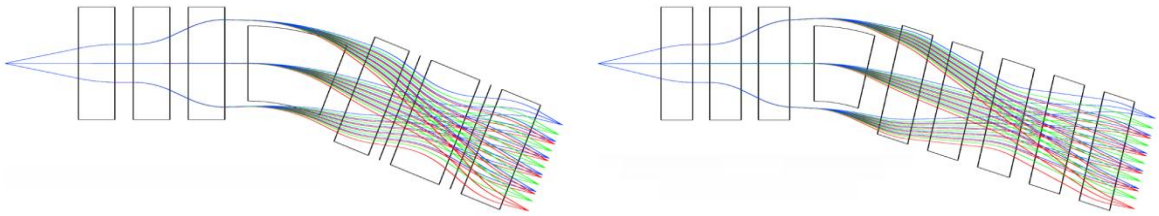

Figure 47: Two options for the first unit of S3, before the dispersive focus on the beam dump at Image 1. The combined multipole option (left) is more compact, but more challenging to build and more likely to suffer from saturation effects and poor sextupole field uniformity. The separated sextupole option (right) allows fewer sextupole degrees of freedom but with stronger, cleaner sextupole fields.

The Q-S-Q-S-Q configuration was tested and performed well in first-order. Losses in first-order angular acceptance were minor, with values achieved above +/- 60 mrad in both planes. In higher order COSY calculations however, the separated sextupole pentuplet solution proved unable to provide adequate correction of optical aberrations, even though the allowed sextupole strength was considerably increased, and the mirror symmetry with the closed pentuplet in the second half of the momentum achromat allowed stronger higher order corrections and more degrees of freedom than the combined open multipole triplet option.

The S-Q-S-Q-S-Q configuration for the beam dump multiplet has so far only been considered in first order. It provides good angular acceptance in both standard and high-acceptance (see Section 3.2.3.4.2) modes but would present some difficulties related to magnification and space, as will be discussed below. In higher orders the sextuplet option might be expected to perform better than the pentuplet option, having both more correction strength and more sextupole degrees of freedom, although the extended length of the system would also be expected to increase aberrations.

The extended second triplet of the separated sextupole systems also results in greater compression of both horizontal and vertical angles, with Image 1 angular magnifications in horizontal and vertical planes of -0.70 and -0.65 respectively for the pentuplet option and similarly -0.47 and -0.39 for the sextuplet option. Though compression of the angles in the early stages of S3 is advantageous in that it

improves angular acceptance of the full system, it will also result in increased first-order spot sizes at the images and—in the case of the horizontal plane—it will reduce resolution both at the beam dump fingers at Image 1 and at the M/Q selection slits at Image 4.

It is not entirely possible to design S^3 to perform as well regardless of these large angular compressions. The momentum dispersion at Image 1 cannot be increased to fully compensate for the magnification effect because of the limited size of the multipole apertures and the desired momentum and charge state acceptances. Therefore, it would be necessary to expand the beam blocking fingers at Image 1 proportionally to reject the primary beam at the same level, resulting in reduced transmission of the products of interest for experiments where the primary beam charge states fall within the momentum acceptance. The second half of the momentum achromat—between Image 1 and Image 2—could be extended to preserve unit magnification at Image 4 and thereby preserve the M/Q resolving power of the system, but the added length would leave little free space after Image 4 for placement of the low energy branch.

Generally speaking, angular compression at Image 1 (with $|(a|a)| < 1$ or $|(b|b)| < 1$) would help to reduce transmission of scattered particles from the beam dump region by magnifying any scattering angles produced there, while also increasing the first order vertical spot size (since $|(y|y)|$ would be greater than one), which would reduce thermal strain on the beam dump fingers. At the same time, however, $|(x|x)| > 1$ would reduce the momentum resolution at the beam dump location and emittance growth in an Image 1 degrader—for settings including a degrader there—would be exacerbated in both planes.

3.2.3.1.2 Symmetry

The degree of symmetry to be preserved in the first-order lattice needs also be decided. Expanded drifts at the object point, Image 2, and Image 4 do not necessarily require expanded drifts at Image 1 and Image 3. Neither do longer multipoles in the second multiplet (the open element in the beam dump region) necessarily require a symmetric expansion of any other multiplet(s). While maintaining first-order symmetry tends to reduce higher order optical aberrations, increasing the compactness of the system also tends to reduce aberrations. Higher order implications will be discussed further in the following section (Section 3.2.3.2). Furthermore, the maximum usable space about the final focal plane—for the placement of the high-resolution mass separator among other equipment—is achieved by producing a shorter system and thus by not expanding the Image 1 and Image 3 drifts, or the other multiplets, symmetrically with the other dimensions of the system. Tuning a symmetric system is simpler, but the angular and energy acceptance of a more symmetric system is less flat (i.e. the angular acceptance for particles of non-central momenta and M/Q drops more quickly).

The current optimized system preserves only 2-fold symmetry in the first half of the system, on either side of Image 1, providing a unit magnification to the intermediate achromatic image. It may be advantageous, as discussed above, to use a shorter triplet immediately after Image 1 rather than building a closed multiplet symmetric with the open multiplet. First order calculations have been carried out with various asymmetric systems to determine the probable resulting magnification at Image 2. In the standard mode optics (i.e. with the target 80 cm from the entrance to the first quadrupole of S^3) an asymmetric third triplet expands horizontal angles, with an angular magnification of 1.12, while compressing vertical angles, with a magnification of 0.8.

The horizontal angular magnification will shrink the beam spot at Image 2 and Image 4, reducing the needed Image 2 aperture and improving the final M/Q resolution for a given mass dispersion; at the same time, the horizontal angular acceptance of the full system will be reduced by the expanded envelope in the second half of the system. The vertical angular magnification will increase the vertical angular acceptance of the second half of the system; at the same time the beam spot size at Image 2 and Image 4 will be increased, which will increase the necessary size of the Image 2 aperture and the filling of the vertical space of the Image 4 detectors. Increasing the vertical angular acceptance in the second half of S^3 does little to improve performance in a standard mode in first order, since the first order angular acceptance of the first half is roughly equal to that of the second half, but given that mounting aberrations could progressively increase the vertical envelope as it travels through S^3, it

could be beneficial to have a larger angular acceptance in the second half of the system. This could also help increase transmission when performing two-step studies, with a reaction target placed at Image 2, which would increase the emittance in the second half of the system.

The consequences of first order symmetry about Image 1 for the high-acceptance mode (see Section 3.2.3.4.2 for a general description) are slightly different. In this case the vertical angles are already compressed at Image 1 and Image 2 to provide expanded vertical angular acceptance in the unaltered system beyond Image 1. Asymmetric T2 and T3 increase the compression of vertical angles by an additional 10% to 20%, which will provide a vertical angular acceptance in the remainder of the system significantly larger than that provided by the first unit of S^3. The horizontal angular magnification on the other hand is reduced about 10%, then roughly equal to unity at Image 2.

3.2.3.2 Higher order considerations

As a large acceptance, high resolution separator spectrometer, the performance of S^3 will be determined by its higher order optical properties. The all order system should provide:

- a small beam spot for primary beam like particles at Image 1 to reduce primary beam particle rates by at least a factor of 10^3 while minimizing losses of the nuclei of interest;
- a small product distribution at Image 2 to allow a small aperture to pass a large proportion of the nuclei of interest while efficiently rejecting scattered particles;
- a high M/Q resolving power at Image 4 to physically separate the nuclei of interest from the majority of non-isobar contaminants; and
- high transmission of the products produced in the reaction target—more than 50% of the full charge state distribution for the two baseline experimental cases (see Sections 2.2.1 and 2.2.2)—requiring both a large angular acceptance and large charge state and momentum acceptances for the low energy fusion-evaporation production mechanism to be chiefly used.

While the first three of these requirements depend on the all-order transfer map from the object to a particular image location, the fourth—the transmission requirement—depends on the optical aberrations throughout the system and is thus the most challenging.

It may be tempting to think of S^3 as being composed of two separable systems, the momentum achromat and the M/Q separator, joined at the intermediate achromatic image (Image 2). The reality, however, is that higher order aberration terms propagate through the full system starting from the target position, so the two halves may only be considered separately in a first-order approximation. Thus, maintaining versatility in the second half of the system will require all, or very nearly all, of the higher order correction elements to be adjustable throughout the system (as opposed to fixed corrections built into curved dipole faces or shaped quadrupole iron). Curved dipole entrance and exit boundaries could be used to add higher-order corrections, which may be especially useful about the beam dump where higher order correction elements will be more limited in both number and strength. Quadrupole poletips, if present, could also be shaped to include some fraction of higher-order correction terms—as was done in VAMOS, for example—but this would limit tune flexibility. If static corrections prove to be necessary, extensive modeling work should be undertaken to demonstrate their compatibility with the wide variety of operating modes envisaged for S^3 (see Section 3.2.3.4). So far, model results indicate that the desired mass resolving power can be reached without using any such fixed corrections.

Because of this strong coupling of the full system, correction elements at the beginning of S^3 must be tuned to produce the optimum balance among the size of aberrations for primary-beam-like particles at the beam dump and the sizes of aberrations for product-like particles at the intermediate achromatic image and the M/Q dispersive final focal plane. In highly asymmetric fusion production cases, when the primary beam charge states do not fall within the momentum acceptance, the aberrations for primary-beam-like particles at the beam dump are inconsequential and could be ignored. In two-step

reaction experiments, the reduction of aberrations at the secondary reaction target at Image 2 may be of particular importance. In heavy and superheavy element studies, high M/Q resolution at Image 4 will be of particular importance, though it will also be necessary to keep a small aperture at Image 2 to reduce the transmission of scattered particles to the Image 4. In each case, specialized correction tunes could be used to make the best use of the available higher-order strength to correct aberrations intelligently, according to need.

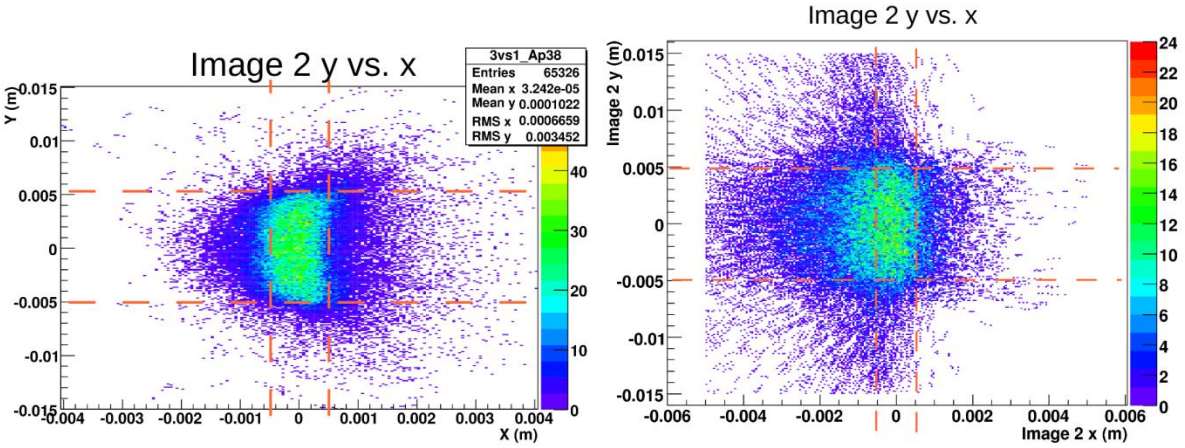

Figure 48: Particle distribution at the intermediate achromatic image (Image 2) after optimizing corrections in the momentum achromat only up to Image 2 (left) and after re-optimizing the full system to achieve M/Q resolving power at the final focal plane (right). The orange dashed lines indicate the size of the initial beam spot, the full-width of the uniform vertical distribution and one sigma of the Gaussian horizontal distribution.

Correction elements will necessarily be of limited strength, and correction tunes should generally be designed to allow high-resolution operation up to the full system rigidity of 1.8 Tm. So far, all of the correction tunes have been designed to be used up to the full system rigidity. Since much of the experimental program will be carried out at much lower rigidities, however, it could also be useful to develop stronger correction tunes that could only be used for lower rigidity settings.

Aberration correction at Image 1, and even at Image 2, is complicated by the need for open-sided multipole elements following the first dipole. A separated-sextupole solution would remove the complication of producing combined, open multipole elements and permit a considerably larger maximum field derivative in the sextupole correctors (see Figure 47), but so far, two separated, open sextupole elements placed in the second triplet have proved unable to correct the aberrations to the intermediate achromatic focus. This is possibly due to the reduced degrees of freedom offered by the one fewer sextupole between the first dipole and Image 1. If so, introducing curvature in the entrance and exit faces of the first dipole could provide sufficient sextupole correction strength to replace the lost degree of freedom; an additional physical separated sextupole could also be added between the dipole and the first open quadrupole to provide this correction. These two further solutions have yet to be investigated in higher order calculations.

More symmetric ion optical systems generally exhibit reduced image aberrations. At the same time, more compact systems also tend to produce reduced aberrations. In the design of S^3, symmetry and compactness are in competition. In the second half of S^3 (the M/Q separator), the maximum symmetry that can be achieved is 2-fold, about the centers of the electric and magnetic dipoles in the third and fourth quarters of the system respectively. In the first half of S^3 (the momentum achromat), 2-fold or 4-fold symmetry would be possible. The unique requirements of the beam dump area between the first dipole and the dispersive image (Image 1) place unique technical demands on the second multipole triplet, which are not shared by the other three triplets in the momentum achromat. Also, the free spaces required after the production target, about the dispersive image (Image 1), and before the achromatic image (Image 2) are not necessarily the same.

The free space required after the production target is likely less than 80cm. Reduced drift space between the production target and the first multipole would improve the angular acceptance of the system. The space required at Image 1 will depend on detailed designs of the high-power, multi-finger

beam dump system and its associated fixed and movable shielding, whose dimensions have yet to be determined, but reduced drifts about Image 1 would clearly improve first-order angular acceptance. Free space before Image 2 would be valuable to enable the placement of high-efficiency gamma-ray and charged particle detector arrays at this point, for experiments in which a secondary target will be placed there.

Thus, a fully symmetric momentum achromat would mean unnecessarily expanding the drift after the production target and about the beam dump to match the large drift desired at Image 2 and similarly expanding the physical size of all four multipole triplets to that required for the open-sided element. While the symmetric system clearly is disadvantageous in terms of space and material cost, the difference in terms of optical performance is not self-evident. Looking at the RMS aberrations present at the end of the momentum achromat at each order and in both the vertical and horizontal planes for system configurations of increasing symmetry (see Figure 49) suggests that in this case, increasing symmetry increases the total optical aberrations. Similar results are seen if the total aberrations are considered more holistically by looking at the uncorrected achromatic spot size produced at Image 2.

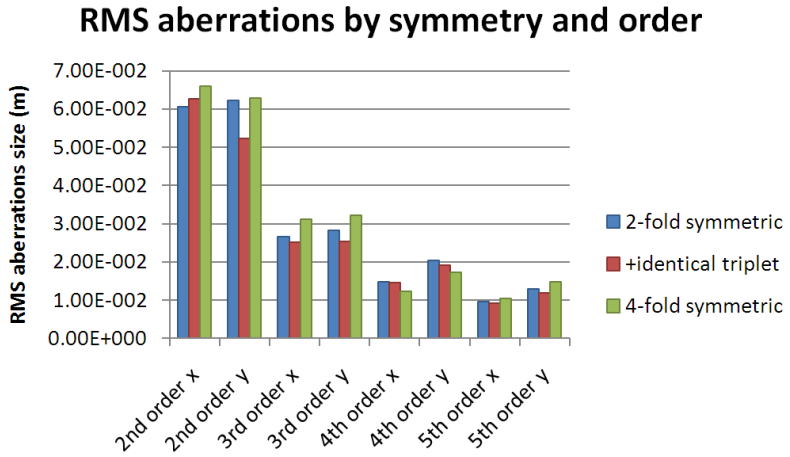

Figure 49: The root of the sum of squared aberrations at Image 2 by order and plane are shown for three, increasing degrees of symmetry in the momentum achromat. These are the initial aberrations before any corrections are applied. The longer, 4-fold symmetric system produced larger total aberrations.

We may also consider breaking the 2-fold symmetry about Image 1 in favor of a more compact multipole triplet following the beam dump, but breaking the 2-fold symmetry might over complicate operational tuning of S^3. The issue of 2-fold symmetry in the first half of S^3 is discussed in more detail in Section 3.2.3.1.2.

Significant higher order harmonics are present in the magnetic multipoles to be used in the system (e.g. see Figure 26). While further optimization of the designs will improve the field purity, the unwanted harmonics cannot be removed completely. More correct treatment of the evolution of the position dependent strengths of the multiple harmonics present in any given multipole requires the use of more generalized routines in COSY or, for a truly realistic treatment, the use of full 3D field map based ray tracing codes such as Zgoubi.

Multiple attempts to produce a system including only sextupole correction elements that meets all the design specifications (chief among them the M/Q resolving power) have proven unsuccessful. Thus, octupole corrections will be needed, at least in the second half of S^3 (the mass separator). Because the proposed room temperature, large-aperture combined quadrupole and sextupole elements are already at the limit of the capability of room temperature magnet technology, this implies the use of superconducting multipoles in this part of the system. Adding octupole correction elements to the momentum achromat so far does not seem to improve the M/Q resolution significantly, unless octupoles may also be included in the second triplet. Adjustable octupole correctors could not be included in the proposed room temperature open multipoles, but may be able to be included in the MOSAR superconducting open multipole, pending further progress on the next generation of the conceptual design of MOSAR.

Open multipoles that produce a sextupole field by using various configurations of dipole coils of opposite polarity—such as the Super-ACO type or the present, more advanced, room-temperature open sextupole discussed in the following chapter—will excite not only higher order multipoles, but will also produce residual dipole components. The coil configuration may be designed such that the integral of the dipole field along the optic axis is zero or such that the dipole field is zero at the center of the element, but both conditions cannot be satisfied at once. Furthermore, the integral—or the central value—of the strength of the dipole component depends on the radius chosen for the harmonic analysis, so neither can the integral of the dipole component be zero at all radii within the multipole. In any case, the residual dipole component will produce steering in the open multipoles which will shift central rays off of the optic axis and may result in undesirable behavior, including degraded M/Q resolving power and reduced beam rejection efficiency. The all-order resolving powers based on field maps of various open sextupole designs are given in several figures of Section 3.2.2.2. For the cases shown, the performance of the superconducting elements is significantly better than the room-temperature multipoles, although room-temperature elements with significantly improved field quality and reduced dipole component have yet to be similarly evaluated.

The methods of modeling the fringe fields of the elements of S^3 in each case are discussed in the sections above addressed to the application of specific ion optical codes to S^3.

3.2.3.3 Transmission and resolving power for the nuclei of interest

The more approximate methods of modeling have shown great success at meeting the specified system performances for S^3. Specifically this has been achieved using hard-edge, all-order ray tracing models and Enge fringe-field, third-order Taylor expansions. More than 50% of the full charge state distribution was transmitted by the system, both for the ^{100}Sn and superheavy element production baseline experimental cases, and M/Q resolving power specifications are met across the full charge state acceptance (i.e. for all 5 charge states in both cases). Early work with un-optimized, fifth-order Taylor expansions also produces encouraging results (Figure 30). Most promising, TraceWin calculations of a new two-fold symmetric layout—again including realistic multipole field maps—now give mass resolving powers above 400 across the full M/Q acceptance (Figure 45). Though, the challenge remains to meet the specified performances when adding realistic electric and magnetic dipole elements in full field-map-based ray tracing simulations. Thus, the task is two-fold: first, to design and construct elements of sufficient field quality—particularly the open multipole triplet and the electric dipole—and second, to design an optical lattice capable of achieving the desired system performances with elements of whatever field quality can finally be achieved. Specific results for particular optimized lattices were given above, according to the model used, in Sections 3.2.2.1 and 3.2.2.2.

3.2.3.4 Alternate optical modes

S^3 is a multipurpose device and as such will operate in a variety of optical modes optimized for particular experimental conditions. The high-resolution mode is the primary operating mode that has been the subject of detailed higher order optimizations discussed elsewhere in this report. Alternate optical modes have so far only been considered in first-order calculations and only for those experimental settings expected to be most useful to the users. Higher order studies will be needed to determine their actual feasibility and the system performances under these conditions.

While it may be possible to produce alternate first order tunes by adding additional optical devices after the final focal plane of S^3 (i.e. a refocusing section), the presence of a high-resolution mass analyzer after Image 4 leaves little space for such additions, and so the discussions in this section will be limited to what can be achieved with only the standard S^3 device between the object and Image 4.

3.2.3.4.1 Converging charge states mode

The standard S^3 detection is designed to accommodate a focal plane of 20 cm in the horizontal direction by 10 cm in the vertical direction. In some cases it may be advantageous to reduce the size of the final focal plane. A smaller focal plane would allow the transmitted particles to be collected

within a smaller detector or gas cell entrance window, but would likely require a reduced M/Q dispersion and consequently a reduced M/Q resolving power. In the case of an ANL type gas cell (Q = 1+ extraction), the total gas volume and thus the size of the entrance window is not critical. In the case of a LISOL type gas cell, however, the extraction efficiency depends critically on the total gas volume, since all of the extracted gas must pass through a narrow region to allow for efficient laser ionization of the neutralized products. Thus, the focal plane distribution should be as small as possible to minimize the required area of the entrance window.

The ideal tune for a LISOL type gas cell mode would have no M/Q dispersion at the gas cell entrance window—allowing the smallest possible gas volume—but would preserve some M/Q resolving power by producing an M/Q dispersive image at some earlier point in the system. This would allow some reduction in the total particle rate entering the gas cell. We refer to such a setting as a "converging-charge-states" mode, since the different charge states of the transmitted products are dispersed at some point but are converging at that point so as to reach a non-dispersive condition soon after. See Figure 50 for a comparison of the two settings.

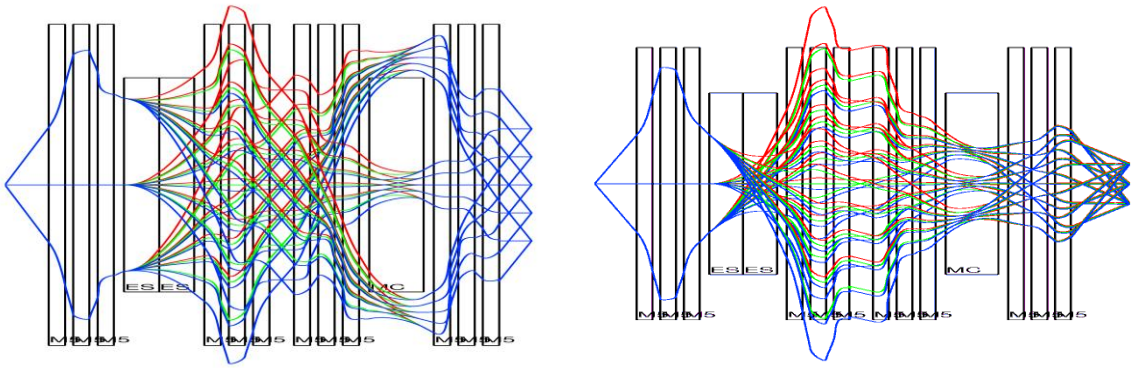

Figure 50: Horizontal space plots of the second half of S³ for the standard, high-resolution mode (left) and the converging-charge-states mode (right). The optic axis has been straightened for the sake of clarity and rays are plotted for three horizontal angles, three momenta and five charge states. In the standard mode the five charge states are dispersed and approach Image 4 parallel to one another. In the converging-charge-states mode the M/Q dispersive plane is much closer to the exit of the last multipole and the five charge states have converging angles at this point. The final spot-size depends purely on the width of the angular distribution.

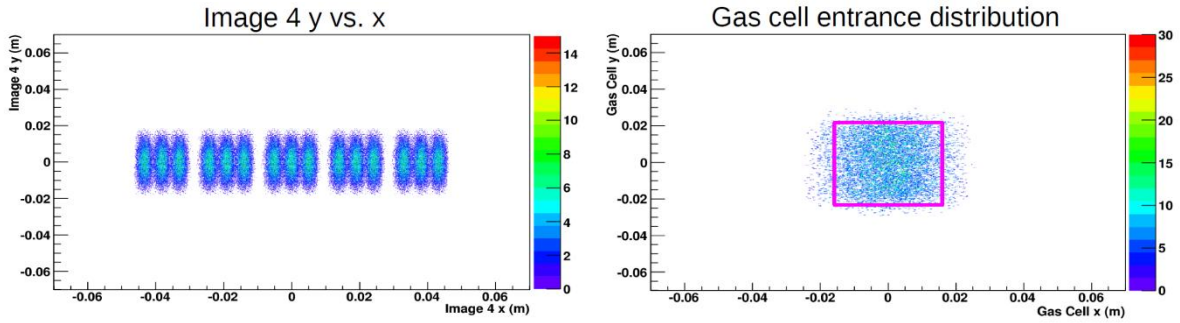

Figure 51: Particle distributions in first-order Monte Carlo calculations of the converging-charge-states mode at the M/Q dispersive image (left) and at the position of the gas cell entrance window (right). The magenta square indicates the width of 94% of the distribution in each plane and has dimensions of 3.3 cm horizontally by 4.2 cm vertically.

In the case of certain stopped decay spectroscopy experiments to be performed at Image 4, it will be desirable to preserve M/Q selectivity as far as possible while fitting the full charge state acceptance within a single implantation detector. This would allow a more compact, and thus more efficient, configuration of surrounding charged particle and gamma ray detectors. Such experiments could make use of this mode or an intermediate setting between this and the standard high-resolution mode with a moderately reduced focal plane size and a better M/Q resolution.

3.2.3.4.2 High-acceptance mode

A high-acceptance mode would be useful for products with a particularly large angular divergence, e.g. $^{22}Ne + ^{238}U \rightarrow ^{255}No + 5n$. This mode would reduce the beam envelope within the system as much as possible to increase the angular as well as momentum (and therefore charge state) acceptance of the final system. The enhanced angular acceptance is most easily produced by moving the production target closer to the first optical element of S^3. Retuning the first two triplets to again provide a dispersive focus at Image 1 produces a system up to that point with a similar horizontal angular acceptance but an increased vertical angular acceptance of roughly +/- 100 mrad. At the same time, the vertical angles are slightly compressed at Image 1—as compared to the standard mode—such that this larger vertical envelope will be transmitted through the rest of S^3 without the need for any physical alterations to the downstream elements. This magnification will increase the vertical spot size at the final focal plane by roughly 30%, but this would seem to be of little consequence.

In this case, the momentum dispersion at Image 1 is kept fixed, such that the quadrupole settings through the rest of S^3 are identical to those of the standard high-resolution mode. It may also be possible to reduce the dispersion at Image 1, which would increase the momentum and charge state acceptance of the first half of S^3. The horizontal angular magnification at Image 1 is very nearly the same as in the high-resolution mode, providing a magnification at Image 4 very close to unity and thus preserving the potential for high M/Q resolving power. Higher order multipoles will need to be adjusted for this mode, however, meaning that the final M/Q resolution achievable—or the maximum magnetic rigidity for which a given resolution may be achieved—may be slightly different than for the standard mode.

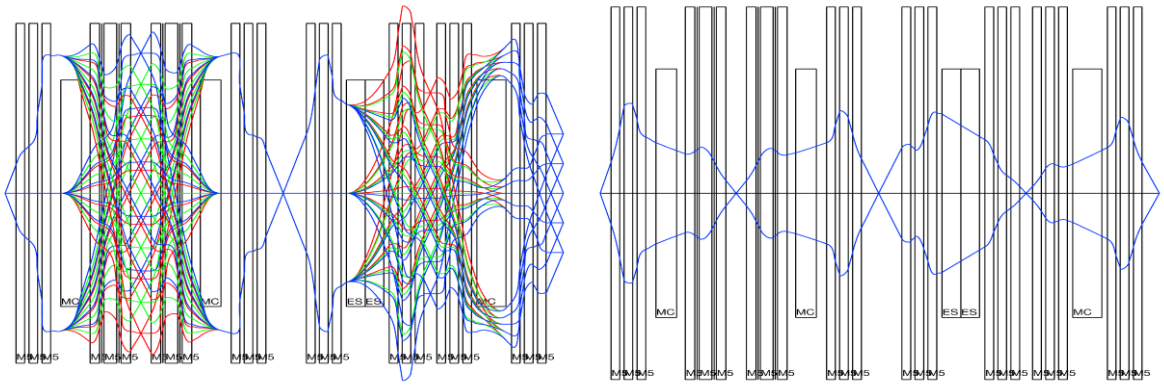

Figure 52: Horizontal (left) and vertical (right) space plots of the full S^3 system for the high-acceptance mode. Rays are plotted for three horizontal angles, two vertical angles, three momenta and five charge states. The extreme angles shown are +/-50 mrad in both planes and the element apertures are shown correctly, except for the vertical space in the third dipole (the electric dipole) which is actually equal to the vertical aperture of the neighboring multipoles.

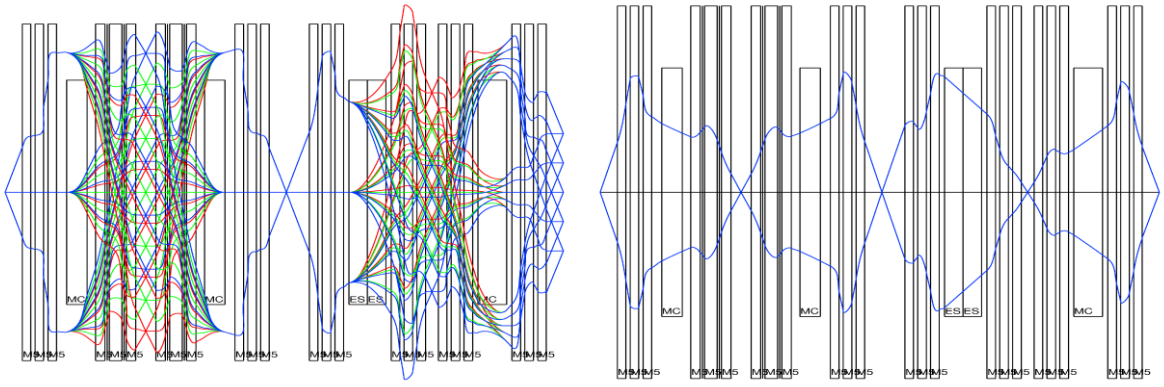

Figure 53: For comparison to Figure 52, similar horizontal and vertical space plots for the standard, high-resolution mode. Note particularly the global expansion of the vertical envelope.

3.2.3.5 Primary beam rejection

The very intense projectile beams of 10pμA or more provided by LINAG must be managed carefully to protect the many sensitive downstream elements along the S³ beam line, including the electric dipole which is required for the high mass resolution. Hence, the goal of the momentum achromat is to perform a preliminary rejection of the beam, such that 0.1% or less of the beam will be transmitted to the mass spectrometer. We have studied the beam trajectory for the direct (Z = 116) and symmetric (^{100}Sn) fusion kinematics (*Figure 54* and *Figure 55*).

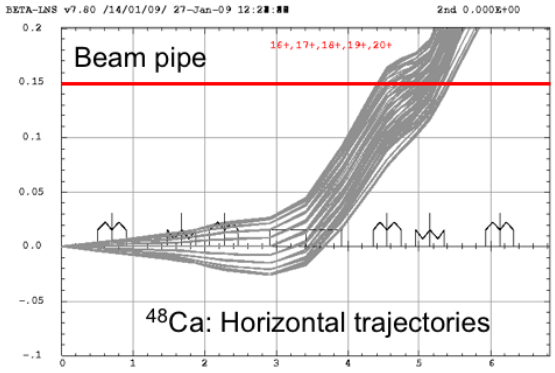

Figure 54: All order beam trajectories between the target and the beam dump for direct kinematics: $^{48}Ca+^{248}Cm \rightarrow ^{292}116+4n$.

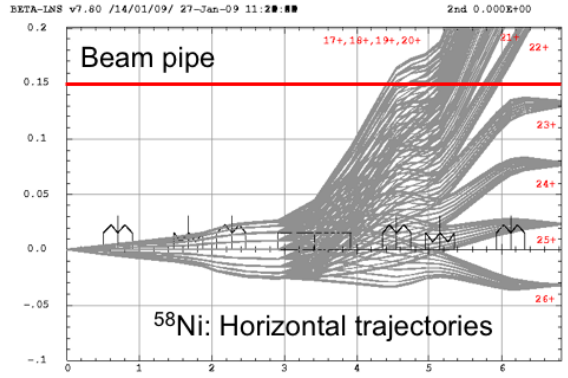

Figure 55: All order beam trajectories between the target and the beam dump for symmetric kinematics $^{58}Ni+^{46}Ti \rightarrow ^{100}Sn+4n$.

According to these simulations, the beam would be stopped in two main sectors:

- Outside the beam pipe, after going through the first multiplet located after the first dipole. In the direct kinematics (SHE production, for example ^{292}116) case, 100% of the beam impinges in this zone. In the ^{100}Sn setting, 73% of the ^{58}Ni primary beam would be stopped in this region. A beam stopper is necessary to protect this area. The magnets of this multiplet have to be 'open' in order to allow the beam extraction.

- At the intermediate focal plane of the momentum achromat, at several well-defined points, depending on the projectile charge-state. 27% of the primary beam would be stopped in this region in the ^{100}Sn setting. Water-cooled fingers with a width of about 1cm can be inserted at each of these positions (which vary according to the kinematics). Each finger would stop up to a few tens of % of the projectile beam. Transmission simulations show that the presence of fingers with a horizontal width of 1 cm in this focal plane would cause a loss of 19% of the ^{100}Sn evaporation residues.

The distribution of ^{58}Ni charge-states at the intermediate focal plane is shown in *Figure 56*.

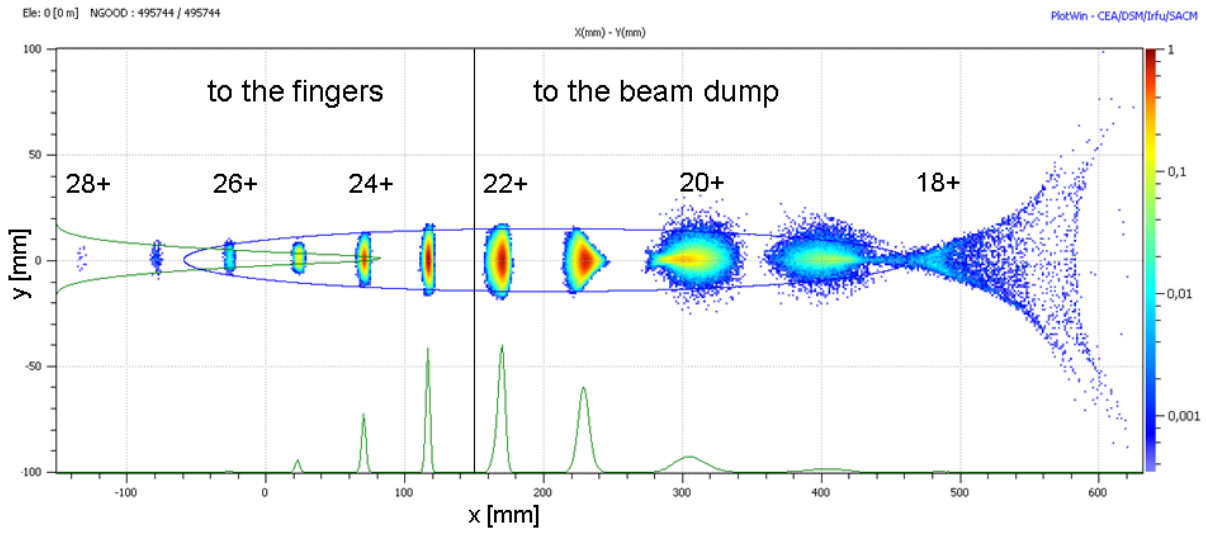

Figure 56: Charge-state distribution of the ^{58}Ni beam at the intermediate focal plane. The beam pipe area limit at x = +150 mm is indicated by a black line. The more positive horizontal positions correspond to higher rigidities.

In the beam pipe area, the distributions are well defined, as the projectile beam has a small momentum and angular distribution. The maximum area necessary for a finger to stop each charge state is around (10 x 20) mm^2.

The charge states going outside the spectrometer acceptance have a much less defined distribution because they travel through the vertical gap of the open magnets, where the field is no longer quadrupolar. Therefore they can have a very large horizontal and vertical distribution when hitting the beam dump. In the case of ^{58}Ni this is less critical because the most exotic charge-states are weakly populated, but with very asymmetric fusion reactions it could be more problematic. The beam dump should have a total height of about 400 mm.

A small collimator will be placed at the image point of the momentum achromat to remove most of the scattered ions. After this first stage of primary beam rejection (Image 1 plus Image 2), the beam counting rate is reduced to a tolerable fraction that can acceptably impinge on the electrode of the mass spectrometer. This is where the majority of the remaining primary beam particles will be lost, given their dramatically different electric rigidity from that of the residues of interest. The high resolving power of the mass spectrometer is then used to suppress all the evaporation residues with masses close to the nuclei of interest.

3.2.4 Summary

The design presented here achieves a combination of beam suppression, evaporation residue transmission and mass channel selection unique in the world. It will allow for unique experiments like in-flight mass measurement of superheavy elements, or studies of very weak evaporation channels (^{100}Sn like). It has a two-stage selection (magnetic rigidity and mass) that will achieve very good rejection of both the beam and adjacent mass channels of reaction products. It is especially optimized for fusion evaporation reactions in direct and symmetric kinematics and the delayed study of rare channels.

In some experiments where the momentum selection is sufficient (e.g. transfer on light nuclei), the first momentum achromat part can be used as a standard magnetic spectrometer with the final focal point used for a secondary target.

4 Hardware Designs

4.1 Room temperature multiplet option

4.1.1 Closed multipole (standard configuration)

In order to have a good mass resolution combined with a high acceptance, it is necessary to correct optical aberrations. As mentioned previously, the multipoles combine quadrupole and sextupole fields for this purpose. Room temperature (RT), iron-dominated, magnets are a proven solution for high performance, low energy nuclear physics instruments due to the quality of the field produced and their low maintenance profile. Room temperature magnets have been extensively used at GANIL and in the plans for SPIRAL2, and the infrastructure has been planned to power and cool this type of magnets.

In the closed solution studied:

- The quadrupole field is produced by shaping the iron pole with a hyperbola.

  The gradient is made homogeneous for the different radii by adjusting this shape. The pole is chamfered in order to adjust the magnetic length.

- The sextupole is made of six “air core” coils, wound on the vacuum chamber (see ***Figure 57***). The feasibility of this solution is being investigated together with an industrial company which is finishing a prototype, in order to check the winding position precision, and the resulting thickness (see Figure 58). There is only a limited interaction between the two fields in the iron but additional dipolar coils are necessary to cancel out a small dipolar field produced by the interaction of SX with the iron. These coils are only low power correctors.

- Octupoles of significant strength (90 T/m^3) cannot be included due to the limited current density available in standard conductors.

- It is possible to adjust the length (and thereby the effective length) of the coils according to the demands of the optics and mechanical space requirements.

- The alignment of the two magnetic axes will be done mechanically.

The resulting multipole has been used successfully in optical simulations of the momentum achromat portion of the separator.

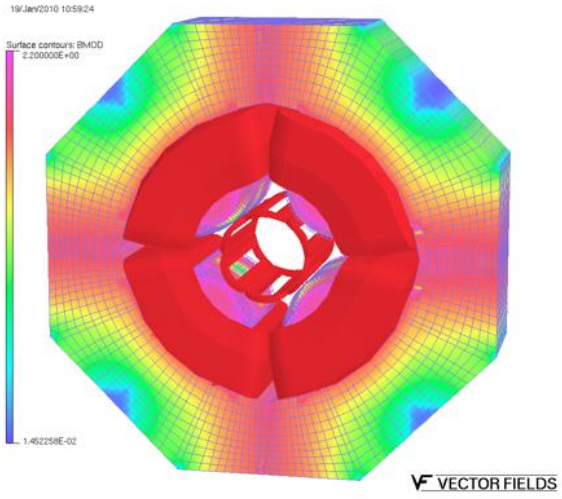

Figure 57: Room-temperature closed multipole, including quadrupole and sextupole components.

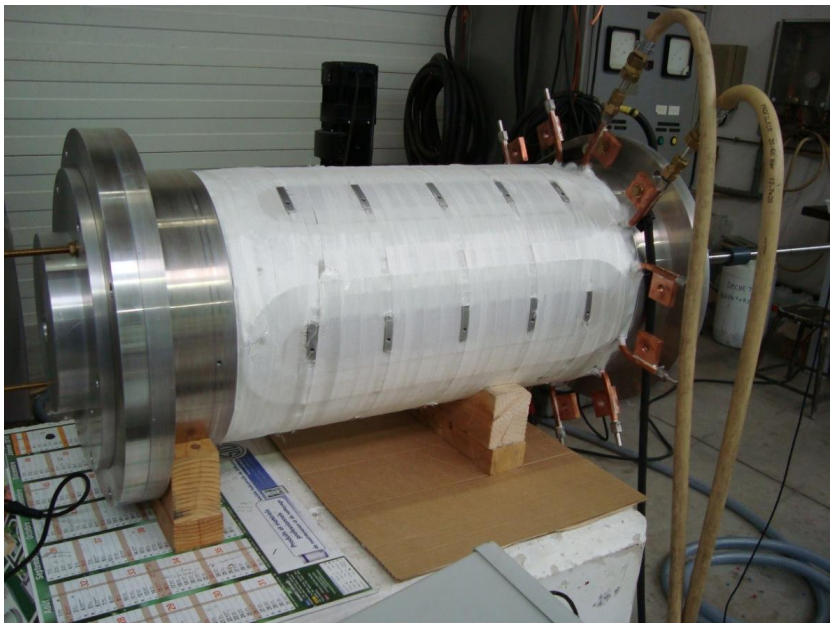

Figure 58: Room-temperature, closed sextupole prototype.

4.1.2 Open multipole (GANIL design)

For the multipole triplet in the beam dump region, a second-generation, open-sided solution has been designed, minimizing the dipolar effects found in the previous solution (i.e. the SuperACO like solution). This open room temperature solution uses a combination of two dipolar coils—both in close proximity to the beam pipe—to create a kind of sextupole field. The curves below (see Figure 59) show how the sextupole is created. Green and blue represent the fields of the two dipole coils, and the solid black curve shows the resulting sextupole field. The red, dot-dashed curve shows the theoretical ideal sextupole field for the sake of comparison.

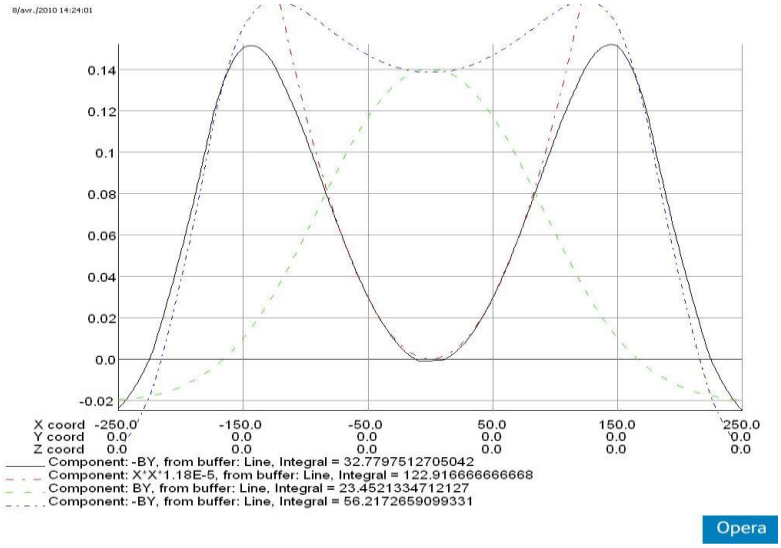

Figure 59: Comparison of an ideal sextupole and the GANIL room-temperature open sextupole. The good field region extends, in this case, to around 100mm.

This design has yet to be fully optimized, but the result will remain in some ways significantly different from an ideal sextupole field. The shapes and lengths of the two coils will be adjusted to minimize the residual dipolar effect. This design will require high current density in the coils, and significant power.

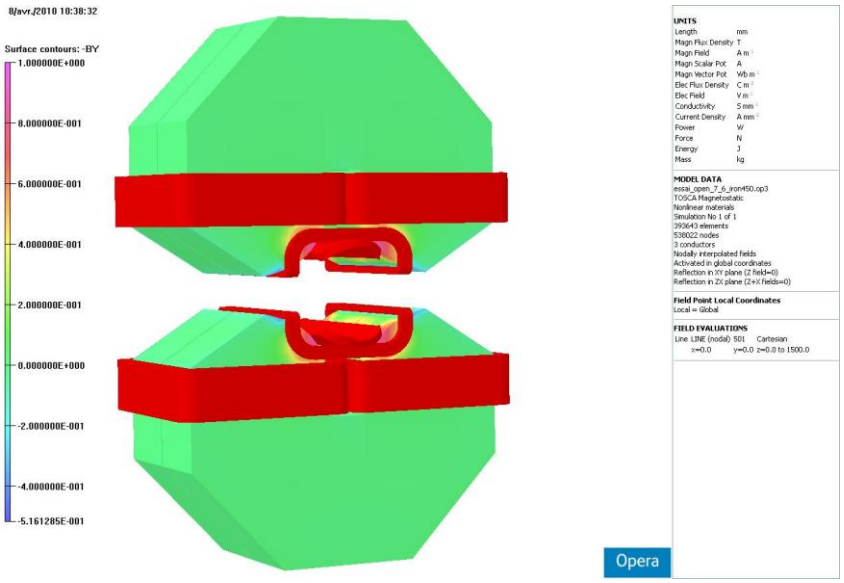

Figure 60: The GANIL room-temperature, open multipole, including quadrupole and sextupole components.

Different lengths of the room temperature multipole designs—both closed and open—have been modeled and studied in different optical solutions.

4.1.3 Open multipole (Saclay design)

The quadrupole design was developed with an approach similar to that of the GANIL closed quadrupole design, except that a return leg is added; the open sextupole field is produced with one dipole coil near the beam pipe and the other on this return leg. The first studies showed a high saturation of the quadrupole iron. The pole geometry was optimized (see Figure 61) in order to reduce the saturation down to 1.55 T when the sextupole component is turned off (see Figure 62). For 51764 Ampere turns per coil, a maximum quadrupole gradient of 5.7 T/m is reached.

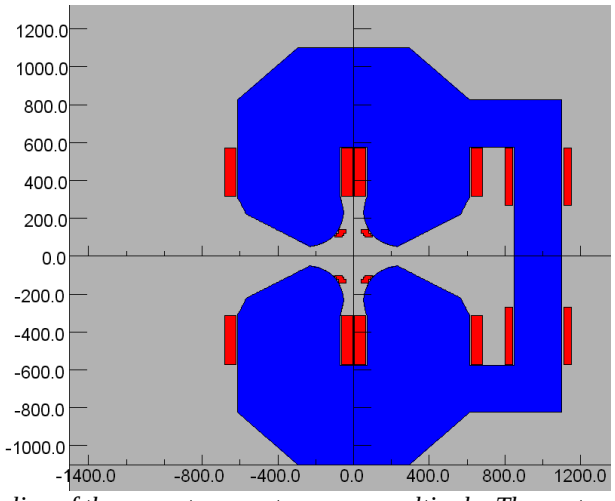

Figure 61: Transverse slice of the room temperature open multipole. The sextupole is obtained with the combination of the dipolar coils close to the magnet pole and the coils placed around the return leg.

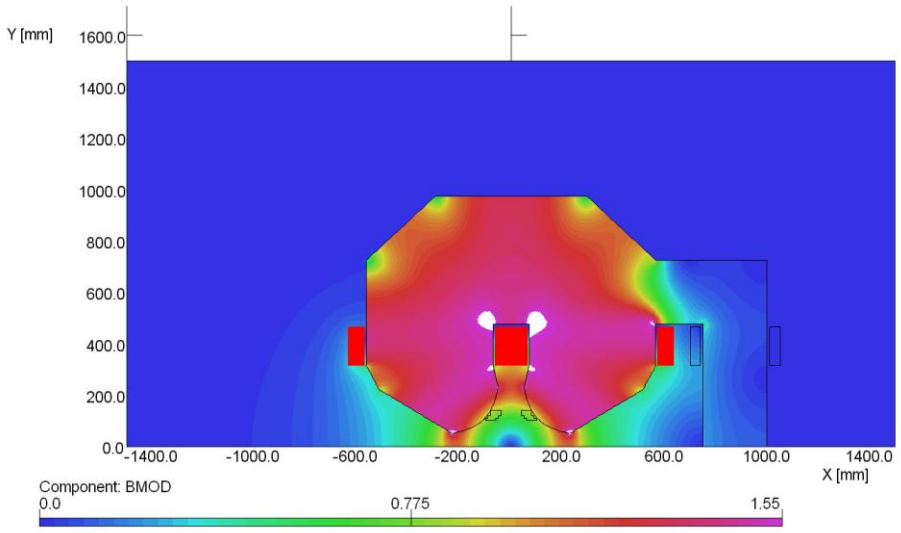

Figure 62: Magnetic field values produced by the quadrupole coils.

The horizontal and vertical gradient at the magnet center are shown in Figure 63. A small slope is observed on the horizontal gradient (though not in the vertical gradient), due to the « C » shape of the iron. A fraction of the magnetic flux goes through the leg, depending on the proximity between the leg and the pole.

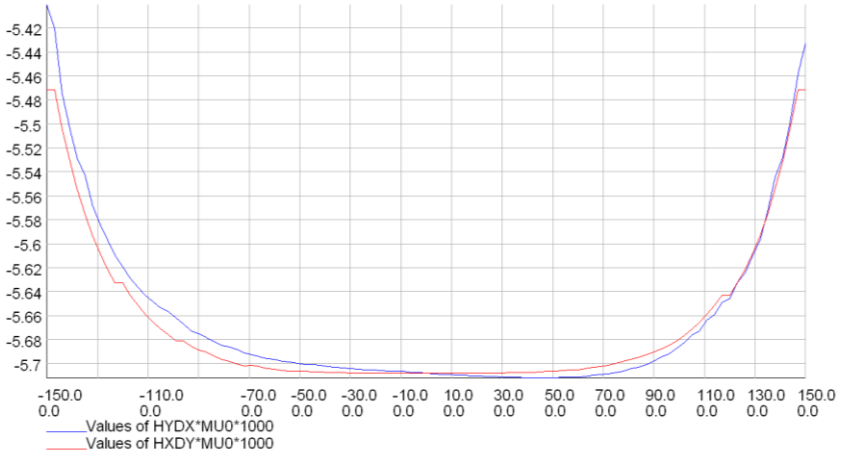

Figure 63: Quadrupole gradient evolution along the horizontal and vertical axes.

The sextupole component is achieved by the subtraction of two dipolar fields. One is produced by coils around the return leg (S1), the other by dipolar coils close to the quadrupole pole tips (S2). The geometry of the S2 coil is critical. Its shape and its position—around an angle of 45° near the pole tip—have a strong influence on the sextupole field quality. The S2 coil's geometry has been optimized in order to reduce the required current density. Each coil must be placed above the 45 degree line and its surface minimized close to this position. Figure 64 illustrates the optimization results.

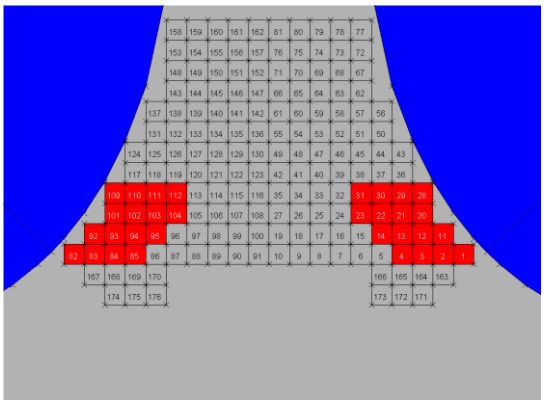

Figure 64: Final geometry (in red) of the dipolar coil close to the magnet pole. The numbers indicate the area tested for the coil position.

With the following setting—NI = 10500 Ampere turns per coil for S1 and NI = 23500 Ampere turns per coil for S2—the sextupole strength obtained is about 10 Tm^{-2}. The superposition of the quadrupole and sextupole naturally produces a difference in the pole saturation (see Figure 65) due to the added dipolar field. The peak field in the iron increases from 1.55 T to 1.7 T.

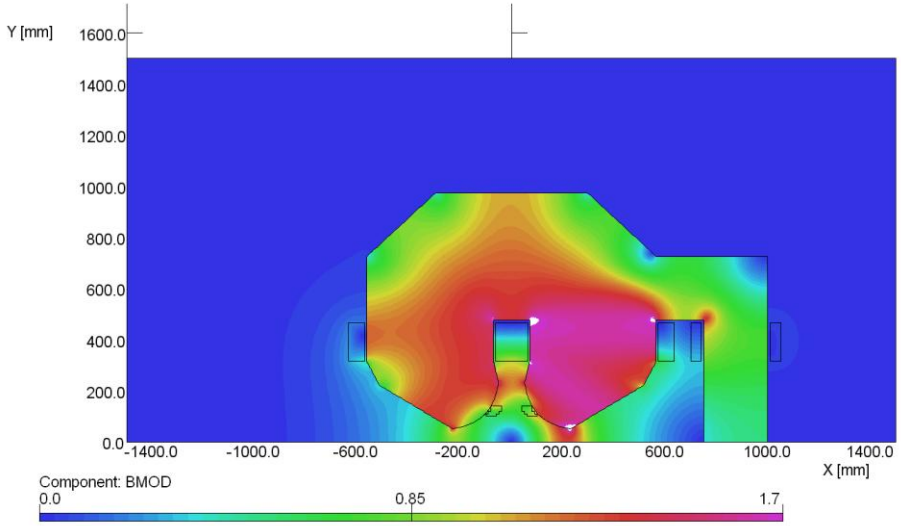

Figure 65: Magnetic field values of the superimposed quadrupole and sextupole.

The field maps have been produced in a full triplet configuration to take into account the close proximity of the multipoles. Figure 66 illustrates a triplet configuration where all quadrupoles are switched on, without sextupoles.

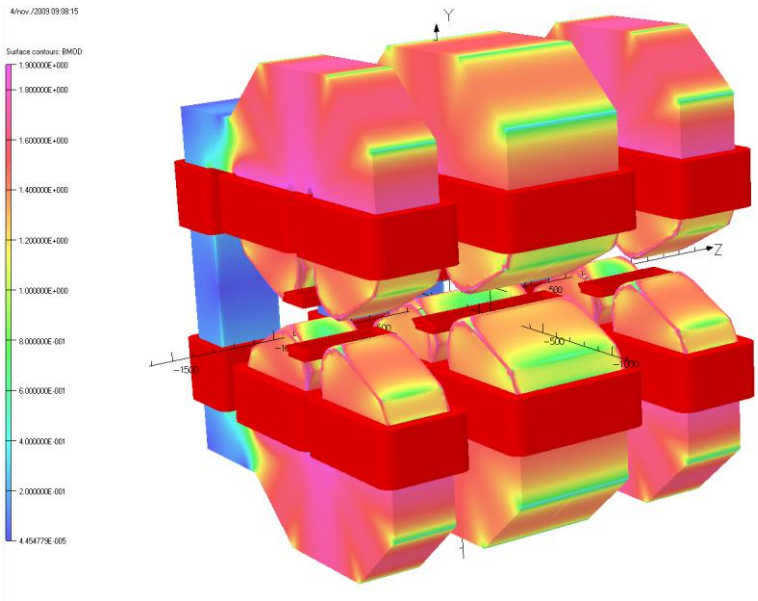

Figure 66: Saturation plot of the room temperature open triplet with all quadrupoles switched on.

For each field map calculation, each element of the triplet is switched on or off. The harmonic analysis of the field produced by the quadrupole coils in a half-triplet is shown in Figure 67. In addition to the first natural harmonic of the quadrupole, the dodecapole (C6), dipole (C1) and sextupole (C3) terms appear.

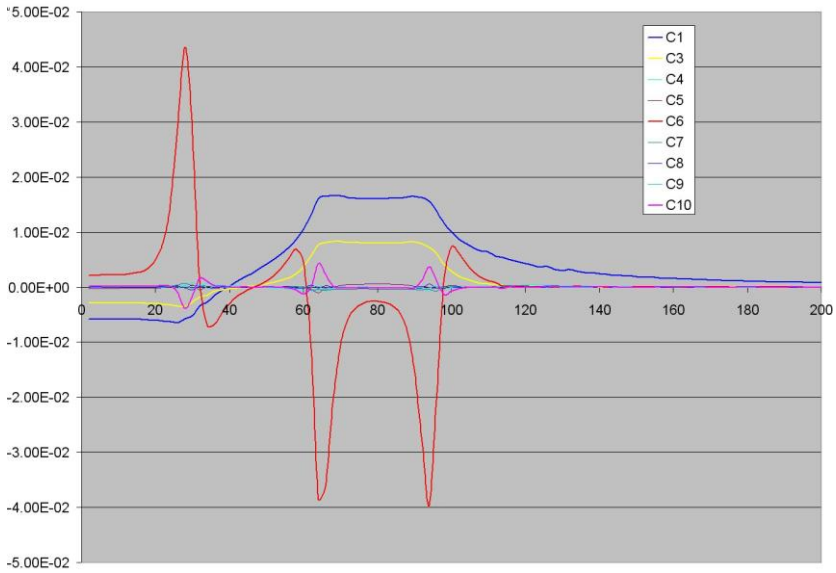

Figure 67: Harmonic analysis (in units relative to the main component) of a quadrupole half-triplet along the longitudinal axis, at a radius r = 120 mm.

The harmonic analysis for the sextupole component in a half-triplet is shown in Figure 68. In addition to the unwanted natural harmonics of the dipole, the decapole (C5) the tetradecapole (C7) and the octadecapole (C9), a strong dipole (C1) term remains in the fringe field region.

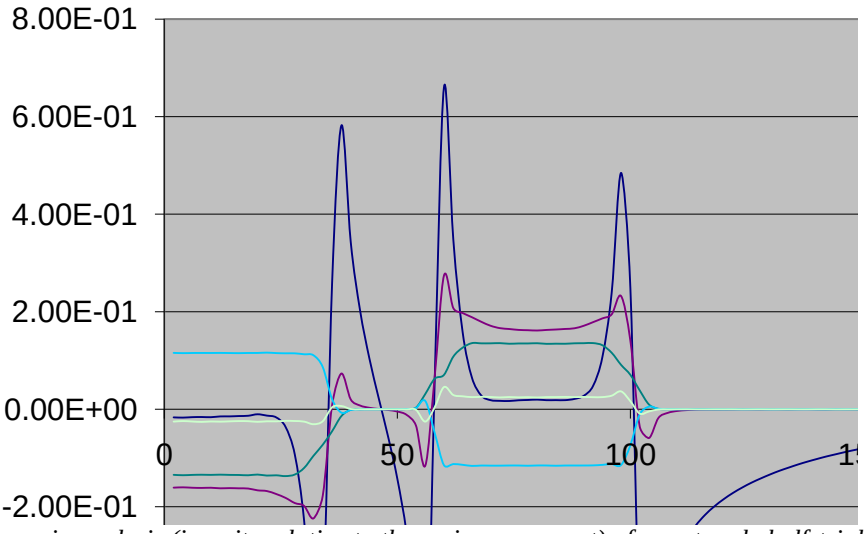

Figure 68: Harmonic analysis (in units relative to the main component) of a sextupole half-triplet along the longitudinal axis, at a radius r = 120 mm.

Figure 69 shows the harmonic analyses for the GANIL and SACLAY designs along the longitudinal axis. The calculation presents the same components for both systems but with a lower amplitude for the GANIL proposed design. Moreover, the residual dipolar field, which induces the most significant deterioration of the beam quality and the mass separation power, is also lower in the GANIL design (see Figure 70).

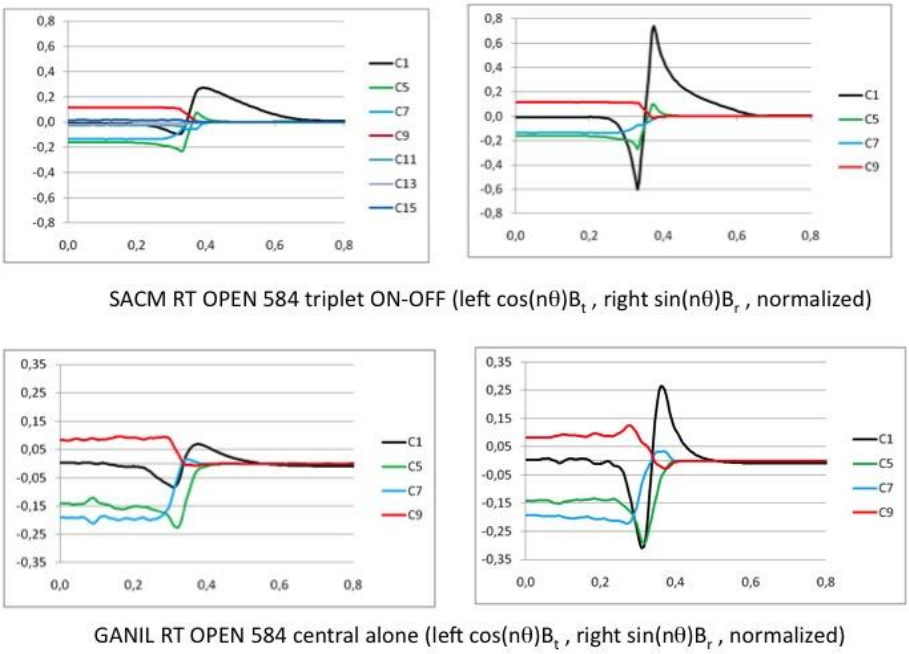

Figure 69: Harmonic analysis of the Saclay (top) and GANIL (bottom) room-temperature, open multipole. Note the difference in the vertical scale.

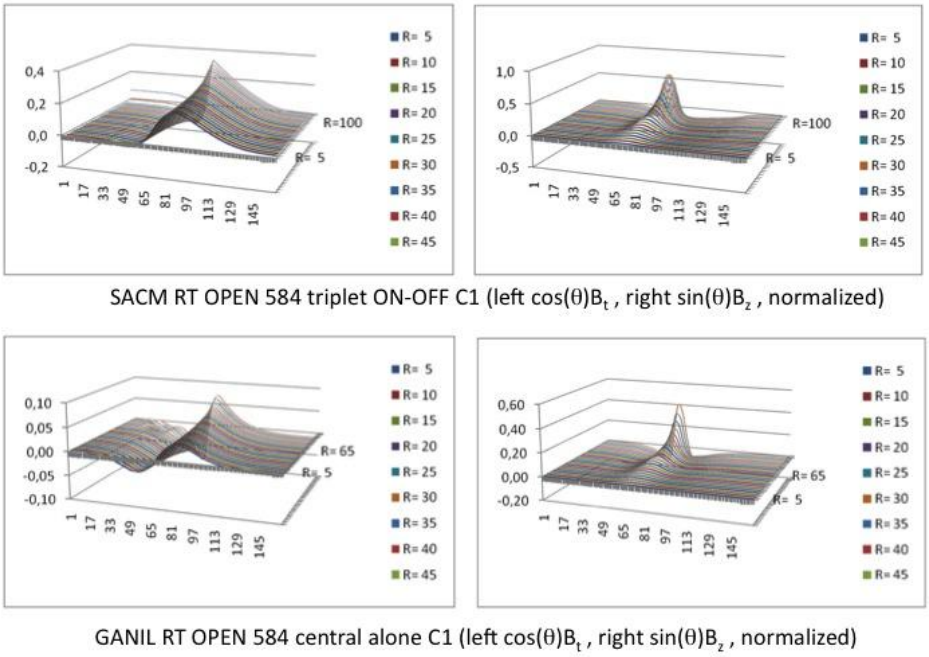

Figure 70: Residual dipolar component of the Saclay (top) and GANIL (bottom) room-temperature open multipoles along the longitudinal axis at different radii from the optic axis.

4.2 Superconducting multiplet option

4.2.1 Closed multipole (saddle coil design)

A preliminary design study and cost estimate for superconducting quadrupole triplets have been carried out. The proposed solution is for each of these multipole magnets to have quadrupole, sextupole, and octupole components. These coils are to be wound on the surface of cylinders as indicated in Figure 71. They are an approximation to cos(nθ) coils optimized to minimize higher-order mulipoles in the integrated field components. The magnet design consists of three layers of coils one each for the quadrupole, sextupole and octupole component. The innermost layer of coils produces the octupole component. The outer most layer of coils produces the quadrupole component and the coils generating the sextupole component are sandwiched between these two. The order in which the layers appear is subject to further optimization.

Table 8 provides some of the characteristics of the magnetic multipole triplet. The design is first carried out in an air-core model and then a cylindrical iron return path is added outside the cryostat radius. Figure 72a shows the air-core quadrupole coefficients A2 and B2 evaluated at a radius of 15 cm. The cylindrical iron adds roughly 20% to the magnetic field strength and produces no saturation effects. Its placement outside the cryostat results in a very small cold mass as well as a small total mass of the triplet. Figure 72b shows the coefficients of the first allowed term, the dodecapole, in the quadrupole field also evaluated at 15 cm. The quad coil widths can be adjusted in the design to make the integral of the error term be zero or any other value that optics simulations might indicate to be optimal. The total mass of each of these superconducting multipoles is 3 tons, with about 2.5 tons being the warm iron cylindrical yokes. In this preliminary design the operating currents being used to achieve high quality fields for up to 2 Tm magnetic rigidity are in the 200-400 ampere range. This requires 9 pairs of leads and 9 power supplies per triplet. The proposed solution for the leads is to use HTS leads between 4.5 K (temperature of the coils) and 80 K, at a liquid nitrogen cooled shield temperature. The leads will be vapor cooled with N_2 gas from the 80 K shield to room temperature. The power supplies are very small and can be mounted near each triplet to minimize the length of the copper leads.

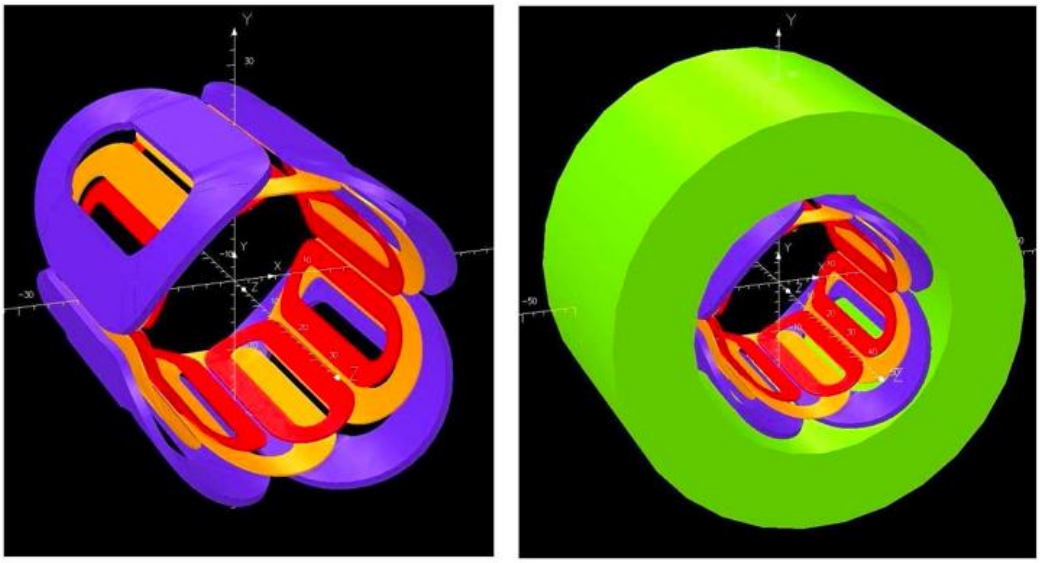

Figure 71: Superconducting multipoles, including quadrupole, sextupole, and octupole components, both without (left) and with (right) an outer iron shell.

Warm bore diameter	30 cm
Effective length	40 cm
Reference radius (R_{ref})	15 cm
Quadrupole component at R_{ref}	1.0 T
Sextupole component at R_{ref}	0.3 T
Octupole component at R_{ref}	0.3 T

Table 8: Characteristics of the magnetic multipole at its maximum field setting.

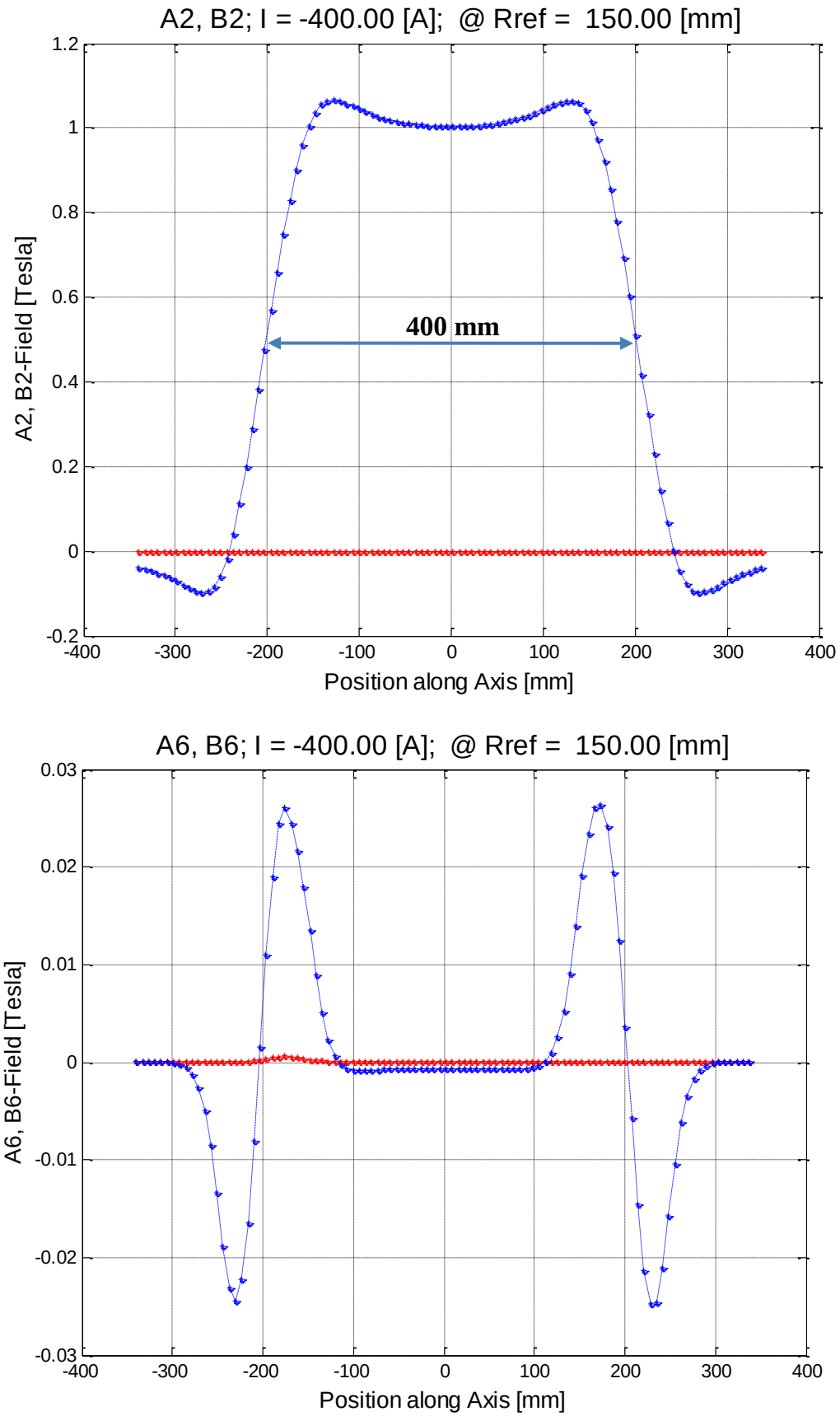

Figure 72: a) Amplitudes of the quadrupole harmonic coefficients at 15 cm radius, and b) the amplitudes of the dodecapole coefficients at 15 cm radius with the coil design adjusted to cancel the integral of this error term.

4.2.2 Cryogenics

If all 8 triplets in S^3 would be superconducting, a significant fraction of the cryogenic heat load will be from the current leads. There are 3 pairs of leads per multipole magnet, i.e. 9 per triplet and 72 total. The total current in all leads at the maximum rated rigidity is 36 kA. In this situation it is cost effective to use HTS leads cooled by conduction between liquid nitrogen temperature and liquid helium temperature and cooled by liquid nitrogen boil-off vapor from liquid nitrogen temperature to room temperature. In this case the leads provide about 1 watt of heat per triplet at liquid helium temperature and they also require the boil-off vapor from about 2.5 liters per hour of liquid nitrogen per triplet. The total helium refrigeration heat load at 4.5 K would be about 50 Watts, including the static load of the cryostats, the heat from the HTS conduction-cooled current leads, the valve boxes, and the distribution system. In addition, 20 liters per hour of liquid nitrogen are used for shield and vapor cooling of the leads from 80 K to room temperature. Two solutions for the cryogenics infrastructure for the superconducting multipoles are being considered. One option is a stand-alone liquid helium refrigerator of a type made by either Air Liquide or Linde. A standard Linde model, for example, provides 130 W of refrigeration at 4.5K with LN2 pre-cooling and requires only 45 kW of compressor electrical power. A preferable option is to provide the 50 watts of liquid helium refrigeration for S^3 by coupling it to the SPIRAL2 superconducting linac central refrigeration plant. This coupling should be done using heat exchangers that prevent mixing of the helium gas between the central plant and the S^3 cryostats. This can be achieved, for example, by using a recondensing system in each triplet as is commonly implemented these days with cryostats that utilize cryocoolers (as used, for example in the RIKEN superconducting fragment separator triplets).

4.2.3 Closed multipole (Saclay flat racetrack coil design)

The use of flat racetrack coils simplifies the coil winding, which has an impact on the magnet cost. A homogenous field can be obtained over a large area with a careful positioning of the coils. The coils are placed in order to have a current distribution following a cos(nθ) law. All the needed multipoles (quadrupole, sextupole, octupole) can be easily superimposed within a single element. The gradients required for the highest rigidities are achieved with reasonable currents. A 2D schematic of the coils arrangement is shown in Figure 73.

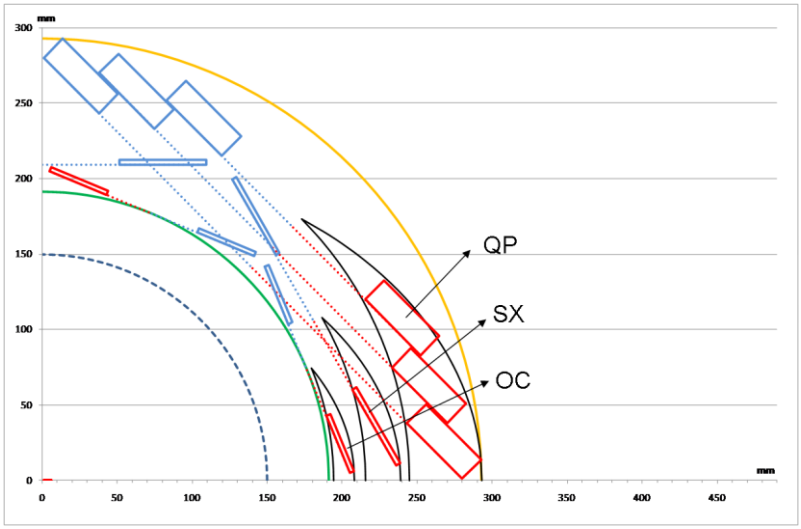

Figure 73: Schematic of flat racetrack coil configuration for the closed superconducting multipole design.

3D studies performed with Opera3D (see Figure 74) show the influence of the coil return, especially on the quadrupole. Harmonic analyses for the three multipoles are shown in Figure 75, Figure 77 and Figure 76. The remaining higher-order harmonics are only the first natural harmonics of each multipole, and all are less than a factor of 4×10^{-3} of the main component. The second natural harmonics are already negligible.

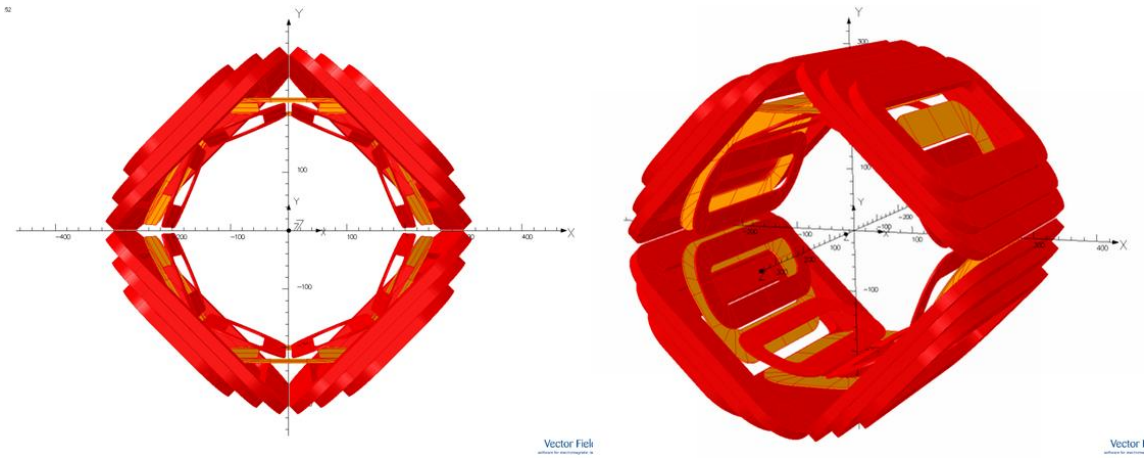

Figure 74: 3D view of the flat racetrack superconducting multipole.

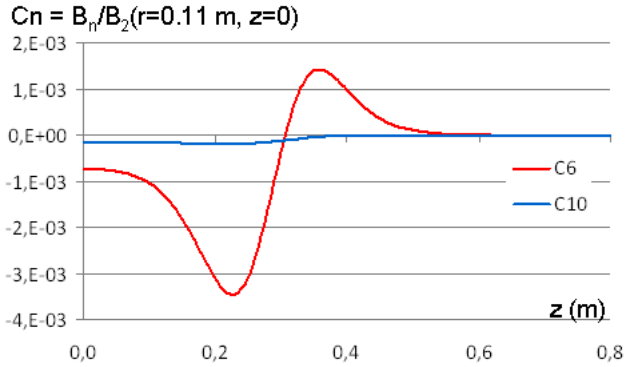

Figure 75: Harmonic analysis of the superconducting quadrupole along the longitudinal axis z. The calculation was performed on a half-magnet.

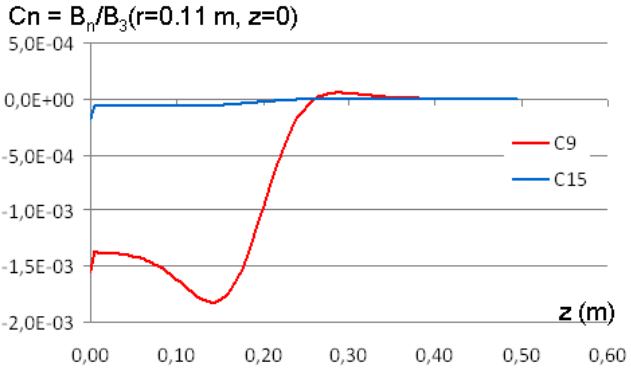

Figure 76: Harmonic analysis of the superconducting sextupole along the longitudinal axis z. The calculation was performed on a half-magnet.

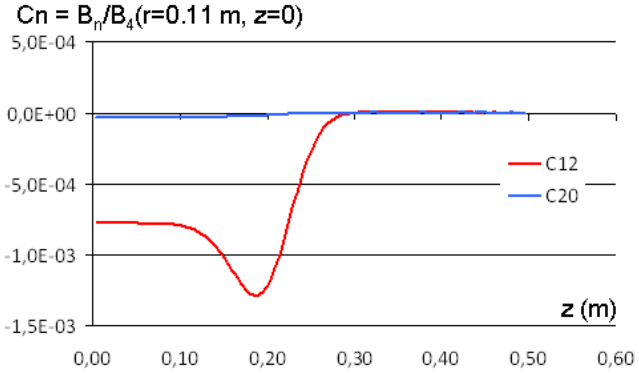

Figure 77: Harmonic analysis of the superconducting octupole along the longitudinal axis z. The calculation was performed on a half-magnet.

4.2.4 Open multipole (Saclay MOSAR design)

MOSAR ("Multipole Ouvert Supraconducteur à grande Acceptance basé sur des bobines Racetrack plates") is the French acronym equivalent to "Open Superconducting Multipole with large Acceptance based on flat Racetrack coils." The flat racetrack concept has already been successfully applied to standard closed superconducting multipoles (see previous section).

This multipole must include at least quadrupole and sextupole components. The quadrupole coil configuration is in standard 45° symmetry but the coil extension is reduced to leave a vertical gap free. Consequently, due to a mismatch between the current distribution and the cos(2θ) law, the main quadrupole windings create a dodecapole component, which is compensated by an opposing quadrupole winding. For the sextupole, the first approach was the same as in the open room temperature quadrupole case; the sextupole field was produced by two opposing dipolar windings which naturally create a sextupolar harmonic. In order to cancel the next natural harmonics of the dipole coils, the decapole—a third dipolar winding—was added. Figure 78 shows a transverse cross-section of this multipole.

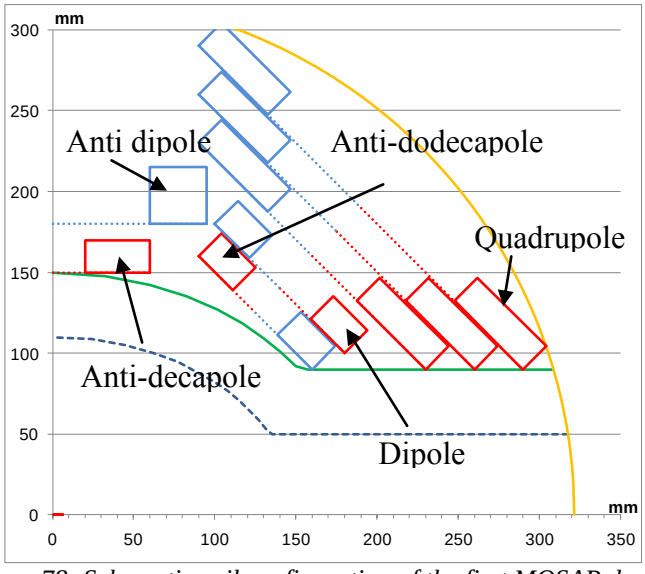

Figure 78: Schematic coil configuration of the first MOSAR design.

As the sextupole is produced by a combination of two dipolar fields with different horizontal extent, a residual dipolar field remains, which varies along the horizontal plane (Figure 79). This induces a deterioration of the beam quality and reduces the mass separation power.

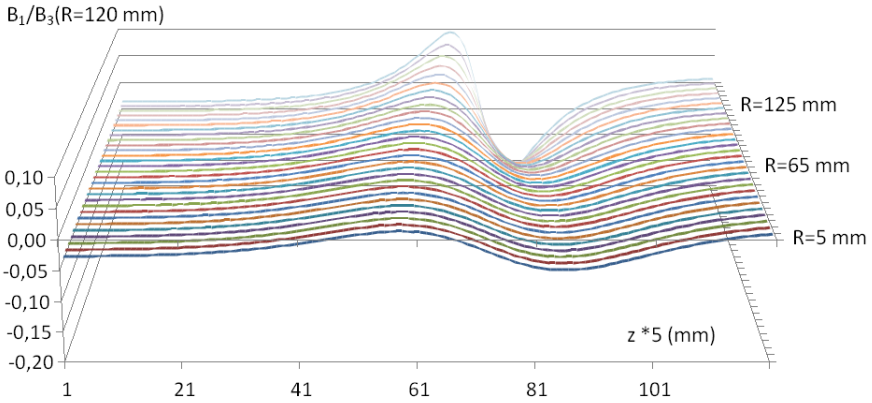

Figure 79: Residual dipolar component of the MOSAR sextupole along the longitudinal axis at different radii.

A new design of the MOSAR magnet was developed to suppress the unwanted residual dipolar component. In order to achieve this, the MOSAR multipole components (sextupole, and octupole if needed) are obtained with sets of coils which are placed according to the standard multipole symmetries, while keeping a free vertical gap of about ± 90 mm for the primary beam extraction and for additional mechanical elements (Figure 80). An octupole could be inserted similarly, if needed. The field quality obtained, in terms of higher order excited multipole harmonics, is comparable to that of the closed magnets (warm or superconducting). The harmonic analysis of the quadrupole component is presented in Figure 81. The additional higher-order harmonics produced in the sextupole and octupole are their first natural harmonics, the 18-pole and the 24-pole, respectively. At a radius of 120 mm the relative strengths of these components are below 3×10^{-3} of the main component. By symmetry, the dipolar field disappears completely from the sextupole field. At full excitation of the coils, the maximum field on the coils is about 5.6 T (Figure 82), which is compatible with a superconducting state of the NbTi coils.

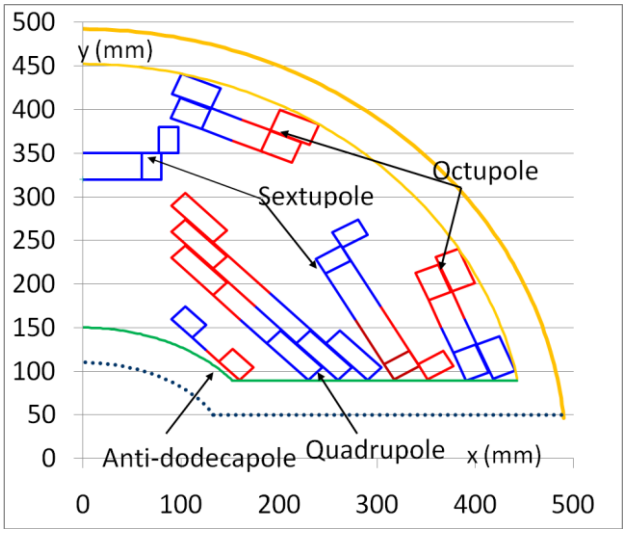

Figure 80: Schematic coil configuration of the second MOSAR design.

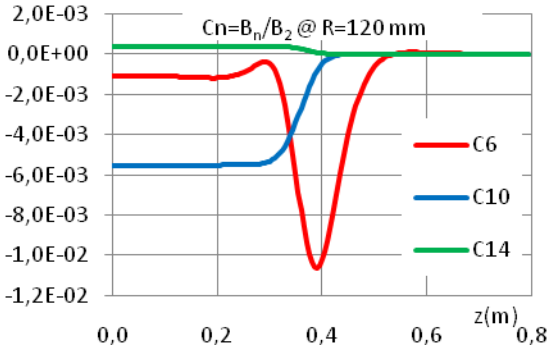

Figure 81: Remaining higher order harmonic components of the quadrupole field along the longitudinal axis z.

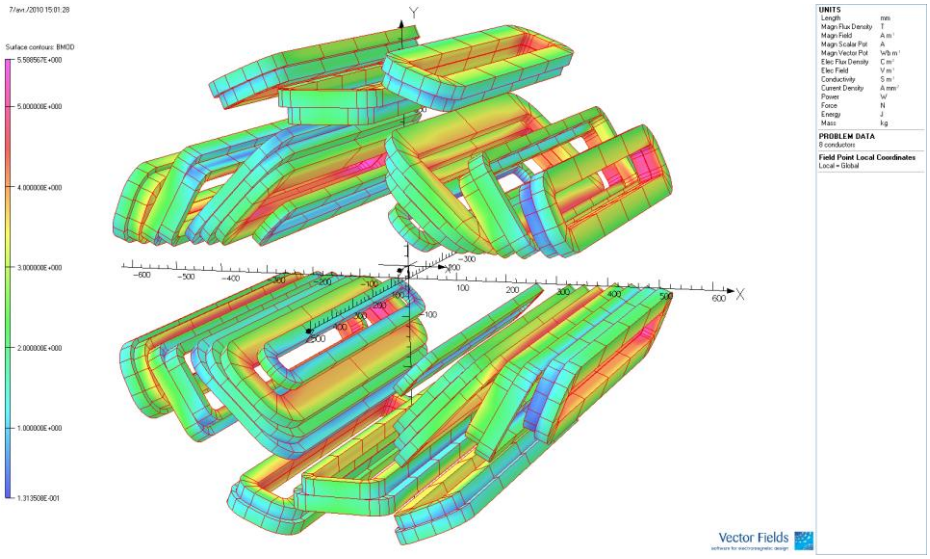

Figure 82: Magnetic field distribution on the coils calculated by Opera3D.

4.3 Magnetic dipole

The three magnetic dipoles will most likely use room temperature coils, due to the low magnetic fields required. Magnetic rigidity requirements are modest for direct kinematics and symmetric fusion reactions, $\lesssim$ 1 Tm. The designs can accommodate magnetic rigidities up to 1.5 Tm or higher with peak magnetic fields still less than 1 T. The dipoles have a rather small deflection angle and low field intensity. A large air gap is required for transmission with the best homogeneity possible and—as far as is possible—a low fringe field extension. A preliminary design for an H-shaped dipole (see Figure 83) demonstrated that a homogeneity of 5×10^{-4} can be achieved.

The particular designs discussed here are those of the first two dipoles, those in the momentum achromat. The third dipole will be of a very similar design but with a larger bend angle, and it will therefore have different geometry, weight, cooling, etc. specifications than those discussed here below.

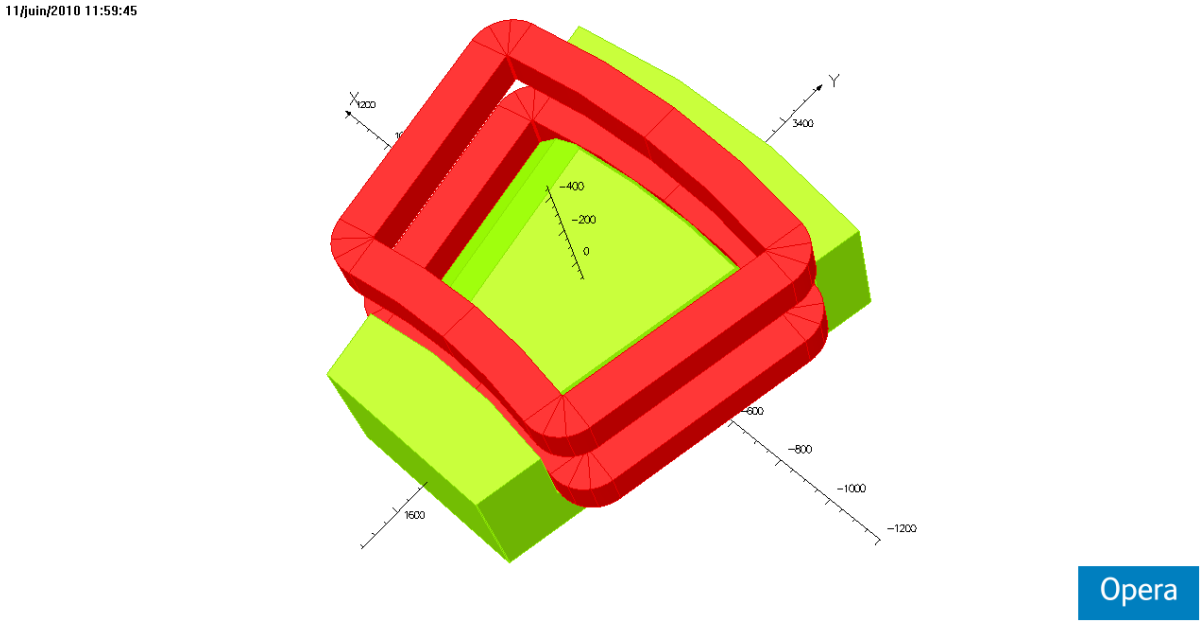

Figure 83: 3D view of the magnetic dipole calculated by Opera3D.

A large double chamfer enables adjustment of the magnetic length (possibly with removable shims). The fringe field extension could be limited further by the use of shielding plates around the coils in future designs. The power dissipation is limited by the use of large conductors.

Correction coils are possible to allow for steering or to enable a pair of dipoles to use the same power supply. The mass of the dipole could be optimized by reducing the horizontal extent of the good field region to precisely match that which is needed.

MAGNETIC	
Angle	21.88º
Curvature radius	2500 mm
Face Input angle	0º
Face Output angle	0º
Magnetic induction (max)	0.7200T useful + cycling around 10%
Magnetic induction (min)	Not specified yet

MECHANICAL	
Gap	H= 240 mm (200mm for beam)
Good field region extension	+/-180mm
Iron weight, estimated	7200kg
Copper weight, estimated	800kg

POWER AND COOLING @Pmax	
Intensity max (cycling)	I= 760A
Voltage	U= 2*50 =100 V
Power dissipation	P= 2 * 38kW = 76kW
Total Resistance (@ I max)	0.132 Ω
Cooling circuits (total)	10
Pressure drop	12 bars
Temperature rise	25º

Water flow	2*22 l/mn = 44 liters/minute

Data for one main coil

CONDUCTOR	
Resistivity (@20 ºC)	1.75 10-^{8}
Height * Width	12 * 12 mm
Hole diameter	6 mm

GEOMETRY	
Number of turns	100
Average turn length	3.85m
Number of cooling circuits (/coil)	5
Cooling circuit length	77 m

Table 9: Preliminary design parameters of the magnetic dipoles.

4.4 Electric dipole

The mass separator stage consists of an electric dipole followed by a magnetic dipole, each sandwiched between two multipole triplets. The electric dipole in the mass separator stage is essential to produce mass dispersion. The bending radius for the reference particle inside the electric dipole was chosen to be 4 m. The electric dipole must have a gap of 20 cm to provide good angular acceptance. At full electric rigidity (12 MV), voltages of ±300 kV are required on the electrodes. Parameters are similar to those for the Lohengren electric dipole at Grenoble and Electrostatic Analyzer for the Hybrid Recoil Mass Analyzer (HYRA) at IUAC (Inter University Accelerator Centre), New Delhi, India presently being constructing by Danfysik [http://www.danfysik.com/].

Beam optics simulations show that an effective bend angle of 24.7 degrees would produce the desired balance of mass dispersion and angular acceptance. The design of the electric dipole consists of two parallel titanium plates (or alternatively a stainless steel anode and aluminum cathode) of 5-cm thickness, 30-cm height and 1.72-m effective length separated by a 20cm gap. Each plate is a section of a hollow cylinder which can be described by the section angle, height, and inner and outer radii. Both plates are positioned concentric to the reference orbit with the face of each plate perpendicular to the dispersive plane. Both plates have the same section angle and height but have different inner and outer radii, +/- 10-cm relative to the central 4-m radius of curvature. The section angle is optimized to get the desired effective bend angle with consideration of the fringe field effects at the entrance and exit.

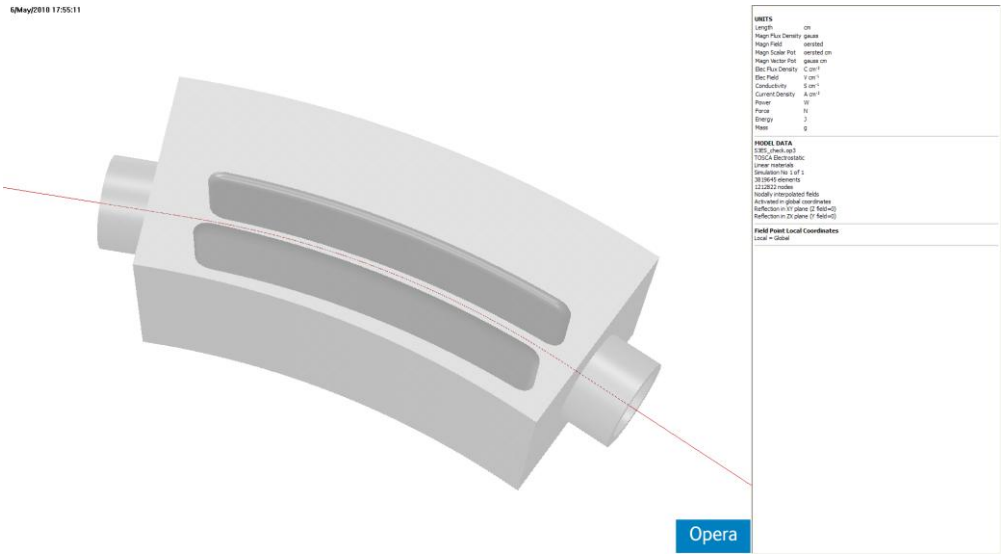

Figure 84: Figure showing the plates, shielding and the reference trajectory for the electric dipole.

To reduce the chances of sparking and minimize the peak field in the plates the top and bottom edges are made smooth by rounding them. The entrance and exit edge of each plate are appended with end caps of 5 cm length. The end caps have a smooth geometry to further reduce peak fields that occur in the entrance and exit regions. The two plates are placed in a stainless steel vessel to provide shielding. The entrance and exit ends of the vessel also become part of the beam line to meet the drift length requirements. There will be a vacuum valve with an internal diameter of 30 cm at each end of the element for isolation during conditioning and maintenance. The connecting edge between the inner wall of the vessel and the inner surface of the beam line is also rounded to minimize the chances of sparking. A TOSCA model showing the two plates and the vessel is shown in Figure 84 and the Table 10 lists some of the parameters for the electric dipole. The Figure 90 shows the contour plot of the electric field on the midplane.

Plate Separation	20 cm
Bending Radius	4m
Bending Angle	24.7 degrees
Plate Height	30cm
Effective Length	1.72m
Plate Material	Titanium
Plate Shape	Cylindrical
Voltage	±300kV
Peak Field (inside)	30kV/cm
Peak Filed (on the plates)	48kV/cm

Table 10: Preliminary design parameters for the electric dipole. These parameters will be fine-tuned to be consistent with the final optical solution and an optimized high-voltage performance.

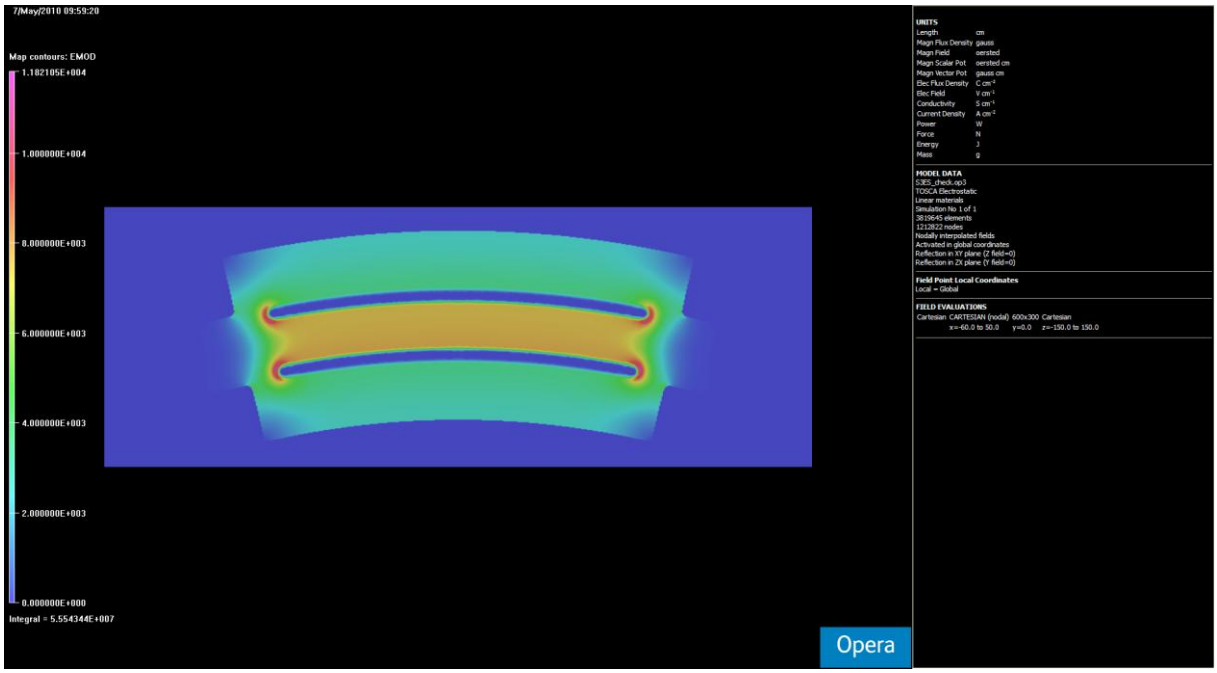

Figure 85: Contour plot of the absolute electric field on the midplane for the SHE case.

Figure 86 shows the preliminary design of the electric dipole and the adjacent multipoles. The high-voltage multiplier stacks will be integrated into the vacuum enclosure similar to the solution implemented at the ORNL/HRIBF RMS and the ANL/ATLAS FMA separators. This eliminates the need for stand-alone external high-voltage power supplies and the associated cables and vacuum feedthroughs.

For direct kinematics and symmetric kinematics fusion evaporation reactions, e.g. for superheavy element studies and studies in the ^{100}Sn region, respectively, the electric rigidity requirements are modest, $\ll$ 12 MV, and the present design of the electrostatic dipole described above is well optimized (±300 kV, 30 kV/cm). For some planned experiments the electric rigidity of the ions in the second half of S^3 exceeds this design constraint. We envision two options for these research programs. 1) For inverse kinematics fusion reactions, the angular acceptance requirement is reduced so that a smaller gap can be used for the electric dipole. In this case a higher electric rigidity can be accommodated by having a set of deflector plates with a smaller gap to replace the standard, base-line set. 2) For some proposed reactions and also for the proposed atomic physics program the second half of S^3 is not required to operate as a mass separator, so the E-dipole can be replaced by a magnetic dipole with equivalent bend angle for these programs.

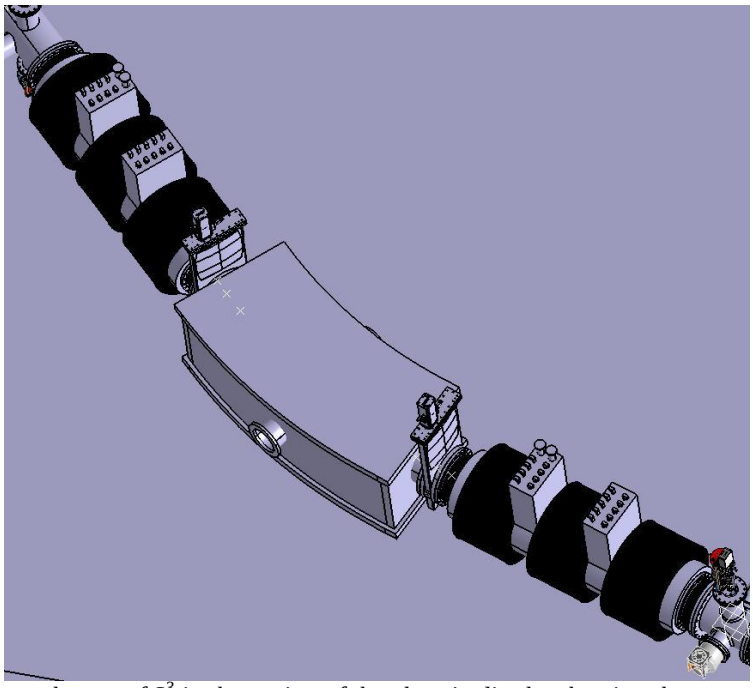

Figure 86: Preliminary layout of S³ in the region of the electric dipole, showing the vacuum box of the dipole and the adjacent multipole triplets.

The treatment of full 3D electric dipole fields in the transfer map based beam optics codes has been a difficult problem due to the lack of any model in the presently available optics codes to describe the electric field in the fringe field regions. This problem has now been overcome with a newly developed maps-to-maps approach. This allows the generation of a multi-order transfer map from the 3D field map of the electric element. It is now possible to use realistic maps to perform beam optics simulations.

4.5 Beam Dump

The beam dump is a critical element of the separator. It has to sustain up to 45 kW of beam within the beam tube of the multiplet (Note: 45 kW is an envelope case for a ^{12}C beam at 1 mA and 14.5 AMeV). For a more typical case of a ^{48}Ca beam at 16pμA and 5 AMeV, the total power in this region would be 3.8 kW. Apart from radiation safety considerations—treated in the "Nuclear Safety" Section—care has to be taken so that a minimal amount of heat is transmitted to the surrounding cryostat. This issue is similar to that encountered in the BigRips (RIKEN, Japan) beam dump design, albeit on a smaller scale, since they had to deal with a 100 kW uranium beam. In their case, an ensemble of water cooled copper tubes was used to cover the vacuum chamber of a dipole. The S³ beam dump design still needs progress on several fronts:

- Exact beam spot position and size, which depends on the experiment
- Encumbrance of the beam dump, which may reduce the acceptance
- Heat transfer to the environment, specifically to the surrounding cryostat.
- Nuclear safety, radiation protection in normal operation and accessibility of the beam dump in case of an incident (see "Nuclear Safety" Section).

We are also studying a zero-degree beam stop at the entrance of the spectrometer, which should block 99% of the beam while having 80% transmission for evaporation residues with a large angular spread.

4.5.1 Functional requirements

4.5.1.1 Dump areas

Nuclei produced in or transmitted through the S3 target are dispersed in p/q by the first half of the achromat in the horizontal plane. The different charge states follow trajectories that will lead them to be stopped in one of three distinct areas:

- The "high magnetic rigidity area" will receive particles exceeding the upper p/q acceptance limit of the spectrometer. This area is of greatest importance in direct reactions (light projectile on heavy target), which will in principle produce the highest primary beam intensities. So this area must withstand the highest power deposition as well as the most significant implantation of radioactive species and material activation.

- The "low magnetic rigidity area" for particles below the lower p/q acceptance limit of the spectrometer. In principle, beam particles entering this area will be of the least populous charge states and the design of this area will therefore be the least demanding of the three areas.

- The "acceptance area", where primary beam particles—depending of the reaction type—can follow trajectories similar to those of the ions of interest, though of smaller emittance.

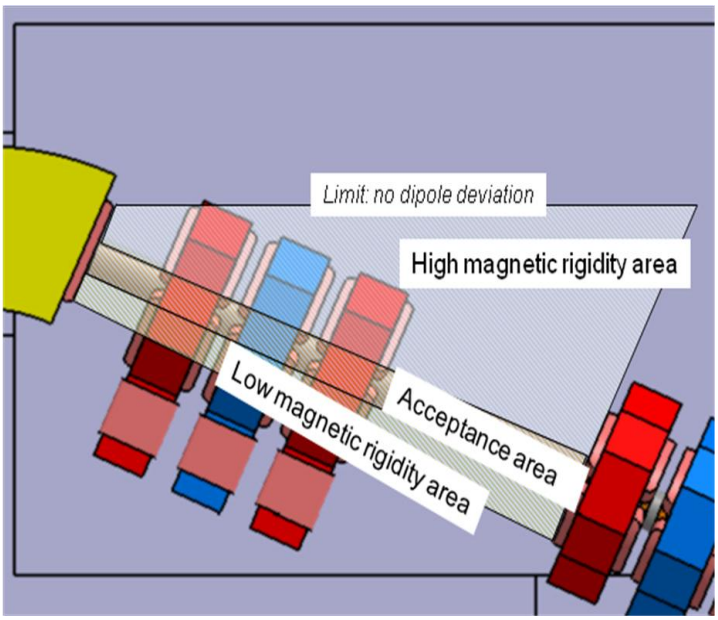

Figure 87: View of the dispersive plane including the three areas covered by the beam dump.

4.5.1.1.1 Acceptance area

In this area, nuclei are distributed in the horizontal plane, at first order, as a function of their magnetic rigidity, the ratio of their momentum to their electric charge (Bρ=p/q). Beam ions momenta depend on the primary beam and the energy loss and straggling in the target. The distinct primary beam charge states are thus separated onto different trajectories.

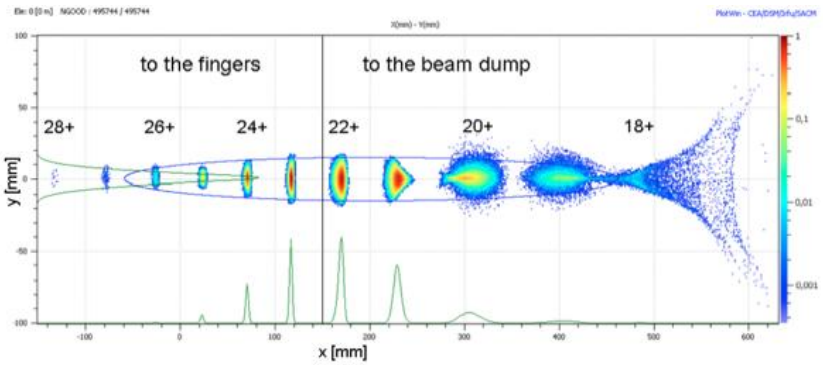

Figure 88: 58Ni charge state distribution at the dispersive plane.

The ions of interest occupy the same area, but generally fill the acceptance with a more uniform distribution because of the much larger energy spread of the evaporation residues. To intercept as few as possible of the product nuclei of interest, we have to minimize the size of the beam dump parts. The idea is to position movable fingers that will specifically stop individual primary beam charge states. Each moving finger will be instrumented to be able to measure the stopped intensity. This will allow fine-tuning of the fingers' positions, charge state distribution measurements and an indirect method of continuously monitoring the integrity of the production target. Shutters will be placed on each side of the acceptance area to stop charge states at the limit of the momentum acceptance and to ensure continuity with the high and low magnetic rigidity regions of the dump.

4.5.1.1.2 High magnetic rigidity area

The primary beam ions transmitted through the target should have a higher magnetic rigidity than the reaction products to be studied. It is then the high magnetic rigidity area beam dump parts that will—in most cases—have to endure the highest rate of primary beam particles, especially in the case of superheavy elements synthesis experiments. These experiments will be the longest experiments to be run at S^3 and will make use of some of the highest beam intensities. Thus, the high magnetic rigidity area is the place where the energy deposition and the neutron production and activation will be the highest.

The different charge states are distributed within an area, bounded on one side by the acceptance region at Image 1 and on the other side by a line corresponding to a straight line trajectory (i.e. no deflection, which implies an infinite magnetic rigidity) through the first magnetic dipole (located immediately upstream). The multipoles immediately downstream of the first magnetic dipole are the open multipoles. This allows trajectories of the beam outside the acceptance to be removed from the optical system without being stopped in the beam pipe or the multipole magnets. It is then possible to stop the beam outside magnetic elements allowing:

- To shield the high magnetic rigidity beam dump—with both fixed and movable shielding—and to limit the dose rate due to its activation
- To limit secondary activation of neighboring materials by neutrons produced in the dump
- To ease human intervention in the beam dump room and the remote handling and maintenance of the beam dump itself.

4.5.1.1.3 Low magnetic rigidity area

Lower energy products and higher charge states will be directed into the low magnetic rigidity area.

These extreme charge states should be the least intense. Nevertheless, we need to consider their impact as far as thermal and radiological aspects are concerned. Moreover, scattered particles from this region could contribute to on the experimental background in the downstream detectors.

The low magnetic rigidity area dump will have to meet the following requirements:

- To shield the vacuum chamber and the magnets against the deposited beam power

- To limit the radiological effect of the implantations
- To limit ion scattering after impact (anti-scattering plates could be implemented here for this purpose).

4.5.2 Functional description, beam dump sub-system breakdown

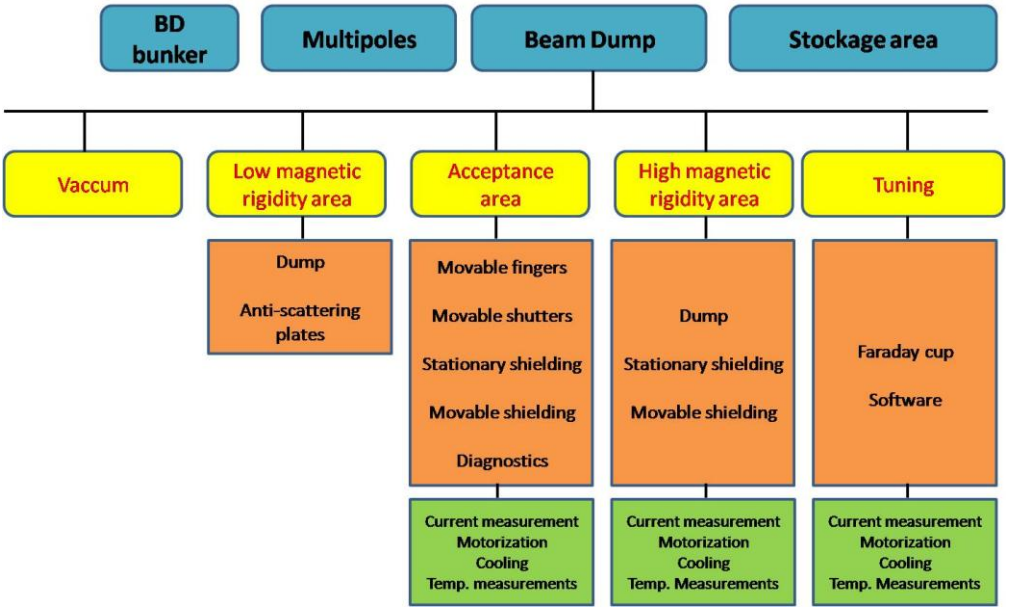

4.5.3 Beam Dump functional sketch (room temperature magnets option)

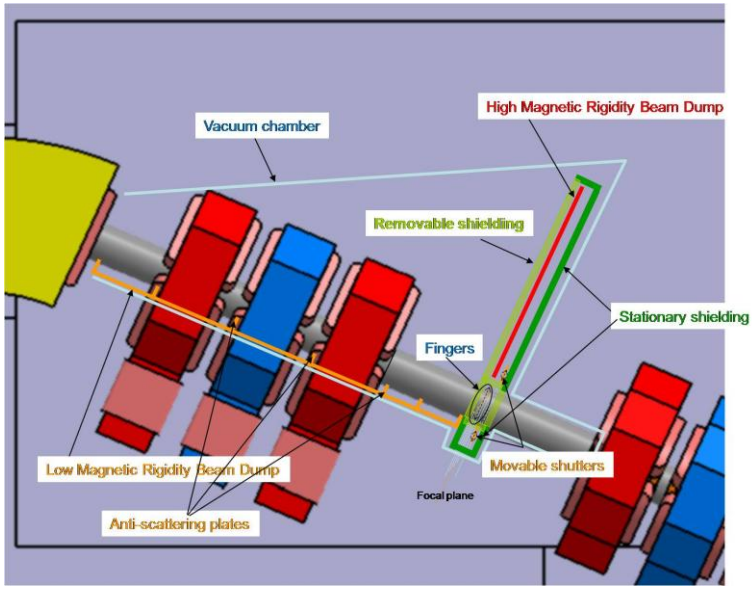

Figure 89: Schematic sketch of the beam dump components, room temperature magnets option.

4.5.4 Current layouts

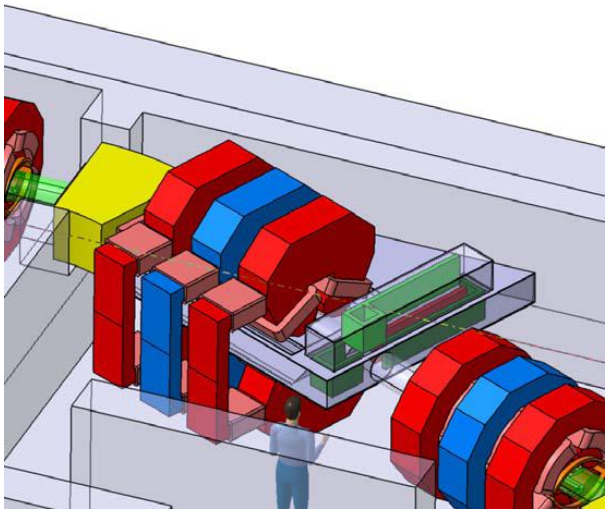

Figure 90: Mechanical design sketch of the beam dump, room temperature magnets option.

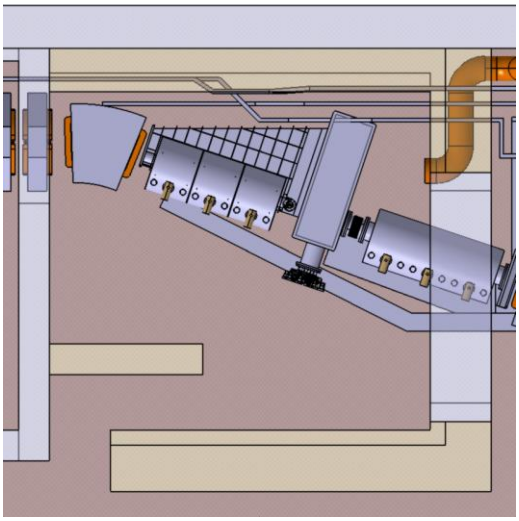

Figure 91: Mechanical design sketch of the beam dump, superconducting magnets option.

4.5.5 Safety

4.5.5.1 Nuclear safety / radioprotection

The beam dump is the most activated material and the primary radiation source. Moreover, it generates neutrons which activate surrounding materials. The residual γ dose rate coming from the beam dump has been calculated, since it is the main contributor to the external dose when the beam is off. For this reason, the first two work packages studied by SENAC are:

- Analysis of the effect of the materials to be used in the dump components. The output of this work package will include:
  - the assessment of the residual dose rate as a function of materials used in the dump components (and any resulting limitations on materials that may be used)
  - the neutron production rate (relevant for the dose rate when the beam dump is in use and for the activation of surrounding equipment),
  - the associated implications for decommissioning and
  - the preliminary definition of the shielding needed;
- Preliminary radiological characterization of the Beam Dump system. The outputs of this work package will give an approximate knowledge of:
  - the neutron flux distribution in the beam dump room and target room
  - the activation of the components of beam dump subsystems and the neighboring fluids (notably the cooling water and the surrounding air) with the associated gamma dose rates
  - the determination of the radiological shielding characteristics

The design must be optimized in terms of the choice of stopping material (for the beam dump) and the material for the surrounding equipment in order to minimize the dose rate. This can also be achieved by using an effective biological shielding (some proposals are given in this chapter) or by using very reliable equipment with low maintenance needs (i.e. limiting the time of exposure - ALARA concept).

The gas pumped from the vacuum in the beam dump sector will have to be collected in storage bottles to allow decay and control before being released. The cooling pipes of the beam dump elements will be connected to a tertiary circuit. A leak on this circuit must be collected in a watertight retention. If the heat exchanger is located outside the Beam Dump bunker it has to be designed and built in a way it complies with the nuclear safety level of the S^3 principal room.

4.5.5.2 Conventional safety

The supports and anchors must be designed such that in case of a SMS earthquake (*Séisme Majoré de Sécurité*) nothing will alter the integrity of the target room, in order to avoid any contamination. The beam dump supports must meet this requirement. This will require specialized support designs, which will, additionally, have to meet mechanical constraints imposed by the large amount of equipment that must be located in the comparatively small beam dump room.

4.5.6 Critical items

The following preliminary critical item list will aid in the definition of the development plan in the very near future, to determine the qualification procedures and equipment and to define the resources needed (financial resources and human resources).

4.5.6.1 Shielding

Due to activation of the beam dump components, shielding will be needed to allow human access to the beam dump room when the beam is off. Movable shielding plates will have to completely enclose the multi-part dump, both in a nominal condition (all fingers and shutters being at their rest location) or in a failure condition (fingers or shutters jammed in the acceptance area). The shielding thickness (under investigation) is a critical point for the beam dump design as it determines the overall mass and the free space needed along the beam line for installation.

4.5.6.2 Cooling

The movable fingers must withstand 1 kW distributed over an area of approximately 1 cm². The power density is thus 10 MW/m². Today IRFU's experience is limited to 0.5 MW/m² but the tokomak Tore Supra has been using solutions to deal with 10 MW/m² for years and current ITER studies are targeting 20 MW/m². A specialized study must be performed at IRFU and we foresee a paper study by the end of 2010 followed by testing on a support model by the middle of 2011.

Fingers' cooling pipes have to be distributed in the horizontal plane to be hidden behind the dump area. Their dimension along the beam axis must be limited, however, in order to allow a compact arrangement of the fingers along the beam axis to ensure that all the fingers will be located close to the optical focal plane. Thus, the pipes will have a limited cross section and be of unconventional design.

4.5.6.3 Vacuum

The pressure inside S^3 vacuum chambers, including the beam dump vacuum chamber, must not exceed $5\ 10^{-8}$ mbar. This will impose constraints on all the parts located in the vacuum chamber. For instance, the shielding, probably lead, must have surfaces or coatings compatible with the required vacuum level or must be enclosed in an adequate box. Baking of the vacuum chambers may be needed and the space allocations to very nearby equipment will have to be carefully considered.

4.5.6.4 Reliability

Access to the beam dump bunker will be controlled and, despite the shielding (movable shielding and stationary shielding) that will completely surround the dump components, the activation of neighboring equipment will necessitate some delay before entering the bunker. A mechanical failure of any of the beam dump devices (fingers/shutters displacement, cooling, current measurement, etc.) may then lead to a non-negligible unavailability period before any maintenance operation can be performed. Thus, we have to ensure a high level of reliability. A very low finger and shutter failure occurrence probability will be specified, which will lead us to pay particular attention to the design and testing of the beam dump devices.

4.5.6.5 Integration with the second (open) triplet

If the second open triplet is made of room temperature magnets, it will be possible to install the magnets in two pieces, placing the upper half of the magnets after the beam dump vacuum chamber is in place. This will not be possible if the second triplet is made of superconducting magnets due to the surrounding cryostat. The open triplet chamber must have a particular profile in the x-y plane due to the beam profile to be transmitted through this region and the necessary clear space in the side of the magnets to pass the primary beam charge states to the beam dump. This implies a "c" shaped profile. So in the case of an open superconducting triplet, we will probably have to slip the chamber into the triplet, requiring some specialized studies of the vacuum flanges and combined studies of the vacuum chamber and the superconducting open magnet design. The limited space in the beam dump room is unlikely to accommodate the sliding assembly operation, which would then have to be performed in the larger S^3 room and the full assembly then installed by crane. The combined study and the very constrained interfaces between the beam dump and the open triplet could benefit by the lodging of these two work-packages in the same institute.

Triplet	Type	Iron length	Inner Diameter H(mm) V(mm)	Multipole components	Fields gradient Integral Homogeneity	Power (kW)	Operating current (Amp)	Weight (singlet)
RT closed B-A-B	A	400 mm* 1650 mm* 1650 mm	H = 270 V = 270	Q = 6 T/m S = 9.8 T/m^2	Q: Mag length 540mm Homogeneity 1% S: Mag length 480mm	Q=60 S =50	Q : 800 S : 1400	5.4t
	B	300 mm × 1650 mm × 1650 mm	H = 270 V = 270	Q = 4 T/m S = 9.8 T/m^2	Q: Mag length 440mm Homogeneity 1% S: Mag length 380mm	NA		4t
RT open (CEA) B-A-B	A	584 mm	H = 180* V = 220	Q = 5.7 T/m S = 10 T/m^2	Q mag Length : 730mm @R=90mm : Quadrupole : 1.2% Sextupole : 100%			12t
	B	310 mm	H=180* V = 220	Q = 5.7 T/m S = 10 T/m^2	Q mag length : 470mm @R=90mm : Quadrupole : 1.2% Sextupole : 100%			9,8t
RT open (GANIL)		450 mm × 1100 mm× 2000 mm	H=180* (good field) V = 220	Q = 6 T/m S = 8 T/m^2	Q: Mag length 600mm S: Mag length 500mm	Q=65 S=60+ 45	Q: 900 S: 1500 +2000	5.6t
SC closed (ANL) A-A-A		400 mm outer radius = 300 mm	H = 300 V = 300	Q = 6.6 T/m S = 13.3 T/m^2 O = 89 T/m^3	< 1.5% deviation from linearity	Q = 2 S = 1 O = 1	Q = 400 S = 250 O = 250	1t
SC open MOSAR (CEA)		Adjusted on closed multipoles Present value : 620mm	H = 300 V = 220	Q = 6 T/m S = 11 T/m^2	@R=150 mm : Quadrupole : 35% Sextupole : 20%		Q : 249 S : 168	3.5t

Table 11: Summary of specifications for the various proposed magnet designs. Homogeneity is defined as the difference between the integral of the gradient close to the axis (10 mm) compared to the integral of the gradient measured at the radius of beam pipe (150 mm).

5 Conventional Safety comparison between room temperature and superconducting magnets

5.1 Magnet weight

Room temperature magnets are much heavier than superconducting magnets:

- The open RT triplet in the Beam Dump area should weigh approximately 17 tons
- The open SC triplet should weigh approximately 10 tons
- Each closed RT triplet should weigh approximately 13 tons
- Each closed SC triplet should weigh approximately 3 tons

The handling methods and procedures for their installation will take this into account.

The magnet supports and anchorages must be designed such that in case of a SMS earthquake (*Séisme Majoré de Sécurité*) nothing will alter the integrity of the target room, in order to avoid any contamination. The magnets concerned are those of triplets # 1, #2 and #3; triplet #3 could alter the integrity of the Beam Dump bunker and this could, consequently, alter that of the target room.

This will demand specialized support designs, which will, additionally, have to meet the mechanical constraints imposed by the large amount of equipment that must be located in the limited available space of these confined areas. Due to their weight, this aspect is more critical for room temperature magnets.

5.2 Oxygen Deficiency Hazard

Superconducting magnets would require the use of cryogenic fluids (Helium and Nitrogen) and leaks of these fluids could displace the oxygen in the S^3 vault or its subspaces, creating oxygen-deficiency hazards. 100 liters of liquid Helium expends to approximately 75 m^3 of gaseous Helium. This gas would then be located near the ceiling of the room. A proper analysis of possible oxygen-deficiency hazards associated with the S^3 superconducting magnets will be performed.

5.3 Conclusion of conventional hazard comparison

With respect to conventional safety, we do not expect significant differences between the two magnet technologies being considered. In each case conventional rules and mitigation methods are well known and detailed safety analyses will be performed—reviewed by GANIL and Spiral 2 safety authorities—to precisely assess the risks and to work on the mitigation of any identified risks from the beginning of the detailed design phase. These hazards are common to accelerators and at the existing GANIL facility. Standard rules and mitigating factors will be applied.

6 Nuclear Safety issues and proposed solutions

The following statements concern the S^3 area, but are elaborated within the framework of the AEL (LINAG experimental rooms, including NFS) and more generally of the SPIRAL2 project safety plan.

The present analysis deals with the nuclear risks related to the normal operation and the accidental conditions of S^3. Even if the aspects related to the dismantling of the facility are considered in a further stage, one must take them into account in the preliminary studies since the waste generation is directly correlated to the activation level.

The following study focus on the beam dump room, the most critical area for radioprotection and safety point of view. The target area is also being considered because of the possibility of using actinides targets. The main objectives for safety issues are:

- target area : no contamination problem, limited activation
- beam dump room : activation limited under the radioprotection control
- main spectrometer area : limited activation, no contamination

Concerning the impact of magnet technology the following safety aspects are:

- equipments activation in the beam dump room
- activation of fluids
- accidental scenario
- maintenance and handling

Present studies focus on activation calculations for the main materials and fluids. This is a key issue in the establishment of the radioprotection constraints and furthermore in the analysis of the maintenance and accidental scenarios.

6.1 Assumptions on operating scenarios

For nuclear safety purposes, four main assumptions are considered for S^3:

- A "covering scenario" used for the design of the S^3 room (wall thickness, beam dump room confinement, underground building…) concerning the interaction of the beam with stopping material. A ^{12}C beam of 14.5 MeV/n and intensity 1 mA (1.6×10^{15}pps for Q=4+) was chosen as the envelope case to determine wall thickness and earth activation. Do note that 1 mA beam of ^{12}C at 14.5MeV/n is an extreme case since it corresponds to the highest, most penalizing energy for A/q=3 with the highest intensity. After interacting with the target, the primary beam is directed towards a beam dump located in a dedicated place in the physics hall. Other reaction products are transmitted by the spectrometer up to a detection plane.
- A "realistic scenario" and "conservative scenario" used to assess the radioprotection issues inside S^3 room and mainly in the beam-dump room. The "realistic scenario" is based on the operating scenario (see 2.7) and used during 10 year of operation. The "conservative scenario" corresponds to a ^{12}C at 14,5MeV/n for an intensity of 30 pµA (1.8×10^{14}pps) intensity which is more realistic than the "covering scenario". These two scenarios are used for activation calculations and its impact in terms of radioprotection.
- The use of thin actinide targets in the target area. Actinides are present as unsealed source (thin layer): the mass is to 45 mg per radionuclide. The radionuclide list and quantities have been established according to physics needs.

These actinide targets will be irradiated by ion beams accelerated to about 14.5 MeV/A (S^3). The reaction products are extracted for analysis in the physics halls. The possibility of using the activities

requested by the physicists will be analyzed in parallel to the definition of operations and associated safety analyses. The consequences of certain statutory requirements on operation must also be taken into account.

6.2 Radiological inventories and nuclear materials

6.2.1 Actinide targets

The radiological inventories identified for the physics requirements are not exhaustive but must be sufficient to define an envelope in order to analyze the risks of exposure to ionizing radiation. For the risks of internal exposure, this envelope will be defined by maximum activity and DPUI.

Only one target at a time can be in use in the physics halls. The other targets are stored in a dedicated cabinet.

Thin targets are considered as unsealed sources. The maximum mass of each radionuclide is estimated at 45 mg. The associated maximum activity is 7.10^9 Bq (^{249}Cf) for hall S^3 (and 2.10^{10} Bq (^{244}Cm) for hall NFS).

6.2.2 Nuclear materials

The values requiring authorization for the held of nuclear materials have been identified further to a preliminary analysis of the regulations:

- $\sum$Pu or ^{233}U > 3 g
- U enriched to 20 % or more in isotope ^{235}U > 15 g.)

The activities requested by the physicists are subject to authorization. Currently, the INB 113 (GANIL) is subject to declaration.

6.2.3 Mechanisms for induced activation

Interaction of primary beams with the material (vacuum chamber walls, beam dumps, etc.) induces activation by two different processes:

- Direct interaction of the primary beam ions with the material,
- Indirect activation by the neutrons produced in nuclear reactions.

The first mechanism is very localised, limited to the path of the ions in the material (of the order of a few hundred micrometers for a Carbon beam) and limited to the elements impacted by the primary beam. Maximum activation is therefore specific to the beam-dump, for which the design is presently in progress. Indirect activation results in specific activity of the surrounding equipments. Note that composition and geometry of the main components of the magnet (for room temperature multiplet and superconducting multiplet) are a key for the calculation of induced activation and associated dose rate.

6.3 Identification of risks

6.3.1 External radiation exposure risks

6.3.1.1 Access management system

This system is dedicated to access management in the various installation areas likely to exhibit an equivalent dose rate (DER) incompatible with the radioprotection objectives. This can occur while the machine is in operation and, depending on the case, due to the gamma emission from activation of some interceptive equipment (beam dumps, targets, etc.), .

This system is divided into two subsystems, the access management unit (UGA) and the marker management unit (UGB).

A dedicated system is used to manage the risks related to X radiation (UGS-X).

6.3.1.2 Actinides

The actinide targets in hall S^3 exhibit no special risks of external exposure (see ^{248}Cm).

Although DER is not incompatible with the use of these targets, these values will require suitable measures, especially during preparation in glove box and transfers for both types of source.

6.3.1.3 Neutron and γ radiation

External radiation exposure risks results mainly from:

- neutron production when the ion beam interacts with the stopping material of the beam dump,
- γ rays emitted by the different activated materials when beam is off.

The external prompt dose rate due to neutron production has been studied on the basis of a preliminary conceptual design of the super separator spectrometer room. The calculations results are resumed in this document and the safety and radioprotection issues discussed in terms of recommendations.

The activation of different materials has been calculated taking into account both primary interaction (ion beam interaction with the stopping material of the beam dump) and the one induced by secondary neutrons in the beam dump and surrounding materials. Residual γ dose rate coming from the beam dump has been calculated since it is the main contributor to the external dose when the beam is off.

The access of workers inside the different rooms must be allowed as soon as possible after operating the S^3 spectrometer. This is necessary for maintenance of equipments and for the preparation of the next experience. It is planned to carry out at maximum 2 runs a year (90 days duration for each experience). To reach this goal, the design must be optimized in terms of choice of stopping material (beam dump) and the material for the surrounding equipments in order to minimize de dose rate. This can also be achieved by using an effective biological shielding (some proposals given in this chapter) or by very reliable equipments with low maintenance needs (limit the time of exposure - ALARA concept).

Preliminary analysis for the first building design

In order to evaluate the external dose rate when the S^3 separator is in operation a first preliminary analysis has been performed. The "covering scenario" was used and two different stopping materials have been considered (copper and nickel). The modelling of the S^3 beam dump location and surrounding material (wall concrete and optical elements) was done based on the first preliminary design. Activation calculations were done for many types of equipment as beam dump, multipole, vacuum chamber…

These first calculations allow recommendations for safety and radioprotection issues:

- S^3 room has been underground in order to optimise the thickness of concrete wall and to limit external dose rate outside the facility. The walls must be at least 60 cm thick in order to limit the activation level of the surrounding earth to 10% of the allowed value. Moreover, the concrete ceiling must be 65 cm thick (plus 2 m of earth above) to reach a dose rate lower than the limit of 0.5 µSv/h at the surface.
- The beam dump room must be circumscribed by a wall of concrete up to 50 cm thick. The backroom wall must be 220 cm thick in order to reduce the neutron flux to an acceptable level of 1 µSv/h (limitation for public access).
- High level of beam-dump activity calculated imposes the use of a setup with a local shielding around the beam-dump to protect workers from external exposure to γ radiation resulting from activation.

- Activation of optical elements must be investigated with the new design and more realistic irradiation scenario. This study is presented in this document for the room temperature multiplet option.

As an example of the first preliminary analysis, Figure 92 shows the results of neutron dose rate inside S^3 room. Presently, the final drawings of S^3 room have been updated by taking into account the above recommendations and with radioprotection margin for concrete wall. This modification must be further validated by new calculations with respect to the radioprotection objectives.

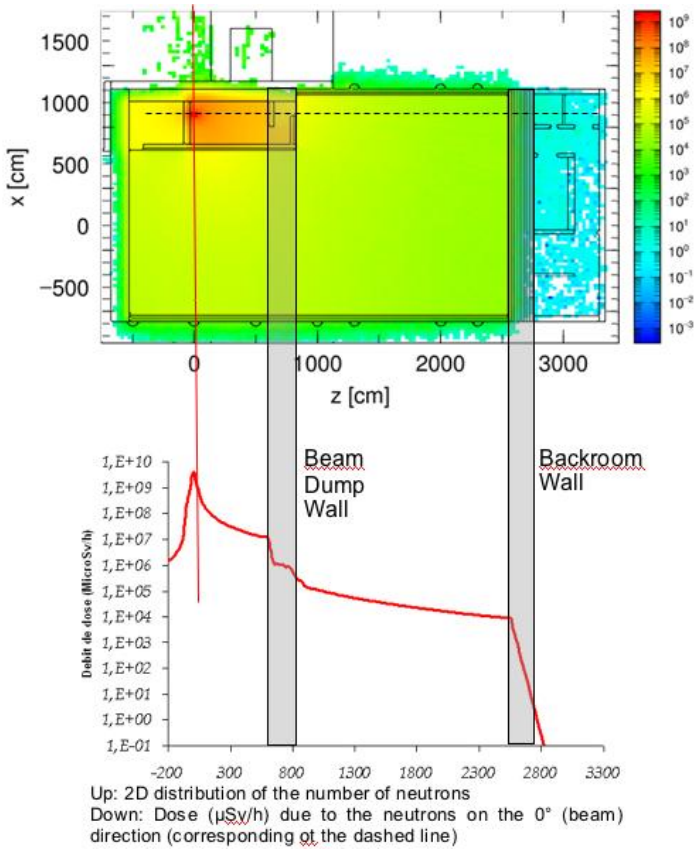

Figure 92 : neutron dose rate distribution from Beam Dump to outside of S^3 room

Methodology for beam dump and classical multiplet option

Methodology used for the first analysis is adopted in the present case for the activation and dose rate calculations by taking into account the last beam-dump and room temperature multiplet design (April 2010). A more complete study for the definition of the beam-dump stopping material was realized but it is not described in this document. PHITS code is used for transport and nuclear reaction calculations while activation calculations have been performed with CINDER'90. Note that other models must be prospected to evaluate the level of confidence of the results. However, few of them (MCNPX(V2.6) and FLUKA(2008)) are not appropriate to model heavy ion interaction at low energy. Equivalent dose rate is evaluated using MERCURAD code and compared with MCNPX results (photon transport).

An example of the isotope yields produced by ^{12}C on Nickel stopping material is shown on Figure 93. At this low energy nuclear reactions are dominated by fusion process and nucleon transfer between beam and target. A large amount of light particles (from neutron to alpha) are also emitted during evaporation and pre-equilibrium phases. These mechanisms are described by PHITS even if it is very difficult to guarantee the quality of the results. Note that the choice of the evaporation model impact on the emission of light particle as neutron (for neutron induced activation, the most conservative model is used for safety margins).

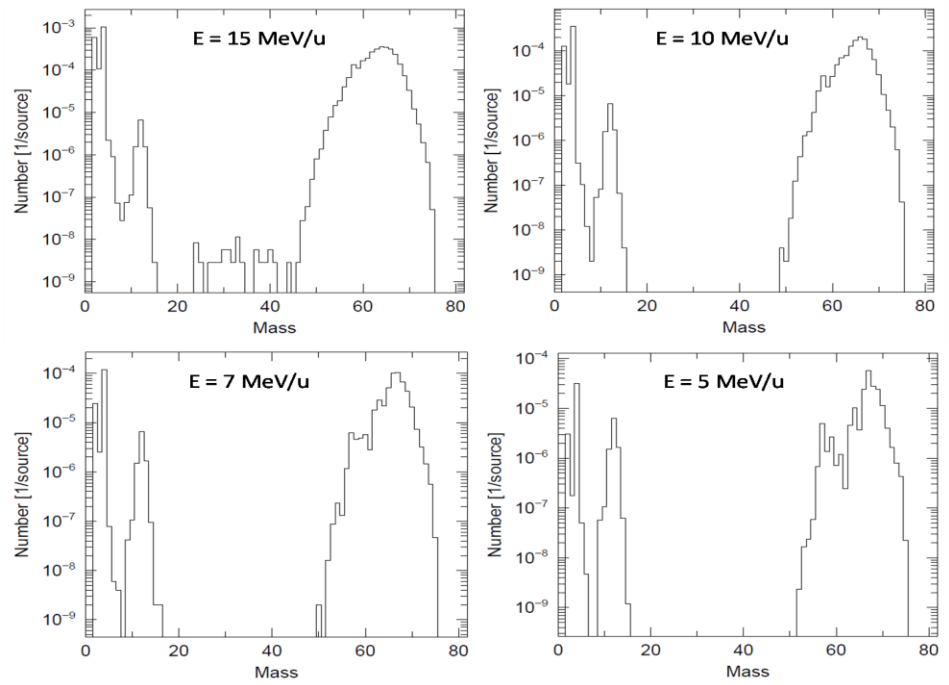

Figure 93 : distribution of isotope yields produced by 12C on Nickel at 5, 7 10 and 15MeV/n.

Radiological impact of the beam dump

As mentioned above, the critical point for radioprotection issues is the activation of the beam-dump. The first analysis shows that a local shielding must be considered. Activation calculations were realized with a large amount of reactions (evolution of beam, energy and stopping material) in order to analyze several radiological spectra reachable during S^3 operation. Activation takes into account direct reactions as well as secondary (neutron and proton induced) reactions. Three irradiation and decay scenarios are take into account for radioprotection and waste management purposes. Dose rate calculations are performed to give information on the thickness of the local shielding according to the feasibility criteria (radioprotection, space limitations, mass...). Lead material is considered as the best choice for photon absorption (good X-ray attenuation coefficient) and due to its low activation expected. Dose rate calculations were performed for several lead thicknesses (from 0 cm to 25 cm) with the most recent beam-dump design. Results are presented in Figure 94 for several configurations (couples beam/target for available energies). In order to agree with the access management (presently the objective correspond to controlled green area under French regulatory legislation, equivalent to the classification of the present GANIL experimental areas), the dose equivalent rate must be below a maximum of 25 µSv/h (red line showing the limit in Figure 94). Figure 94 presents the equivalent dose rate for two decay times (1 hour on the left and 1 day on the right). 10 cm of lead seems to be a good choice to reach this objective. Indeed, the dose rate is below 25µSv/h for each configuration after 1 day of decay time and for most of them after 1 hour. Note that 10 cm thickness of lead is admissible from the point of view of additional considerations (encumbrance limitations, mechanics and mass).

Other considerations have to be evaluated:

Dose equivalent rate coming from other activated materials, mostly from optical element close to the beam-dump. Preliminary results are given later on in this document.

The decay time objectives according to maintenance needs for the equipments.

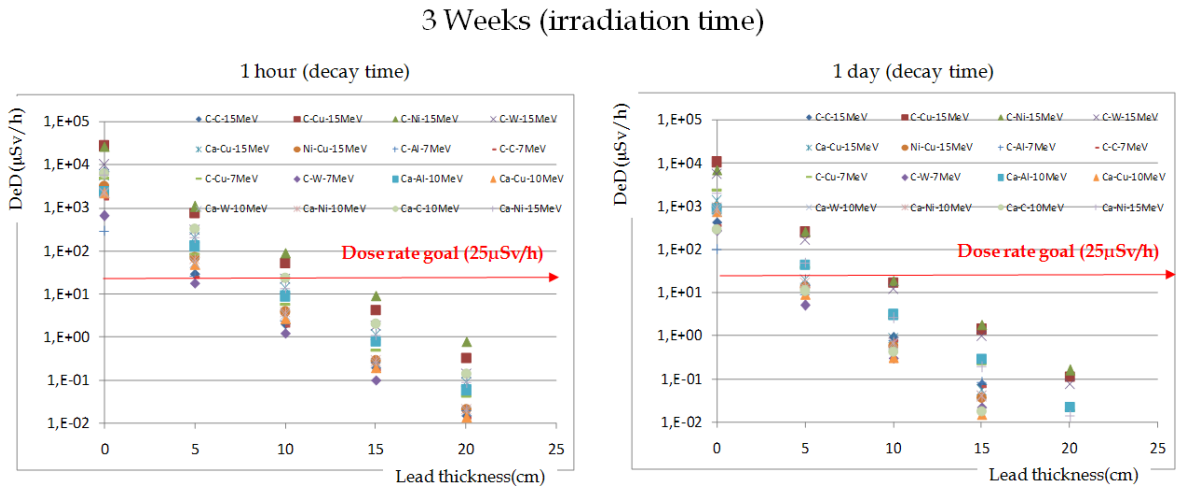

Figure 94 : dose rate calculation for several beam/target configurations as a function of lead shielding thickness

Although the beam dump and its local shielding design are not yet completely defined, the activation of other equipments inside the beam dump room by neutrons produced in the beam dump can be evaluated at this stage, provided that it will not be much affected by the final shielding. Outside the beam-dump room the level of activity is expected to be significantly lower.

Radiological impact of the magnets

Concerning the choice of magnet technology (room temperature multiplet or superconducting multiplet option), only the room temperature option has been studied so far. Indeed, the design of the superconducting multiplet is not defined yet and the cooling fluid is not decided. However, limited information on superconducting multiplet composition is available (it contains mainly steel, iron and Nb-Ti materials). Therefore, we found interesting to evaluate by a preliminary study the radiological impact related exclusively to material composition (without taking into account multiplet geometry).

Activation calculations for the room temperature multiplet option were performed with the two scenarios described in chap 6.1. Results after 10 years of operation are given in Figure 95 for a dose equivalent rate at 30 cm from the most activated opened multipole. This value takes into account the contributions from the three multipoles. The model used for one multipole is presented on Figure 95.

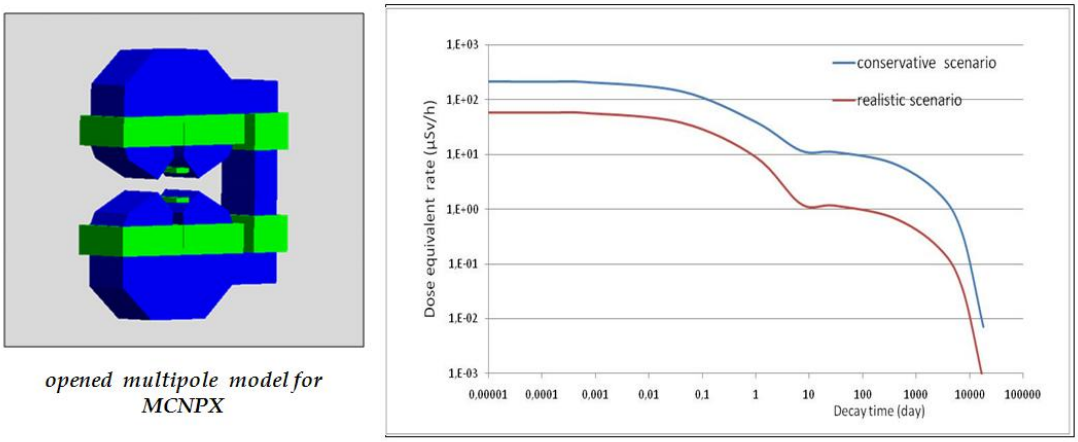

Figure 95 : Multipole model under MCNPX (left) and dose rate equivalent at 30 cm from the most activated opened yoke multipole as function of decay time (right)

After one hour of cooling time (reasonably corresponding to the minimum decay time for entering into the beam-dump room) the equivalent dose rate are close to 170µSv/h (conservative scenario) and close to 40µSv/h (realistic scenario). There values are not compatible with the radioprotection objectives. Consequently, a longer decay time (between 1 or few days) is required before entering the beam-dump area. At this stage, this configuration is acceptable from the radioprotection point view.

As mentioned above, for the superconducting option, geometry design is in progress. To evaluate radiological impact on material (expected for superconducting option), a simple analysis has been performed. Using a reference neutron flux and the same irradiation scenario (6 months/year of irradiation during 10 years of operation), activation and dose rate calculations have been performed with seven materials and plotted in Figure 96 (chemical composition is taken from a data library from GANIL, instead of Nb-Ti where composition was arbitrary chosen 50%Nb and 50%Ti). Nb-Ti seems to be the most penalizing material only for the lowest decay time (accidental scenario, eventually). Copper and Steel are the most penalizing materials for with respect to maintenance activities. Note that for the room temperature multiple, dose rate (Figure 95) mainly comes from copper activation. Aluminum and iron are the most interesting materials (iron for long decay times).

At present the superconducting magnet is planned to be made of steel (but without information on chemical composition), Nb-Ti (very low masses) and probably Iron. Note that mass of the magnet is important for the evaluation of equivalent dose rate, but is expected to be significantly lower than the room temperature option. Also note that steel activation comes partially from impurities as for example cobalt. If necessary, its activity can be decreased by requiring low impurities concentration for the chosen material.

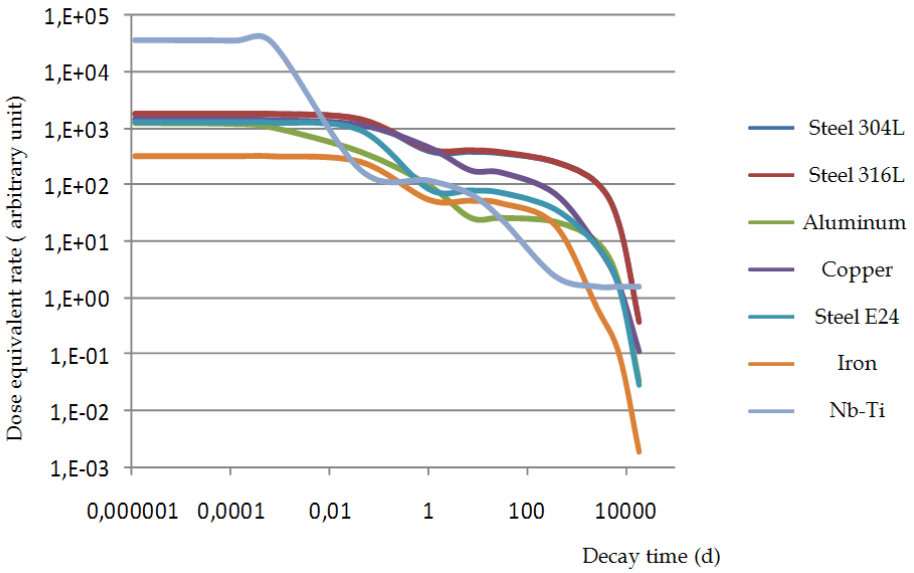

Figure 96 : radiological impact due to γ radiation produced by materials

To go further, geometry must be included for activation and dose rate calculations. This is fundamental to conclude on safety and radioprotection issues. Moreover, activation of cooling fluids is needed to assess the consequence of accidental leakages (contamination) and waste management.

This simple analysis shows that more precise calculations are needed to conclude even if for the moment this solution cannot be yet rejected.

6.3.1.4 Conclusions

There preliminary evaluations have to be considered by taking into account their limits:

- Only one reaction code has been used. A comparison with other codes is underway, as well as a validation by experimental results.

- Concerning the superconducting multiplet option design, activation and dose rate calculations will involve a more detailed design when it will be available.

However, by using several scenarios dedicated to specific goals these calculations allow to obtain orienting values for the activity spectrum and dose rate expected in the S^3 room and more precisely in the beam-dump room. The hall biological protections are designed according to the maximum intensity and energy of the most conservative beam likely to be used in each hall.

Beam dump design

Local biological protections will be installed to limit the external exposure to γ radiation resulting from the activation of the equipment, especially the beam dumps as the main activation comes from the stopping material. The first preliminary results show that a local shielding of 10 cm of lead seems to be appropriate for radioprotection purposes. As previously seen, a more complete calculation must be done with all the equipments inside the beam-dump room, each equipment bringing its own contribution. In addition, a more realistic beam-dump design (based on optical constraints) and more precise beam loss localization is needed to optimize the design of this local shielding. For example, a specific shielding (in term of thickness) is expected around the interceptive fingers. Activation calculation for this local protection has to be investigated even if lead seems to be a good candidate from the activation point of view. In addition, a solution for a removable local shielding is under study. Indeed, this could be an interesting feature under accidental conditions (confinement) and from the radioprotection point of view (replacement if activation too high). Installation of biological protection is clearly a strong link with the global optics design.

Impact on magnet technology

At present, only activation and dose rate calculations for room temperature option have been realized. The results showed an important radiological impact due to the large amount of materials in this case (10 tons of copper and iron per multipole). For radioprotection issues, a delay for access into the beam dump room is needed, according to access management defined by radioprotection objectives. This delay (around 1 day for the worst cases) remains compatible with the operation of the spectrometer. Nevertheless, the reliability of the beam dump is taken into consideration in its design, in order to minimize the required interventions.

Concerning superconducting option, no calculations are available because of the lack of information concerning the preliminary design and material composition. Moreover, one study concerning only the type of material, shown that steel (main component of superconducting element) is not the best candidate from radioprotection point of view. However, the total mass of material is actually lower than in the room temperature option. Therefore, an activation calculation must be done using a realistic geometry to verify the compatibility of radiological impact of this option with GANIL objectives. Remember that activation comes from neutron produced by nuclear reactions into the beam-dump and at this moment no neutron attenuation material is planed around the beam dump.

Finally, for safety issues, fluids activation must be evaluated.

Nuclear safety linked to the actinide target

The target design has no impact on the magnet technology. A summary of this topic can be found in the "Overview of the S^3 project" document.

6.3.1.5 Interceptive equipment

The measures to be implemented when opening the vacuum chamber will be defined after analyzing the risks of internal exposure. The GANIL procedures, at least, will be applied (non-contamination checks, smears, etc.).

6.3.2 Non-nuclear risks

6.3.2.1 Fire

The "fire" approach will be based, in particular, on the decree dated 31 December 1999 modified. This approach will consist in the following:

- Analyze the fire risks for all AELs
- Limit the risk factors (ignition sources, inflammable or explosive materials, etc.)
- Define the fire sectorisation for all AEL premises
- Detect and locate a possible fire A fire in one fire area must not result in loss of fire detection in another fire area. The routing of the detection links is adapted to the fire sectorisation.
- Set off the fire alarm.
- Guarantee the fire resistance of the elements forming the fire sectorisation and of the supporting elements.
- Implement firefighting means (fixed or mobile).

The nuclearised areas will be 2-hour rated fire sectors. It is important to guarantee the fire resistance of the last filtration level (VHE filter, efficiency 10^3) while favouring extraction to limit dissemination outside the second static confinement barrier.

For the "beam dump" areas, the approach will consist in limiting as much as possible the heat load potential and the ignition sources.

6.3.2.2 Handling

Construction measures are implemented to limit or even exclude the risks of falling (handling equipment). In particular, the reaction box must only be transported using the handling equipment.

For workers, the design assumption in accidental situation is fall of the target with loss of confinement. The integrated dose must be calculated considering a 30 second delay for the operators to put on their personal breathing masks.

Similar estimations must be carried out for all stable targets likely to be used in the various physics halls.

6.4 Waste – effluents

The approach will be based on the GANIL waste study. The waste study will have to be modified to include the actinides.

Radioactive solid wastes result from primary beam interaction with the stopping material of the S^3 separator beam dump and from neutron activation of materials surrounding this BD. Activation of main equipments are under study on the basis of the preliminary BD design used for the neutron dose rate evaluation. Calculations are performed by using PHITS and CINDER codes for the following materials:

- the BD (stopping material Ni or Cu, cooling water and cladding in stainless steel),
- the nearest Qpoles (iron, cooling water and support structures),
- the vacuum chamber and its support structure,
- the ordinary concrete of walls.

The activation of different possible shielding materials has not been yet calculated.

Preliminary calculation results are presented in Figure 97. These results have not been yet analysed in terms of activity concentration of the different nuclear wastes to be managed during the operation of

the facility (replacement of equipments for instance) and in view of its future decommissioning (cleaning and dismantling of the structures). Meanwhile the results show a significant level of activity generated during operation and slowly decreasing after operating. The main contributor to the activity is the BD stopping material.

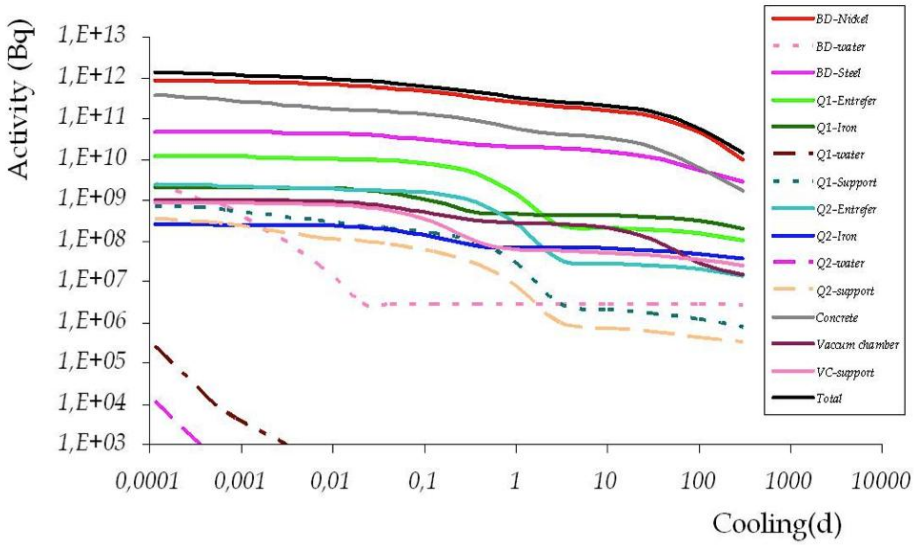

Figure 97: Activity of materials in the S³ zone 1room as a function of decay time

Radioactive liquid wastes can be generated by the use of a cooling system to evacuate the power deposited (40 kW) in the beam stopping material. If water is used to cool down the BD, it is highly recommended to use purified water and to maintain the level of corrosion products as low as possible, eventually by the use of ion exchange resins. In the case of a water cooling loop, tritium can be produced and has to be considered in terms of potential internal dose rate risks during maintenance of the cooling system. Due to the high level of neutron energy and flux, ^{16}N is the main contributor of water activity due to the neutron flux and has to be considered in terms of potential external dose risks as emitter of high energetic γ rays. Consequently a biological shielding should be locally adapted to reduce the contribution of γ rays to the prompt dose in the vicinity of the primary coolant loop including the thermal exchanger.

Cooling systems would be needed for the magnets in the case of room Temperature multipoles too.

Radioactive gas can be generated mainly in the BD room. They are due to air activation with regards to the level of neutron flux and the energy spectrum. It could be needed to use a nuclear HVAC system with air filtered at the inlet in order to avoid the activation of dust particles. If the recycling of air is required to be able to access shortly after operating the BD without specific equipments (face masks), then the recycling rate of activated air with fresh air should be studied in order to minimize the internal dose rate by taking advantage of the decay of the short lived radioisotopes.

6.5 Transport

The activities requested by the physicists require, especially for the ^{249}Cf targets and for ^{239}Pu, type B packaging.

7 Budgets and schedules

7.1 Preliminary cost estimate of the spectrometer

7.1.1 Mass Separator based on superconducting technology {T5-ED-T6-T7-DM-T8}

This separator design is based on one type of SC triplet:	**Cost**	**Margin**
• 4 closed superconducting triplets (T5-T6-T7-T8)	€1.280M	15%
• 1 magnetic dipole (DM)	€0.100M	15%
• 1 electric dipole (DE)	€0.350M	15%
• Slits	€0.045M	15%
• Power supplies	€0.302M	15%
• Vacuum chambers	€0.011M	15%
• Supports	€0.136M	15%
• Diagnostics & controls	€0.098M	15%
• Vacuum system	€0.190M	15%
TOTAL equipment	**2.512M€**	**0.376M€**

7.1.2 Momentum Achromat {T1-DM-T2-T3-DM-T4}

7.1.2.1 Momentum Achromat based on SC technology {T1-DM-T2-T3-DM-T4}

This separator design is based on three types of SC triplets:	**Cost**	**Margin**
- {T1,T4} closed superconducting triplet		
- {T2} open superconducting triplet		
- {T3} closed superconducting triplet with the same dimensions as the open triplet.		
• 3 closed superconducting triplets	€1.100M	15%
• 1 open superconducting triplet	€0.600M	15%
• 2 magnetic dipoles (DM)	€0.150M	15%
• Beam dumps and slits	€0.215M	30%
• Power supplies	€0.187M	15%
• Vacuum chambers	€0.022M	15%
• Supports	€0.136M	15%
• Diagnostics & controls	€0.206M	15%
• Vacuum system	€0.193M	15%
TOTAL equipment	**2.849M€**	**0.460M€**

7.1.2.2 Momentum Achromat based on mixed technology {T1-DM-T2-T3-DM-T4}

The separator design is based on three types of triplets:	**Cost**	**Margin**
- {T1,T4} closed superconducting triplet		
- {T2} open room temperature triplet		
- {T3} closed room temperature triplet		
• 2 closed superconducting triplets	€0.640M	15%
• 1 open room temperature triplet	€0.360M	15%
• 1 closed room temperature triplet	€0.300M	15%
• 2 magnetic dipoles (DM)	€0.150M	15%
• Beam dumps and slits	€0.215M	30%
• Power supplies	€0.379M	15% TBD
• Vacuum chambers	€0.022M	20%
• Supports	€0.136M	20%
• Diagnostics & controls	€0.206M	15%
• Vacuum system	€0.193M	15%

TOTAL equipment	**2.601M€**	**0.430M€**

7.1.2.3 Momentum Achromat based on RT technology {T1-DM-T2-T3-DM-T4}

The separator design is based on two types of triplets:

- {T1, T3,T4} closed room temperature triplet
- {T2} open super-conducting triplet

• 1 open room temperature triplet	€0.360M	15%
• 3 closed room temperature triplet	€0.900M	15%
• 2 magnetic dipoles (DM)	€0.150M	15%
• Beam dumps and slits	€0.215M	30%
• Power supplies	€0.570M	15% TBD
• Vacuum chambers	€0.022M	20%
• Supports	€0.136M	20%
• Diagnostics & controls	€0.206M	15%
• Vacuum system	€0.193M	15%
TOTAL equipment	**2.752M€**	**0.453M€**

Summary of the different options:

	Momentum Achromat	Mass Separator	Total
Option 1	Superconducting	Superconducting	5.361 M€
Option 2	Mixed	Superconducting	5.113 M€
Option 3	Room temperature	Superconducting	5.264 M€

TOTAL Manpower: 20.5 FTE **2.40M €**

In the case of superconducting technology a central cryogenic system is needed. Different approaches are under study. Here we included the price of a central refrigerator, as it would have a much higher efficiency than cryocoolers and it would also enable a much faster cool down of the magnets (makes feasible for idle times of the spectrometer of even a week; see previous section).

The cryogenic refrigerator is based on a complete system of an existing design. It is oversized by about a factor of 2 (130 Watts of 4.5K cooling power with liquid nitrogen pre-cooling) and uses about 45 kW of electricity.

TOTAL refrigerator: 0.600M€

Discussions are underway with SPIRAL2 to see to what extent the SPIRAL2 cryogenic system can be used to serve the needs of S^3.

7.2 Preliminary cost estimates of the other components of the project

-	**Primary target station**	**Cost**	**Margin**
	• Stable target system	€0.070M	15%
	• Actinide target system	€0.140M	15%
	• Vacuum system	€0.040M	15%
	• Supports	€0.012M	15%
	• Diagnostics	€0.030M	15%
	• Containment	€0.075M	15%
	TOTAL equipment	**0.367M€**	**0.055M€**
	TOTAL Manpower, 6.8 FTE	**0.796M€**	
-	**Detection in the final focal plane**	**Cost**	**Margin**
	• Tracking detectors	€0.107M	15%
	• Implantation / tunnel detectors	€0.188M	15%
	• Gamma detection	existing	
	• Electronics & DAQ (600 digitizers and time stamping) *(based on Exogam2 electronics)*	€0.640M	20%
	• Mechanics and supports	€0.040M	20%
	TOTAL equipment	**0.975M€**	**0.180M€**
	TOTAL Manpower, 10 FTE	**1.17M €**	
-	**Low energy branch**	**Cost**	**Margin**
	• Gas catcher and RF cooler	€0.330M	15%
	• High-voltage platform	€0.050M	15%
	• Mass separator	€0.470M	15%
	• Laser system	existing	
	• Roots pumps	existing	
	• Mechanics and supports	€0.030M	15%
	TOTAL	**0.880M€**	**0.132M€**
	TOTAL Manpower, 7.5 FTE	**0.878M€**	
	Total equipment (2.222M€ + 0.367M€ Margin)	**2.589M€**	
	Manpower, 24.3 FTE	**2.843M€**	
	Grand Total (Equipment + Margin + Manpower)	**5.432M€**	

7.3 Schedule according to magnet technology

7.3.1 Room temperature closed and open magnets schedule

The following schedule assumes the use of three room temperature closed triplets and one room temperature open triplet for the momentum achromat.

Nom de la tâche	Durée	Début	Fin
Magnet techno choice	0 jour	Lun 03/05/10	Lun 03/05/10
Optical line geometry optim	2 mois	Lun 03/05/10	Ven 25/06/10
Line mechanical definition	3 mois	Lun 31/05/10	Ven 20/08/10
TDR magnets (DDR, CDR...)	10 jours	Lun 15/11/10	Ven 26/11/10
Project Critical Definition Review OK	0 jour	Lun 13/12/10	Lun 13/12/10
RT closed triplets	**601 jours**	**Lun 03/05/10**	**Lun 20/08/12**
RT closed triplet Optim	3 mois	Lun 03/05/10	Ven 23/07/10
RT closed magnets spec.	3 mois	Lun 26/07/10	Ven 15/10/10
Call for tender RT closed magnets	5 mois	Lun 18/10/10	Ven 04/03/11
Bids and order	1 mois	Lun 07/03/11	Ven 01/04/11
Kick off industry tasks	1 jour	Lun 04/04/11	Lun 04/04/11
Studies at subcontractor	5 mois	Mar 05/04/11	Lun 22/08/11
Supply of raw materials	3 mois	Mar 31/05/11	Lun 22/08/11
tools supplying	3 mois	Mar 23/08/11	Lun 14/11/11
closed multipole #1 manufacturing	4 mois	Mar 15/11/11	Lun 05/03/12
closed multipole #1 fields maps	2 mois	Mar 06/03/12	Lun 30/04/12
closed multipoles #2 to #9 manufacturing	6 mois	Mar 06/03/12	Lun 20/08/12
closed multipoles Field maping	6 mois	Mar 06/03/12	Lun 20/08/12
RT closed magnets ready for installation	0 jour	Lun 20/08/12	Lun 20/08/12
RT open triplet	**501 jours**	**Lun 03/05/10**	**Lun 02/04/12**
RT open triplet Optim	4 mois	Lun 03/05/10	Ven 20/08/10
RT open magnets spec.	3 mois	Lun 23/08/10	Ven 12/11/10
Call for tender RT closed/open magnets	5 mois	Lun 15/11/10	Ven 01/04/11
Bids and order	1 mois	Lun 04/04/11	Ven 29/04/11
Kick off industry tasks	1 jour	Lun 02/05/11	Lun 02/05/11
Studies at subcontractor	5 mois	Mar 03/05/11	Lun 19/09/11
Supply of raw materials	3 mois	Mar 28/06/11	Lun 19/09/11
tools supplying	3 mois	Mar 20/09/11	Lun 12/12/11
open multipoles #1 to #3 manufacturing	2 mois	Mar 13/12/11	Lun 06/02/12
open multipole Field maping	2 mois	Mar 07/02/12	Lun 02/04/12
RT open multipoles ready for installation	0 jour	Lun 02/04/12	Lun 02/04/12

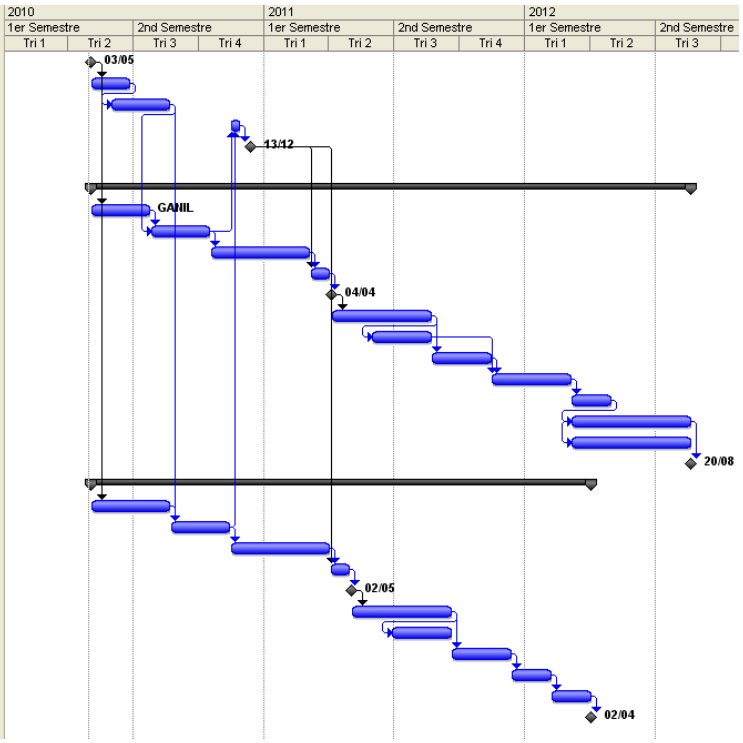

7.3.2 Superconducting open magnet (MOSAR) schedule

		Nom de la tâche	Durée	Début	Fin
1		Magnet techno choice	0 jour	Lun 03/05/10	Lun 03/05/10
2		Optical line geometry optim	2 mois	Lun 03/05/10	Ven 25/06/10
3		Spectrometeer line mechanical definition	3 mois	Lun 31/05/10	Ven 20/08/10
4		TDR magnets	1 jour	Lun 18/10/10	Lun 18/10/10
5		Project Critical Definition Review OK	1 jour	Lun 13/12/10	Lun 13/12/10
6					
7		**SC open magnets (MOSAR)**	**905 jours**	**Lun 03/05/10**	**Ven 18/10/13**
8		conceptual design	6 mois	Lun 03/05/10	Ven 15/10/10
9		Preliminary IRFU technical design	4 mois	Lun 26/07/10	Ven 12/11/10
10		conductor supply (IRFU)	6 mois	Mar 14/12/10	Lun 30/05/11
11		Call for tender	5 mois	Mar 19/10/10	Lun 07/03/11
12		Bids and order MOSARs	1 mois	Mar 08/03/11	Lun 04/04/11
13		Kick off MOSAR subcontract	1 jour	Mar 05/04/11	Mar 05/04/11
14		Detailed design by subcontractor	5 mois	Mer 06/04/11	Mar 23/08/11
15		Production Readiness review	1 jour	Mer 24/08/11	Mer 24/08/11
16		**Coil qualification**	**41 jours**	**Mer 29/06/11**	**Mer 24/08/11**
17		Coil mockup manufacturing and qualif	2 mois	Mer 29/06/11	Mar 23/08/11
18		Coil Status review	1 jour	Mer 24/08/11	Mer 24/08/11
19		**Cryostat**	**180 jours**	**Jeu 25/08/11**	**Mer 02/05/12**
20		MOSAR Cryostat manufacturing	9 mois	Jeu 25/08/11	Mer 02/05/12
21		**Multipole 1 (prototype)**	**301 jours**	**Mer 24/08/11**	**Mer 17/10/12**
22		Multipole 1 (prototype) Coils winding	6 mois	Jeu 25/08/11	Mer 08/02/12
23		Cold mass multipole 1 manufacturing	4 mois	Mer 24/08/11	Mar 13/12/11
24		Multipole 1 (prototype) assembly	3 mois	Jeu 09/02/12	Mer 02/05/12
25		Multipole 1 qualification	4 mois	Jeu 03/05/12	Mer 22/08/12
26		Multipole 1 in MOSAR cryostat	2 mois	Jeu 23/08/12	Mer 17/10/12
27		Prototype review (OK for multipoles 2 and 3)	1 jour	Jeu 23/08/12	Jeu 23/08/12
28		**Multipoles 2 and 3 assembly/qualification**	**220 jours**	**Ven 24/08/12**	**Jeu 27/06/13**
29		Cold mass multipoles 2 and 3 manufacturing	5 mois	Ven 24/08/12	Jeu 10/01/13
30		**Multipole 2**	**160 jours**	**Ven 24/08/12**	**Jeu 04/04/13**
31		Multipole 2 coils winding	4 mois	Ven 24/08/12	Jeu 13/12/12
32		Multipole 2 assembly	1 mois	Ven 11/01/13	Jeu 07/02/13
33		Multipole 2 in MOSAR cryostat	2 mois	Ven 08/02/13	Jeu 04/04/13
34		**Multipole 3**	**140 jours**	**Ven 14/12/12**	**Jeu 27/06/13**
35		Multipole 3 coils winding	4 mois	Ven 14/12/12	Jeu 04/04/13
36		Multipole 3 assembly	1 mois	Ven 05/04/13	Jeu 02/05/13
37		Multipole 3 in MOSAR cryostat	2 mois	Ven 03/05/13	Jeu 27/06/13
38		**Full MOSAR**	**81 jours**	**Ven 28/06/13**	**Ven 18/10/13**
39		Final MOSAR qualification in MOSAR cryost	4 mois	Ven 28/06/13	Jeu 17/10/13
40		Final review and OK for integration in S3	1 jour	Ven 18/10/13	Ven 18/10/13

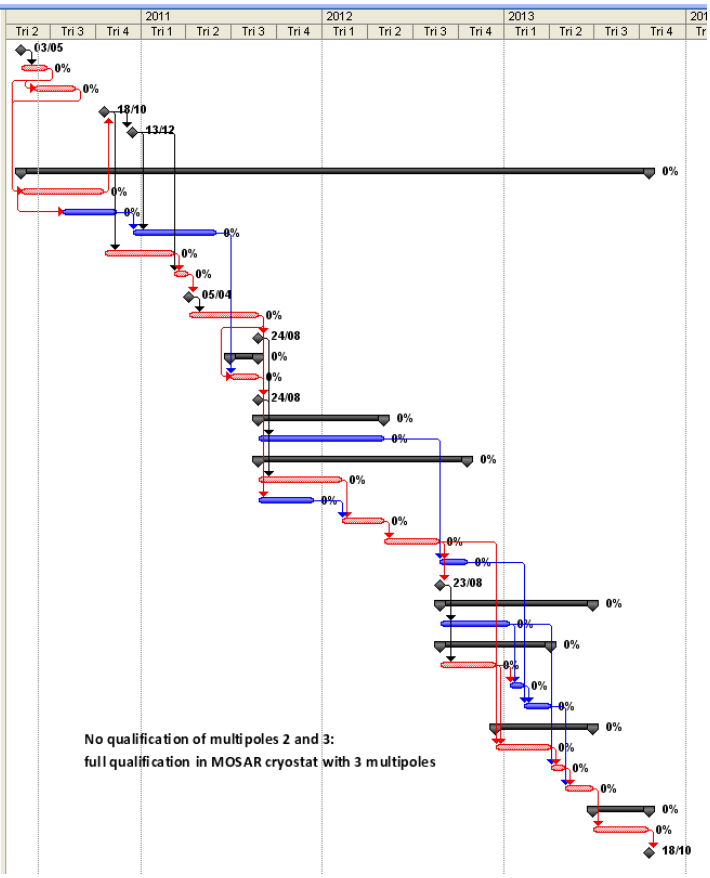

7.3.3 Superconducting closed magnet schedule

The following schedule assumes the use of three superconducting closed triplets in the momentum achromat and four superconducting triplets in the mass spectrometer.

Nom de la tâche	Durée	Début	Fin
Magnet techno choice	0 jour	Lun 03/05/10	Lun 03/05/10
Optical line geometry optim	2 mois	Lun 03/05/10	Ven 25/06/10
Line mechanical definition	3 mois	Lun 31/05/10	Ven 20/08/10
TDR magnets	10 jours	Lun 20/09/10	Ven 01/10/10
Project Critical Definition Review OK	0 jour	Lun 13/12/10	Lun 13/12/10
SC closed magnets	**732 jours**	**Lun 31/05/10**	**Mar 19/03/13**
DOE critical Decision 1	1 jour	Lun 12/07/10	Lun 12/07/10
DOE Critical Decision #3a	1 jour	Lun 13/12/10	Lun 13/12/10
SC closed triplet Optim	1 mois	Lun 31/05/10	Ven 25/06/10
SC closed magnet spec.	1 mois	Lun 23/08/10	Ven 17/09/10
Call for tender SC closed magnets	4 mois	Lun 04/10/10	Ven 21/01/11
Order placement SC closed magnets	1 mois	Lun 24/01/11	Ven 18/02/11
Kick off SC CM study	1 jour	Lun 21/02/11	Lun 21/02/11
SC CM proto manufacturing / validating	3 mois	Mar 22/02/11	Lun 16/05/11
SC CM triplets manufacturing	24 mois	Mar 17/05/11	Lun 18/03/13
SC CM ready for shipping	1 jour	Mar 19/03/13	Mar 19/03/13

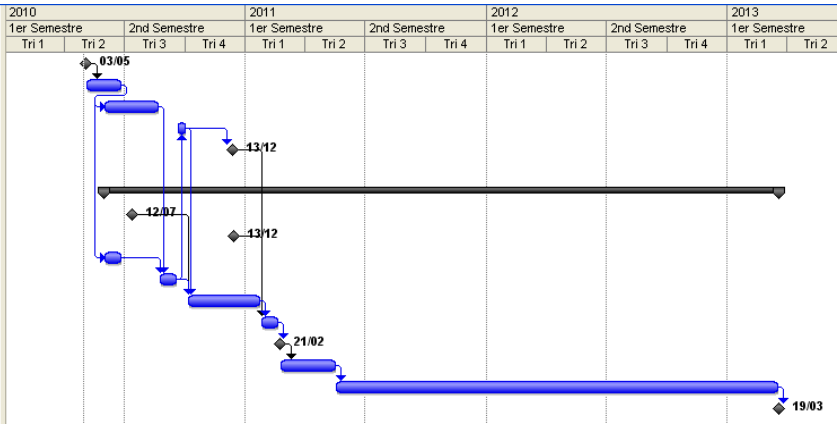

7.3.4 Magnetic dipoles schedule

Nom de la tâche	Durée	Début	Fin
Magnet techno choice	0 jour	Lun 03/05/10	Lun 03/05/10
Optical line geometry optim	2 mois	Lun 03/05/10	Ven 25/06/10
Line mechanical definition	3 mois	Lun 31/05/10	Ven 20/08/10
TDR magnets	10 jours	Lun 18/10/10	Ven 29/10/10
Project Critical Definition Review OK	0 jour	Lun 13/12/10	Lun 13/12/10
magnetic dipoles	**571 jours**	**Lun 26/07/10**	**Lun 01/10/12**
dipoles spec.	6 sm	Lun 26/07/10	Ven 03/09/10
Call for tender magnetic dipoles	5 mois	Lun 01/11/10	Ven 18/03/11
Bids and order	1 mois	Lun 21/03/11	Ven 15/04/11
Kick off industry tasks	1 jour	Lun 18/04/11	Lun 18/04/11
Studies at subcontractor	5 mois	Mar 19/04/11	Lun 05/09/11
Supply of raw materials	3 mois	Mar 14/06/11	Lun 05/09/11
tools suppyling	3 mois	Mar 06/09/11	Lun 28/11/11
magnetic dipole #1 manufacturing	4 mois	Mar 29/11/11	Lun 19/03/12
magnetic dipole #1 field map	2 mois	Mar 20/03/12	Lun 14/05/12
magnetic dipoles #2 and #3 delivery	2 mois	Mar 15/05/12	Lun 09/07/12
magnetic dipoles field maping at Ganil (TBC)	3 mois	Mar 10/07/12	Lun 01/10/12
magnetic dipoles ready for installation	0 jour	Lun 01/10/12	Lun 01/10/12

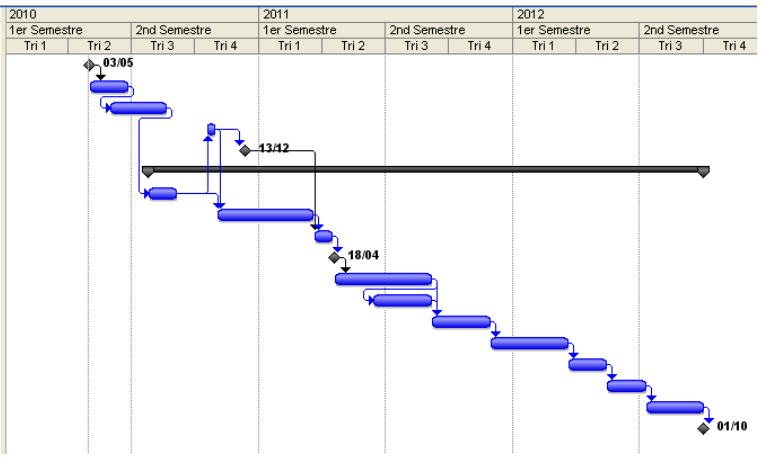

7.3.5 Schedule comparison conclusions

The last superconducting closed triplet is expected to complete fabrication in the middle of March 2013 (to be delivered to GANIL one month later, i.e. mid-April 2013). A room temperature open triplet could be available in April 2012. The choice of this option would make the closed superconducting triplets the last elements to be delivered, i.e. completing delivery in the middle of April 2013. A superconducting open triplet (MOSAR concept) is expected to be available in October 2013. The choice of this option would put this work package on the critical path and would delay the overall S^3 time line by six months. This does not mean that these six months would be lost for other S^3 tasks. The last closed superconducting triplet to arrive in April would still need between two and three months for reception, measurement, and installation; also the overall planning of the closed superconducting triplets would have a time margin of three to four months.

8 S3 organization

8.1 Organization chart

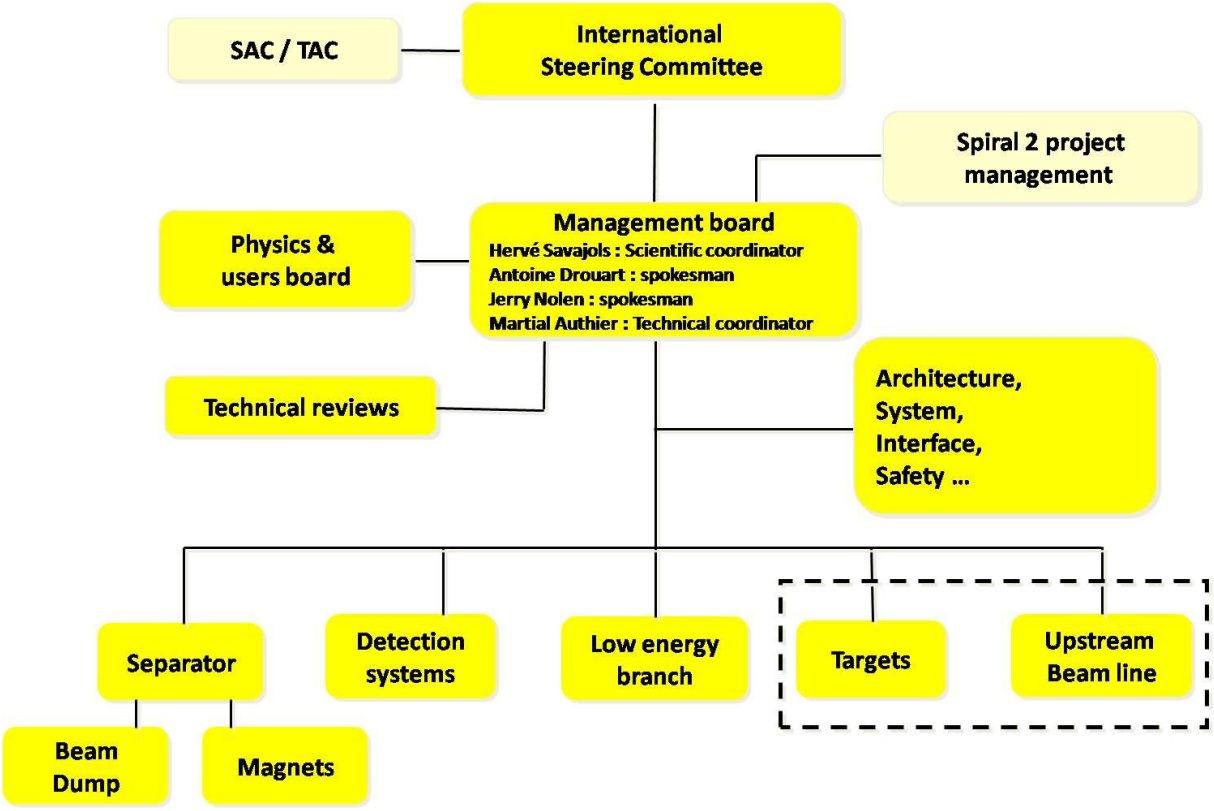

The management board is made up of the scientific coordinator (GANIL), two spokespersons (IRFU and ANL) and one technical coordinator (IRFU). At the upper level of the project a group responsible for the transverse aspects of the project (system, interfaces, safety, etc.) has to manage the technical aspects of the subsystems and ensure the coherence of the whole. S^3 is not in a construction phase yet. Subsystems are organized in a workgroups approach. Once all design choices have been made and the laboratories have committed for the various deliverable products, each subsystem will be headed by a scientific lead and a project manager.

8.2 S3 Steering Committee

Following positive opinions of the SPIRAL2 Steering Committee, the SPIRAL2 Scientific Advisory Committee and the GANIL and SPIRAL2 managements it has been proposed to create a Steering Committee of S^3. This Steering committee will evaluate the various steps to be taken; advise the agencies on courses of action; and help the funding agencies to take the critical decisions on the final design, organization, budget and construction schedule of the project.

It has been proposed that the Committee be initially composed of representatives of the main funding agencies currently likely to contribute to the S^3 construction phase, i.e. the DOE Office of Nuclear Physics, IN2P3/CNRS, Irfu/CEA and GANIL/SPIRAL2.

8.3 Reviews and reports

8.3.1 Introduction

Some reports and reviews will form the communication between the S^3 project and the S^3 Steering Committee and will enable the Steering Committee to clear the future steps of the project. The construction phase will get a green light from the S^3 Steering Committee after an S^3 (CDR).

As the multipoles' procurement is on the project's critical path, this CDR could be preceded by a specific, technical detailed design review at the end of the spectrometer design phase (Detailed Design Review or Technical Design Review), allowing some contacts (calls for tender) with industry before the Critical Definition Review.

There will be overall project reviews commissioned by the S^3 Steering Committee and internal reviews within the institutes—each following their own internal procedures—to precisely examine their work packages and give green lights for their duties, deliveries, and use of financial and human resources: CSTS IRFU/SPhN, DOE Alternative Selection and Cost Range Reviews (Critical Decision 1 review), STP-Physique (GANIL), Irfu Kick-off review, DOE Critical Decision 2 and 3b review, etc.

8.3.2 S^3 project reviews / reports until construction phase

Spiral 2 Scientific Advisory Committee (SAC) reports and reviews

The Spiral 2 Scientific Advisory committee meets on a biannual basis and, most notably, examines the status of Spiral 2 experiments. On every occasion, the S^3 project provides and presents its status report.

Magnet Conceptual Design Report (end of Magnet Preliminary Design Phase)

The aim of this CDR is to present the status of the ion-optical design, magnet designs and technology options, safety studies and mechanical integration of the full S^3 system to provide a basis for a decision on technologies to be used for the hardware components (mainly the technology of multipoles magnets: superconducting or room temperature). This includes performance evaluations, construction and operating cost estimates and a project timeline. This document does not include discussion of sub-systems such as target systems, focal plane detection systems and the low energy branch except where necessary for clarification of interface issues and overall budget estimates.

This is the present report, which is being sent to a panel of experts, with about 1 month for reading and initial feedback. After this review period, further meeting(s) can be scheduled to discuss the comments from the panel of experts.

We then will continue our paper studies of the S^3 beam line with the chosen technologies and so be able to define more precisely the requirements and interfaces for all the other S^3 equipment.

Spectrometer-target Detailed Design Review (end of detailed design phase)
(or Technical Design Review)

In fall, the project will have finished the detailed definition of the spectrometer components (including the upstream beam line and the dispersive plane beam dump system) and a technical analysis will be needed to validate these designs.

The documentation will be the current S^3 status/progress report and specific documentation for the magnets and surrounding systems (specifications, definition, design, risk analysis, development plans, schedule, budgets, commercial approach, safety, and radioprotection).

S^3 project Critical Definition Review

The goal of this review is to give a green light for the project procurement and construction phase.

It will examine the technical conclusions of the Spectrometer-target Detailed Design Review and will review the remaining aspects on the budget needs and availability.

8.3.3 Institutes' Reviews

Added to the former project reviews, institutes may require—following their own procedures—some other reviews to precisely examine their work packages and give green lights for their duties, deliveries, and financial and human resources.

8.3.3.1 Comité de suivie des projets STP-Physique (GANIL)

This committee meets bi-annually, to review work package status reports and preliminary development plans, schedules and assessed resources broken down in time.

8.3.3.2 CSTS IRFU/SPhN = "Conseil Scientifique et Technique » of the IRFU Nuclear physics division (SPhN), June 14

This meeting is organized by IRFU Nuclear Physics division (SPhN) and the goals are:

- To examine the fit between the proposed technical solutions and the main scientific goals.
- To assess IRFU's budgetary needs (useful to work on the division strategy).

The written support to this CSTS is composed of:

- S^3 status report
- IRFU's preliminary work package status report and preliminary development plans, schedules and assessed resources broken down in time.

8.3.3.3 DOE/ Alternative Selection and Cost Range Reviews (Critical Decision 1 review in August)

The goals of the DOE Critical Decision 1 review are to allow expenditure of funds for preliminary design and to approve long-lead procurement if necessary. It is scheduled at the end of the conceptual design phase.

The written support to this CSTS is composed of:

- Preliminary Project Execution Plan (PPEP or management plan, generated by project team). It can include a "Preliminary Systems Functions and Requirements Analysis" and a "Value Management/Engineering Determination."
- Preliminary Acquisition Strategy
- Conceptual Design Report (CDR)
- Preliminary Hazard Analysis and Safety documentation
- Preliminary Risk Management Plan and Risk Registry

8.3.4 IRFU Kick-off review

A CEA-IRFU kick-off review will be planned. It will validate the development options as well as the financial and human CEA/IRFU resources that CEA/IRFU will commit to engage for the construction phase. A dedicated review group, external to the project, is invited to report on the status of the project.

8.3.5 DOE/ Critical Decision 2 and 3b review

This DOE review has the goal to approve the Performance Baseline and the start of the construction. It has the same inputs and outputs as the S^3 project Critical Definition Review.

9 Strategic options

In this chapter, we will present our proposal of the technologies to be used for the hardware components of the S^3 spectrometer, based on the following criteria:

- performance evaluations
- construction and operating cost estimates
- project timeline
- flexibility
- risk analysis

9.1 Scientific requirements

S^3 is optimized for the delayed studies of nuclei produced by fusion-evaporation. Hence, two reference reactions have been chosen for the purpose of optics optimization:

1. $^{48}Ca + ^{248}Cm \rightarrow ^{292}116 + 4n$

   This is an example of superheavy element synthesis with a large angular distribution and a required mass resolving power of 300.

2. $^{58}Ni + ^{46}Ti \rightarrow ^{100}Sn + 4n$

   This symmetric fusion reaction is typical of N=Z nuclei studies. Evaporation residues have a large angular distribution, as well as a large electric rigidity that brings S^3 to the limits of available technology. Therefore, performances for this particular reaction have been considered to compare various hardware technologies while keeping a mass resolving power of better than 300.

In the following we will often use tables to enable a quick glance at the important parameters. The following notation will be used:

<Q>: central charge state

dQ = Q - <Q> We can consider that 5 charges states are significantly transmitted to the detection plane.

Trans = Transmission in % of the total number of the nuclei of interest produced in the target.

WRP : Weighted resolving power = M/dM. (average of the mass resolving power on each charge state weighted by the transmission of each of them).

9.1.1 Description of the different configurations:

- Superconducting Closed Multipoles (SCCM): “Ideal” configuration using realistic field maps of superconducting closed multipoles. Octupole corrections are included in all triplets except the second one. Since the second triplet has to be open-sided for the beam dump, this configuration is not realistic but is used as a reference for maximum performance estimates.
- Room temperature in MA + MS: The multipoles in this configuration include only quadrupole and sextupole components, i.e. no octupole coils.
- Room temperature in MA: Superconducting multipoles with quadrupole, sextupole and octupole fields are used in the mass separator, but no octupole corrections are used in the momentum achromat.

- SCCM + [open magnet]: configurations with superconducting closed magnets on all triplets except the second one which is an open magnet of a specific type:
    - RT Irfu: Room temperature open magnet designed by Irfu
    - RT Ganil: Room temperature magnet designed by Ganil. *These magnets are not represented in the following simulations, but they should give comparable or better results than the Irfu magnets since they are more optimized.*
    - Mosar I: Open superconducting magnet MOSAR. The sextupole field is generated by the residual field from two compensating dipole coils.
    - Mosar I + Octupoles: Same as previous with an additional octupole correction.
    - Mosar II: Open superconducting magnet Mosar with a better sextupole field generated by symmetric sextupole coils.
    - Mosar II + Octupoles: Same as previous but with an additional octupole correction.

9.1.2 Performance comparison by magnet configuration

Magnet types used for closed magnets	WRP	Transmission
Room Temperature in MA+MS (no octupoles)	**103,4**	**52,8**
RT in MA, Superconducting in MS	**288,4**	**52,8**
Superconducting Closed Multipoles in MA+MS (all with octupoles)	**299,4**	**53,3**

Table 12: Average simulated weighted resolving power (WRP) and transmission for the ^{100}Sn case for configurations with different closed magnet types. Only closed magnets are used.

Magnet types used for triplet 2	WRP	Ratio	Transmission
Superconducting Closed Multipoles	**299,4**	1.	53,3
SCCM + Open Room Temperature	**256,3**	0,86	53,1
SCCM + Mosar I design	**255,5**	0,85	49,9
SCCM+ Mosar I design (+ octupoles)	**275,4**	0,92	49,7
SCCM + Mosar II upgrade design	**284,3**	0,95	53,1
SCCM + Mosar II upgrade design (+ octupoles)	**292,9**	0,98	53,1

Table 13: Average simulated weighted resolving power (WRP) and transmission for the ^{100}Sn case for configurations with different open magnet types.

9.1.3 Influence of octupole correction

Table 12 shows the influence of placing octupole corrections either in the mass separator only or both in the momentum achromat and mass separator, compared to a solution with no octupole corrections (corresponds to the use of room temperature magnets in all triplets). In order to reach the required performances:

- Transmission better than 50% for large emittance experiments. **We see that there is little or no impact of the configuration on the transmission.**
- Mass resolving power better than 300.

We need:

- Sextupole corrections in all the quadrupoles of the beam line
- **Octupole corrections embedded in the mass separator multipoles**
- **Octupole corrections in the momentum achromat, at least in the three triplets excluding the second (T2) in the beam dump area.**

These corrections require the use of superconducting technology to embed both sextupole and octupole correctors within a quadrupole.

9.1.4 Open magnet triplet

Table 13 summarizes the resolving power and transmission of configurations using different types of open multipoles. Simulations show that slightly better results are obtained with superconducting magnets than with room temperature magnets. In addition, superconducting technology may allow the addition of octupole corrections. These corrections are shown to slightly increase the resolving power. But since these magnets represent a very innovative design, mechanical feasibility has yet to be verified decisively.

The room temperature open multipoles designed by Ganil have not yet been implemented in the full simulations. They are an improvement over the Irfu room temperature open design (SuperACO) and give much better performance so far with characteristics (weight and power consumption) that are also a great improvement over the previous room temperature design. They remain, however, more preliminary than the MOSAR designs. While the mechanical feasibility is not an issue in this case, a significant improvement in optical performance may be achievable with additional effort; the present designs represent a first attempt. Specifically, there remains a dipole component that is not fully optimized. They are, so far, the best solution for room temperature open magnets.

Finally, one aspect that has not been considered in the TraceWin calculations, whose results were discussed in Section 9.1.2, is the quality of the focus at the achromatic point. A collimator at this point will be used to eliminate many of the ions scattered in the momentum achromat, which otherwise might be transmitted to the final focal plane. The nuclei of interest are concentrated in the center, in an exact image (in first order) of the object (the beam spot on the production target). Octupole corrections in the first part of S^3 may be important to increase the higher-order quality of that image point—improving the beam rejection ratio while maintaining high transmission—while preserving the desired mass resolving power at the final focal plane. This will be the subject of further optimizations.

9.2 Cost (construction, infrastructure, maintenance and operating cost)

9.2.1 Construction

The overall cost estimates for the different technological choices are addressed in Chapter 7 and we don't foresee differences exceeding ~4% of the spectrometer cost for any of the different technical choices.

9.2.2 Infrastructure

The main impacts on the infrastructure are listed below.

Room temperature magnets:

- 250 m^2 is needed in a full room temperature option to install power supplies in a conventional section of the facility.
- Long, high current electrical cables are required to connect the power supplies to the magnets. A savings of 300 k€ in copper is estimated with a full superconducting option as compared to a full room temperature option.
- The power dissipation needed in the framework of a full room temperature technology requires dedicated air cooling in the target and beam dump caves.
- The weight of the room temperature magnets exceeds the lift and crane capabilities and requires a 2-piece design for handling.

Superconducting magnets:

- The need of nitrogen and helium refrigerator and lines for the cryogenic system.

9.2.3 Operating cost

The operating costs are driven by:

Room temperature magnets:

- Electrical power needed is about 1.5 MW in case of a full room temperature technology operating at maximum magnetic rigidity

Superconducting magnets:

- Electrical power needed for superconducting magnets is about 150 kW at maximum magnetic rigidity
- Total installed electrical power is 150 kW + 100 kW (Low energy beam line) + 250 kW (Dipoles). A savings of a factor of three in electrical power is estimated with a full superconducting option as compared to a full room temperature option, giving a savings of around 130 k€ for 6 months running at maximum magnetic rigidity (1 kW/h = 0.06€)
- The need for nitrogen and helium lines for the cryogenic system
    - Nitrogen: requires 2 l/hour per triplet; 5 k€ for 6 months running (0.07 €/l).
    - Helium: requires either a stand-alone liquid helium refrigerator or a heat exchanger to tap helium cooling from the central SPIRAL2 linac cryogenics system.

9.3 Safety issues

As stated in Chapter 5 we don't expect significant differences in conventional risks for superconducting or room temperature magnets with respect to conventional safety. The use of liquid gas needed by superconducting magnets will require administrative and engineering controls to prevent oxygen-deficiency hazards.

A preliminary comparative assessment of nuclear safety issues for both room temperature and superconducting multipole options didn't preclude the selection of either option.

The main topics to be addressed are the differences in the magnet materials (type and mass) and the safety issues relative to cryogenic fluids:

- For a constant mass, iron (room temperature magnets) is preferable to stainless steel, which usually contains traces of Cobalt (superconducting magnets); the procurement of specialized stainless steel with low Cobalt content should be possible and the mass of stainless steel (superconducting option) will be much lower than the mass of iron (room temperature option). The activation calculations for the superconducting option will be completed in October by Irfu/SENAC, for comparison with the room temperature magnet simulations already complete.
- We don't expect any critical issue with respect to the use of cryogenic fluids but this issue will be properly studied by Irfu/SENAC by means of activation calculations (final report scheduled for October 2010). The impact of a liquid gas leak in the cave that could induce a contamination risk will be addressed too (final report scheduled for March 2011).

9.4 Timeline

3 Magnetic dipoles

- Start of call for tender: November 2010
- Order placement: April 2011
- End of qualification of magnetic dipole #1: May 2012
- End of production and qualification of magnetic dipoles #2 and #3: October 2012

1 Electric Dipole

- End of studies and end of discussions with IMP Lanzhou: December 2010
- Manufacturing and qualification of the electric dipole: March 2012

7 Superconducting closed triplets

- Start of call for tender: October 2010
- Order placement: February 2011
- End of qualification of prototype coils: August 2011
- End of production (24 months): March 2013
- Delivery of the last superconducting triplet at Ganil: April 2013

1 open triplet

Superconducting option (MOSAR based triplet)

- Start of call for tender: November 2010
- Order placement: April 2011
- End of qualification of prototype (multipole 1): August 2012
- End of production (multipoles 2 & 3, packaged triplet): October 2013

Or Room temperature option

- Start of call for tender: November 2010
- Order placement: April 2011
- End of production: April 2012

Detailed planning for the upstream beam line / target system, the beam dump and the detection setup has not been performed yet but we assume that the overall critical path for S^3 is for the spectrometer magnets.

As far as the delivery of the last magnet is concerned we have to compare two options:

- Case of the choice of a superconducting open triplet: the critical path is then the delivery of this superconducting open triplet: i.e. October 2013. The start of S^3 commissioning will then be possible in January 2014.
- Case of the choice of a room temperature open triplet: the critical path would be the delivery of the last superconducting closed triplets, i.e. April 2013. The room temperature open triplet being delivered in April 2012. The start of S^3 commissioning could then be possible in summer 2013.

We assume in both cases that the critical path is not the SPIRAL 2 LINAC itself since first physics beams are today scheduled at the end of 2012.

Choice of the open triplet

We can see that the choice of the superconducting open triplet leads to a beam commissioning phase about one year after Spiral 2 beams are foreseen to be available and that the choice of a room temperature open triplet would lead to a beam commissioning phase about 6 months earlier.

With respect to the risk analysis of Section 9.6, if the 2010 studies of the superconducting open triplet conclude that the MOSAR concept is not feasible within a given time compatible with the milestones above, it will be possible to choose the use of a room temperature open triplet without impact on the planning, since a room temperature open triplet needs 18 months less than the superconducting open triplet to be studied, manufactured and delivered.

9.5 Flexibility

The Spiral 2 Scientific Advisory Committee reported in January 2010 that "Flexible multipole elements appeared as essential to achieve the best performance of the separator spectrometer" and recommended "a very careful choice of the solution that preserves the maximum quality and flexibility for a long term use of this important device".

9.6 Compared Risk assessments for the two options of the open triplet

We focus here on the comparisons of risks for the open triplet.

The superconducting closed triplets are definitely chosen for the Mass Spectrometer (4 triplets) and we assume that the choice of 3 additional superconducting closed triplets in the Momentum Achromat does not increase significantly the risk levels of the project.

9.6.1 Performances risks

As stated above, the best performance is theoretically achieved by using superconducting technology for all the magnets. One has to compare the risk of potential loss of performance between theoretical and real world magnets for both the room temperature and superconducting magnets with respect to key issues in each case. This risk assessment doesn't show that issues are very critical; it is used to identify the needed manpower (amount and skills) and development plans.

Superconducting open triplet key issues:

- The mechanical design has to cope with strong magnetic forces without changing the coils' positions.
- The vacuum chambers have a specific shape and must be threaded into the triplet from one end while still allowing a flange on both ends of the chamber.

Room temperature open triplet key issues:

- The profiles of the entrance faces have to be very precisely designed and controlled during manufacturing.

9.6.2 Planning risks

Superconducting magnets require more study and a longer qualification process than room temperature magnets. Estimated planning shows that a room temperature open triplet would be available in spring 2012, while a superconducting open triplet would only be available in fall 2013. Meanwhile, the last superconducting closed triplet would be expected to be delivered in spring 2013. Thus, we lose 6 to 7 months studying and manufacturing a superconducting open triplet instead of a room temperature open triplet. This issue is addressed in Chapter 7.

As far as planning risks are concerned, it is obvious that any planning risk attached to the superconducting open triplet option will impact directly the overall S^3 planning.

9.6.3 Human Resources risk

The skills needed for the study and manufacturing follow-up of superconducting magnets are not exactly the same as the skills needed for the study and the manufacturing follow-up of room temperature magnets. Some parts of the team that we have to build and maintain are not the same in both cases. Both skills exist, and we may write that we assume competent people will be available for either case.

9.6.4 Financial resource risk

The financial resources needed for the different technological choices are addressed in Chapter 7 and we don't foresee differences exceeding 4% of the spectrometer cost for any of the proposed technical choices. As the design and the manufacture of a superconducting magnet are not as simple and straightforward as those for a room temperature magnet, under estimates or unforeseen events leading to financial risk are a bit more likely with superconducting magnets.

9.6.5 Programmatic risks

This risk is real, as no MoU has been signed and not all the institutes are committed to date, but we don't foresee a more significant risk for superconducting magnets than for room temperature magnets in this respect.

9.7 Option proposed

9.7.1 Proposal for closed magnets:

Superconducting closed triplets are definitely chosen for the mass separator (four triplets) and we assume that the choice of three additional superconducting closed triplets in the momentum achromat will improve performance and flexibility, while not significantly increasing the risk level of the project.

9.7.2 Proposal for the open magnets:

- *MOSAR V2:*
  - Best performance on paper
  - Possibility to add octupoles (increase performance and flexibility)
  - Work is still needed to finish mechanical design
  - Timeline and, of lesser importance, the budget are drawbacks of MOSAR
- *Room temperature open magnet:*
  - Performance is presently worse than MOSAR
  - No octupoles possible
  - Mechanical design is essentially completed
  - Field quality could still be optimized further
  - Timeline is not on the critical path

We would propose to still continue with the MOSAR design in order to make a decision for the open multipoles no later than the end of 2010 (it will be possible to decide the use of a room temperature open triplet at a later date without any impact on the planning, since a room temperature open triplet needs 18 months less than the superconducting open triplet to be studied, manufactured and delivered)

We would like to emphasize that this process should not delay any decision on the other system components such as the mass separator.